POLITECNICO DI TORINO

Master of Science in Biomedical Engineering

New bioink formulations exploiting polyurethane hydrogels obtained by thiol-ene photo-click chemistry

Supervisors:

Prof. Valeria Chiono

Prof. Gianluca Ciardelli

Dr. Monica Boffito

Eng. Rossella Laurano

Candidate:

Ludovica Midei

December 2019

Index

Abstract

3D-bioprinting is an emerging additive-manufacturing technology which is attracting widespread interest in tissue engineering/regenerative medicine due to the possibility to fabricate scaffolds able to perfectly adapt to natural tissues. Indeed, this technique allows the deposition of biological materials (i.e., hydrogels eventually loaded with cells/biomolecules) in a very precise and spatially controlled way according to CAD models. In this process, a key-role is exerted by the extrusion material (i.e., the bioink) as it has to comply with some specific requirements: (i) easy printability at low pressure to avoid cell damage; (ii) capability to maintain its printed shape; (iii) good cytocompatibility and (iv) high stability in a watery environment. Hence, the design of smart bioinks with proper chemical, physical and mechanical properties as well as good cytocompatibility is gaining increasing interest. In this scenario, the high versatility of polyurethane chemistry allows the synthesis of polymers with tuneable properties by simply changing their building blocks (i.e., macrodiol, diisocyanate and chain extender), thus paving the way to the development of smart bioinks. Therefore, the aim of this work was the design of smart thermo- and photo-sensitive polyurethane-based hydrogels suitable to be used as bioinks for the fabrication of tissue engineered constructs. Specifically, hydrogel thermosensitivity was exploited to tune bioink viscosity during the printing process, while hydrogel photo-responsiveness allowed the formation of photo-induced covalent bonds in the printed structure, ensuring improved shape-fidelity and mechanical properties.

To this purpose, an amphiphilic poly(ether urethane) (PEU, acronym DHP407) was first synthesized starting from an amphiphilic triblock copolymer (Poloxamer® 407), which ensured polymer thermosensitivity, an aliphatic non-toxic diisocyanate (1,6 hexamethylene diisocyanate) and a chain extender containing a Boc-protected secondary amino group (N-Boc diethanolamine). The success of DHP407 (M_w 30000 Da) synthesis was assessed by Attenuated Total Reflectance Fourier Transform Infrared (ATR-FTIR) spectroscopy through the appearance of the typical absorption bands ascribable to the formation of urethane linkages. Subsequently, DHP407 was subjected to an acidic treatment to remove Boc caging groups (acronym of deprotected poly(ether urethane) D-DHP407), thus exposing a high amount of secondary amines (10^{19} units/$g_{D\text{-}DHP407}$ as calculated through Orange II Sodium salt assay). The exposed functional groups were then exploited to graft photosensitive moieties, thus providing the resulting polymer with responsiveness to UV/Vis light irradiation. Specifically, Thioglycolic acid (TGA) and 5-Norbornene-2-Carboxylic acid (NBE) were grafted to PEU-

NH through carbodiimide chemistry to expose thiols (S-DHP407) and norbornene (NB-DHP407) moieties, respectively. The successful grafting of the molecules was first assessed by ATR-FTIR spectroscopy, through the intensification of the characteristic bands of newly formed amide bonds. Then, thiol (10^{19} groups per gram of S-DHP407) and norbornene (10^{17} groups per gram of NB-DHP407) groups were quantified through a colorimetric assay (Ellman's method) and Proton Nuclear Magnetic Resonance (^{1}H-NMR) spectroscopy, respectively. Polymeric chain arrangement into micelles upon heating up to 45 °C was also investigated through the measurement of the average hydrodynamic micelle diameter (Dynamic Light Scattering), which turned out to be approx. 30 nm for both S-DHP407 and NB-DHP407 solutions at 0.5% w/V. On the other hand, the photo-click thiol-ene reaction mechanism was first studied through UV-Vis spectroscopic analyses on virgin molecules (i.e. TGA and NBE) to identify the proper concentration of the photo-initiator (Eosin Y, EY, 0.1mM – 2mM). Then, by using the optimized EY concentration (0.5 mM), similar analyses were carried out to clarify the role exerted by the co-initiator tyrosine (TYR, 1mM – 10mM), which turned out to negatively affect bond formation upon irradiation. Hence, EY was selected as the only photo-initiator for the preparation of the thiol-ene photo-click hydrogels. Then, S-DHP407/NB-DHP407 hydrogels at 18%w/V concentration and 1:1 stochiometric ratio of thiol-ene moieties were photo-crosslinked through irradiation at 525 nm. The successful formation of new covalent bonds among the polymeric chains upon light irradiation was proved by the increased micelle hydrodynamic diameter (from 29.4 ± 0.4 nm to 31.0 ± 1.1 nm) and the decreased intensity of norbornene and thiol bands in ^{1}H-NMR and ^{13}C-NMR spectra. Subsequently photo-crosslinked hydrogels were rheologically characterized by exploiting their retained thermo-reversibility upon exposure to green light. Results reported that the photo-curing process induced the formation of significantly more developed gels (storage/loss moduli crossover frequency at 37 °C at 0.18 rad/s and < 0.1 rad/s for thermo and photo-crosslinked S-DHP407/NB-DHP407 hydrogels, respectively) with higher storage and loss moduli with respect to the control (not photo-crosslinked hydrogels). Additionally, the negative effect exerted by the co-initiator on photo-induced bond formation was further proved by the frequency sweep tests, showing lower mechanical properties for TYR-containing samples. Finally, the optimized bioink formulation was 3D-printed according to two different CAD models, i.e. square grid and honeycomb structure, by properly adjusting the working pressure and temperature. Specifically, the multilayer constructs were obtained by combining the layer-by-layer hydrogel deposition in the semi-gel state and the successive photo-click stabilization through visible-light irradiation, thus allowing the scaffold to keep their morphology and show enhanced

mechanical properties. Hence, the herein developed bioinks could effectively open a new era in the biomedical field thanks to their high versatility that could potentially allow 3D print matrices based on them to match the physical properties of almost all soft tissues of the human body.

Introduction

1.Hydrogels

Hydrogels are finding widespread application in the biomedical field as 3D systems suitable for the design of biomimetic structures. Indeed, their high-water content and their strong hydrophilicity perfectly reproduce the complex geometry, soft characteristics and three-dimensionality of the extracellular environment. The first application of hydrogels in the biomedical field took place in 1960, with the fabrication of soft contact lens based on hydrophilic matrices of crosslinked poly(2-hydroxyethyl methacrylate) (pHEMA) [1].

During the last few decades hydrogels have been attracting increasing interest in the research community, as suggested by the growing number of papers published on this topic from 1995 on (**Figure 1**).

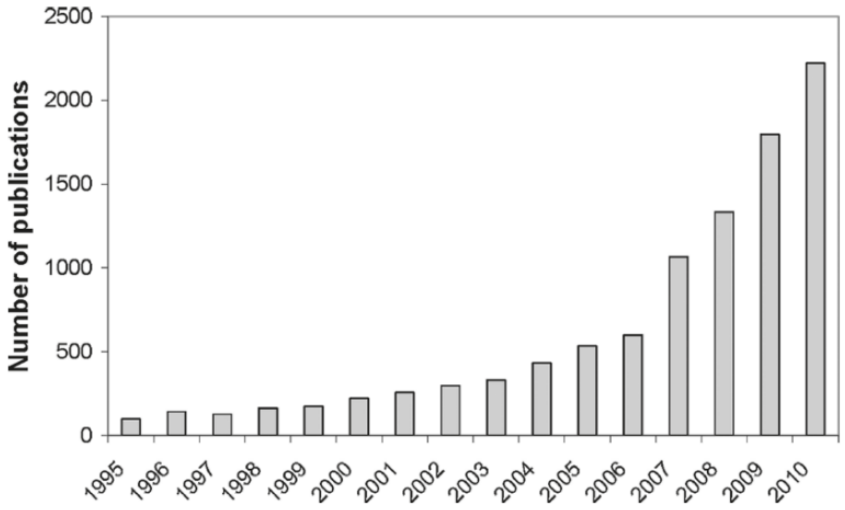

Figure 1 *Overview of the growing number of publications focused on hydrogels during the last few decades. [1]*

1.1 Definition and properties

The most common definition refers to hydrogels as crosslinked, hydrophilic and three-dimensional networks of polymeric materials capable to swell in water or body fluids, increasing from ten up to thousands times their initial dry weight. In this latter case hydrogels are referred to as super-adsorbent [2]. Hydrogel swelling capability, and thus their high network hydrophilicity, can be

correlated to the polar functional groups (e.g., amines, carboxyl and hydroxyl groups) they expose, which can be involved in hydrogen bonds with the molecules of the surrounding fluids(**Figure 2**) [3].

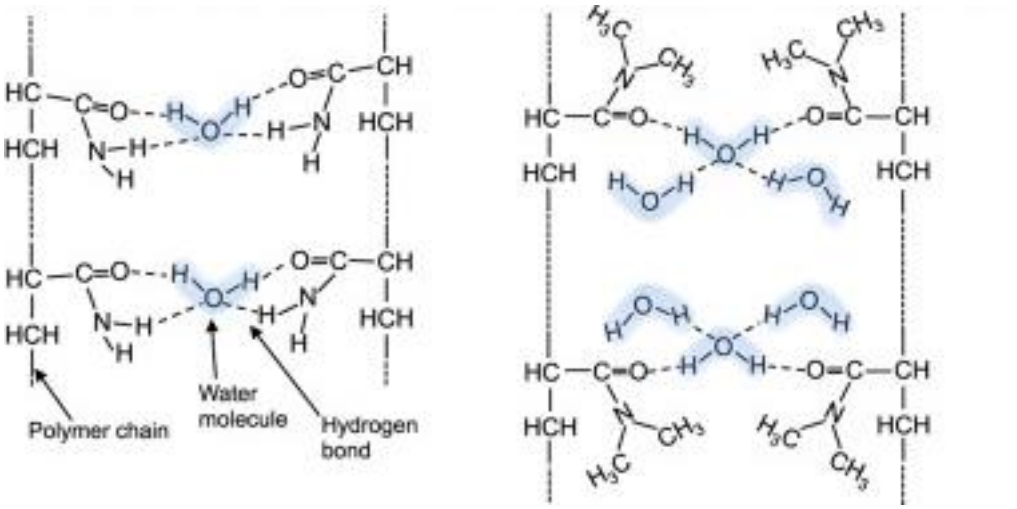

Figure 2 *Examples of H-bondings between hydrogel polymeric chains and the surrounding water molecules.[3]*

A large number of classifications has been reported in the literature to distinguish hydrogels based on (i) the nature of the polymeric component (i.e., natural or synthetic hydrogels); (ii) the kind of the interactions occurring between the polymeric chains (i.e., physical or chemical hydrogels), and (iii) their stimuli-responsiveness capability (i.e., thermo-, photo-, analyte-, pH-sensitive hydrogels).

Hydrogels have found widespread application in the pharmaceutical and medical industry because of their high water-content, which results in soft and rubbery consistence, giving them a strong resemblance to living soft tissues.

Concerning mechanical properties, hydrogels show an intermediate behaviour between solids and viscous liquids. The aqueous solution of the initial pre-polymer, in which the bonds between the chains have not been formed yet, usually shows the behaviour of Newtonian fluids. After gelation, the resulting three-dimensional network exhibits a viscoelastic behaviour, with the exception of some particular materials in which purely elastic properties can be reached [4]. For instance, Zhao et al. designed alginate hydrogels able to display stress-relaxing or purely elastic behaviour according to the crosslinking method. Indeed, ionic-crosslinked gels display a rapid relaxation behaviour, while covalently crosslinked alginate hydrogels undergo elastic deformation due to water migration out of the gel [5]. Hydrogel mechanical properties depend directly on different factors, such as (i) the original stiffness of the polymeric chain, (ii) the polymerization degree, (iii)

the gelation mechanism, and (iv) the swelling rate, which in turn depends on the ratio between hydrophilic and hydrophobic moieties.

One of the main pros in the use of hydrogels consists in the possibility to finely tune their characteristics. Indeed, the mechanical (stiffness and elastic modulus) and physico-chemical (electrical charge and porosity) properties can be adjusted by changing the kind of polymer, its content and its gelation mechanism or by blending different polymeric materials in order to obtain composite hydrogels [6]. For instance, Hutson et al. reported the possibility to tailor the mechanical properties of a polye(thylene glycol) (PEG) and methacrylic gelatin (GelMA) composite hydrogels by simply varying the concentration of the two starting materials. Specifically, the final hydrogel compression module and capability to absorb fluids increased with increasing GelMA initial concentration. [7]

Hydrogel biodegradability is another crucial feature for their use as scaffolds for tissue engineering or as vehicles for cells or therapeutic molecules. The degradation/dissolution time, which mainly depends on the natural or synthetic origin of the material, is a parameter that must be controlled and properly tuned. Concerning tissue regeneration, the hydrogel degradation rate must be time-coordinated with the formation of the new tissue or with the gradual release of payloads or cells in the target site. The hydrogel degradation process can be hydrolytic or enzymatic, depending on the chemical structure and the mechanical properties of the starting materials [4].

Biocompatibility is another fundamental issue in the design of systems suitable for biomedical applications. In general, material biocompatibility is defined as its ability to behave as a substrate capable of supporting appropriate cellular activity, with no local or systemic side effects in the host. Specifically, hydrogel biocompatibility depends on both polymer origin (i.e., natural or synthetic) and its gelation mechanism, which often requires the addition of potentially cytotoxic crosslinking agents. However, the presence of high water content and the soft consistency of hydrogels generally make the biocompatibility of these systems easily achievable [8].

1.2 Hydrogels classification

Hydrogel classification may be based on several characteristics, such as hydrogel physical properties, material origin, nature of crosslinking, type of swelling, preparation methods, electric charge, sensitivity to different stimuli. A general classification is shown in **Figure 3** [9]. Although hydrogels can be classified according to these several features, they are usually categorized into three different classes according to:

1. *Material Origin*: natural or synthetic polymers.
2. *Crosslinking method*: physical or chemical polymerization.
3. *Responsiveness to external stimuli*

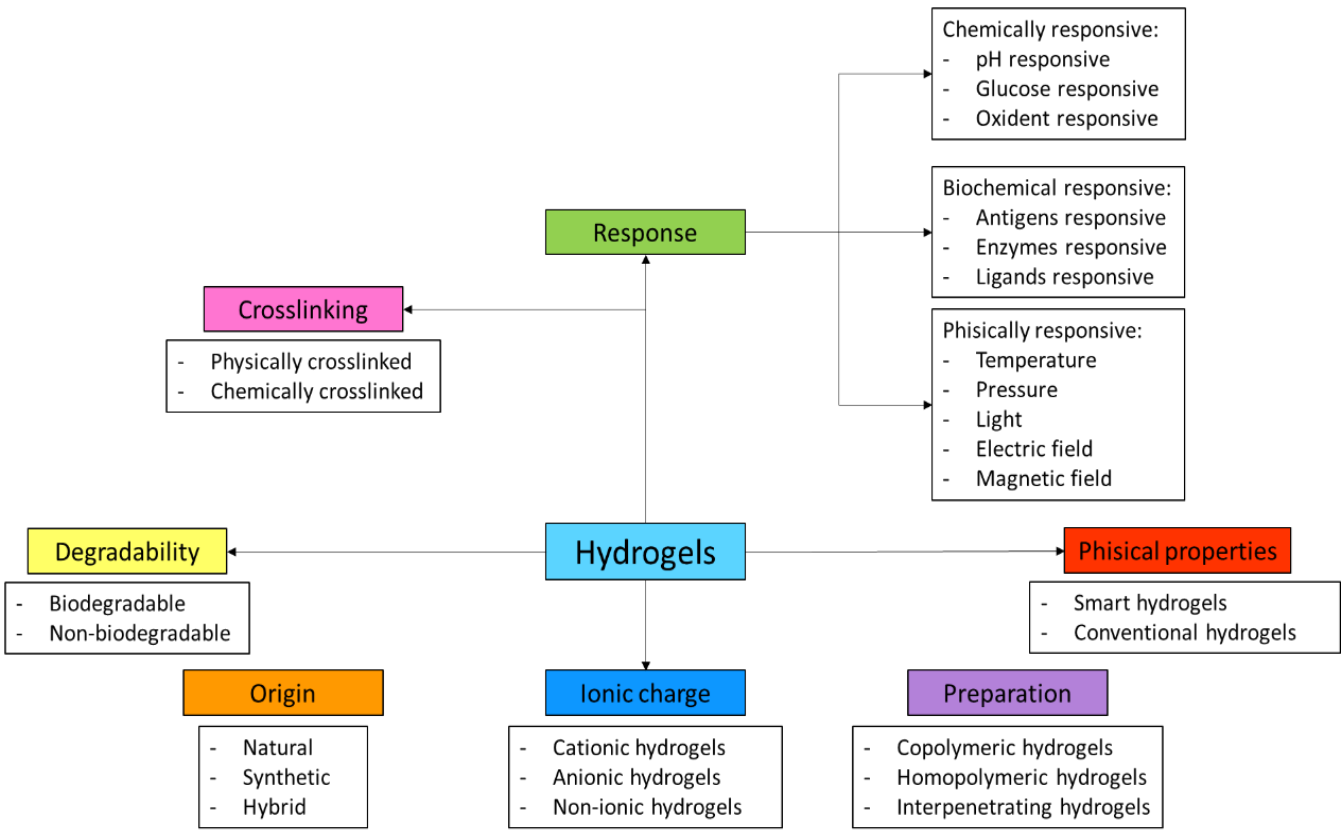

Figure 3 *Hydrogels classifications based on several different properties [8]*

1.2.1 Classification of hydrogel: Material Origin

The first classification distinguishes hydrogels based on the natural or synthetic origin of the starting material.

Natural hydrogels may be derived from proteins or polysaccharides polymers. Among these natural polymers, collagen is particularly interesting as it represents the most abundant structural protein of the organism. Other examples of protein-based hydrogels are those composed by gelatin (collagen derivative), fibrin, laminin and silk fibroin. On the other hand, chitosan, alginate and hyaluronic acid stand out among hydrogels based on polysaccharides [10]. These hydrogels are generally characterized by high biocompatibility, biodegradability and bioactivity in terms of cells adhesion and viability. In addition, they show a high affinity for proteins, such as fibronectin and integrins, thus further improving hydrogel capability to promote cellular adhesion. Indeed, cell adhesion occurs preferentially on surfaces exposing peptide sequences [1]. However, the mechanical properties of natural hydrogels are often weak, leading to a rapid hydrogel dissolution/degradation [11]. In addition, processes required to extract natural polymers suffer for a high variability between different batches, making difficult to definitively characterize their properties. Finally, the biological origin could potentially cause pathology transmission and contamination.

Alternatively, poly-α- hydroxy acids (polylactic acid, PLA and polyglycolic acid, PGA), poly(ε-caprolactone) (PCL) and poly(ethylene glycol) (PEG) are the most commonly explored synthetic biodegradable polymers used to design bulk materials for *synthetic hydrogel* development. Hydrogels based on synthetic polymers show relatively good and easily controlled mechanical properties and they are characterized by more flexible and reproducible production processes [5]. Furthermore, synthetic hydrogels also allow the encapsulation of cells that remain viable and metabolically active [12][13]. However, lacking bioactive structures, they are not able to promote integration activities with biological processes. For this reason, they often need functionalization to succeed in actively interacting with cellular components. These modifications, which consist in introducing peptide sequences or proteins along the material backbone, can be obtained exploiting physical or chemical methods [5]. The simplest physical technique consists in the introduction of bioactive binding sites through the encapsulation into the hydrogel network of extracellular matrix (ECM) proteins, such as collagen, laminin or fibronectin, or growth factors. For instance, the

immobilization of vascular endothelial growth factor (VEGF) in dextran and PEG diacrylate gels induced an increase in the angiogenic capability of the resultant biomimetic matrix [14]. The chemical modification of the polymeric chains consists in the covalent grafting of bioactive proteins or peptides (such as the Arg-Gly-Asp (RGD) peptide sequence [15] or the GGGPQG↓IWGQGK peptide sequence which is sensitive to matrix metalloproteinase (MMP) activity [16]) to the polymer backbone. In a recently published work, E. Leslie-Barbick et al. described the functionalization of PEG molecules with a synthetic sequence (named QK) with the aim to mimic the natural VEGF. Results reported the development of an hydrogel with angiogenesis properties comparable to those shown by the same hydrogel functionalised with VEGF [17].

1.2.2 Classification of hydrogel: Crosslinking

Hydrogel can also be categorized into physical or chemical hydrogels based on their gelation mechanism, which may include the formation of physical or chemical interactions, respectively. [18] *Physical interactions* include the formation of hydrophobic, ionic or hydrogen bonds among the polymer chains (**Figure 4**). For instance, in the presence of polymeric chains composed by hydrophobic and hydrophilic segments, a sol-to-gel transition can occur with increasing temperature, due to the different interactions of the polymer building blocks with water molecules which lead to progressive micelle formation and packing into an ordered network. In this kind of hydrogels, the polymer concentration, the balance between the hydrophobic/hydrophilic content,

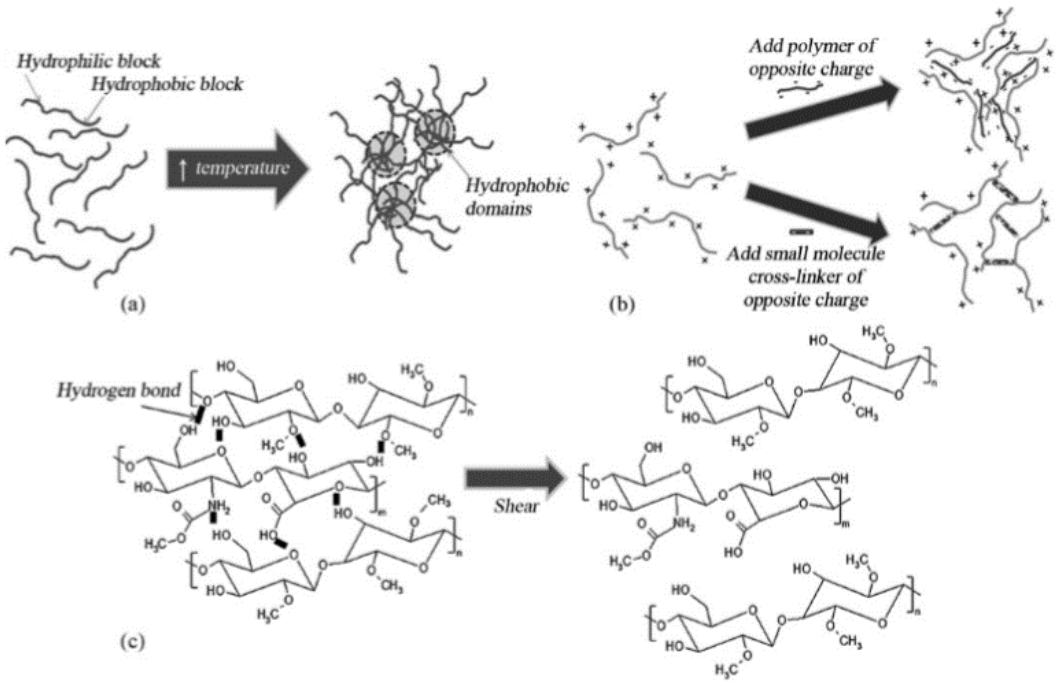

Figure 4 *Formation of physical gels in situ through (a) hydrophobic interactions, (b) charge interactions, (c) hydrogen bonds, which can be destroyed by application of a shear. [19]*

as well as the length of hydrophobic and hydrophilic blocks contribute to the identification of the temperature at which this phase transition takes place. Alternatively, the formation of hydrogel can also occur via ionic interactions between a charged biopolymer and a charged molecule or between two biopolymers with opposite charge. Finally, physical hydrogels can also be the result of hydrogen bonds, which are defined as physical bridges between two polymeric chains.

Being hydrogen bonds the weakest among non-covalent interactions, these physical hydrogels can be easily destroyed by the application of share stresses.

Although these methods of polymerization do not lead to the establishment of permanent bonds, they are able to prevent fast dissolution of hydrogels in water [19].

Chemically crosslinked hydrogels can be obtained via radical polymerization, chemical reactions occurring between complementary groups, high-energy irradiation and enzymatic polymerization. Covalent interactions are much stronger than non-covalent interactions and provide greater mechanical stability than that achievable with physical hydrogels. In addition, the addition of crosslinking agents is often requested and this can lead to biocompatibility issues as they can induce cytotoxic effects [20].

The most common technique used to design hydrogels is radical polymerization (**Figure 5**). Inactive low-molecular weight side groups exposed on monomers are activated in free radicals upon UV or visible-light irradiation in the presence of photo-initiators enhancing the formation of covalent bonds which macroscopically result in an assembled gel.

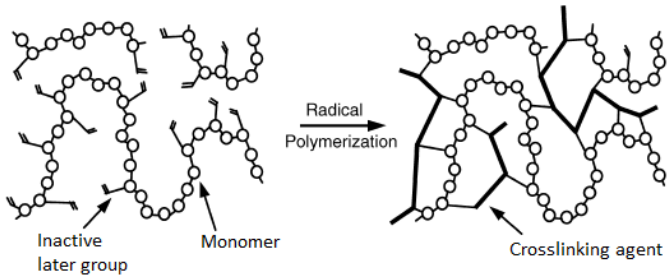

Figure 5 *Schematic representation of chemically crosslinked hydrogels formed by radical polymerization. [19]*

Chemically crosslinked hydrogels can also be obtained by exploiting the reaction occurring between polymeric chains functionalized with groups of complementary reactivity [4]. For instance, condensation reactions involving hydroxyl or amino groups reacting with carboxylic acid derivatives such as isocyanate or activated esters can be exploited to develop chemical hydrogels. As an example, Eiselt et al. improved the mechanical properties of alginate-based hydrogels by

crosslinking alginate, which contains carboxylic groups, and PEG-diamines through carbodiimide chemistry [21].

Another covalent-crosslinking technique involves high energy irradiation, in particular electron and gamma beam. Upon irradiation of the polymeric aqueous solution, radicals form on the polymer backbone by the homolytic scission of the available chemical bonds (e.g., the C-H bond). In addition, hydroxyl radicals can form through radiolysis of water molecules, which consequently attack polymeric chains by participating in macroradical formation. The progressive interaction of macroradicals through covalent bonds finally leads to the formation of the polymerized structure. The possibility of executing the polymerization process in aqueous media under mild conditions (room temperature and physiological pH), without the need of potentially toxic crosslinking agents represents an important advantage of this methodology. On the other hand, the toxicity of the irradiation process itself must be verified before cells or biological substances are encapsulated in the hydrogel.

Finally, among chemical crosslinked hydrogels, wide investigation has been reported also on enzyme-crosslinked systems. For instance, Sperinde et al. studied the formation of a PEG-based hydrogel through enzymatic reaction (driven by transglutaminase) between PEG macromolecules functionalised with lysin terminal groups or glutamine groups. [22]

1.2.3 Classification of hydrogel: Responsiveness to external stimuli

The last hydrogel classification regards their responsiveness to external stimuli, i.e. gel capability to modify their properties in response to small and rapid changes in the surrounding environment, such as temperature and/or pH changes, light irradiation [23].

The main feature of such responsive hydrogels is their capability to modify their network from a collapse state, in which the interactions between the polymeric chains predominate, to a swollen one, in which the interactions between the polymeric chains and the solvent predominate, in response to changes in temperature, pH, electric/magnetic fields, small molecules or biomolecules concentration, and light irradiation intensity (**Figure 6**) [24][25].

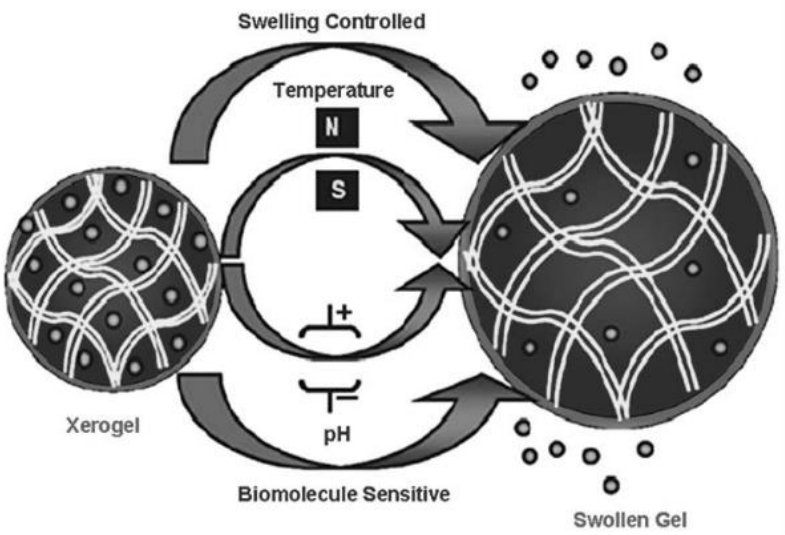

Figure 6 *Stimuli-responsive hydrogels [23]*

pH-responsive hydrogels

pH-responsive hydrogels are systems able to swell or de-swell in response to external pH changes as a consequence of the protonation/deprotonation of functional groups (e.g., carboxylic groups, amines) exposed on the polymer backbone. Specifically, all pH-sensitive polymers (known as polyelectrolytes) expose pendant acidic or basic groups that can release or accept protons in response to variations in environmental pH. In the case of anionic hydrogels (e.g., gels containing carboxylic groups) swelling occurs when the environmental pH is above their pK_a, while in cationic gels (e.g., systems showing pendant amine groups) the increase in volume is a result of an external pH lower than their pK_b.

Therefore, the hydrogel behaviour is not only dependent on the ionic charge and pK_a or pK_b of the ionizable groups exposed along the polymer chains, but also on the pH, ionic strength and counterions of the medium absorbed by the gel. The combination of all these factors allows to finely tailor hydrogel swelling according to their final application [19].

One of the most common polyanions for biomedical applications is poly(acrylic acid) (PAA), that becomes ionized at high pH [27]; meanwhile, polycations as poly(N,N'-diethylaminomethyl methacrylate) (PDEAEM) becomes ionized at low pH [28] (**Figure 7**).

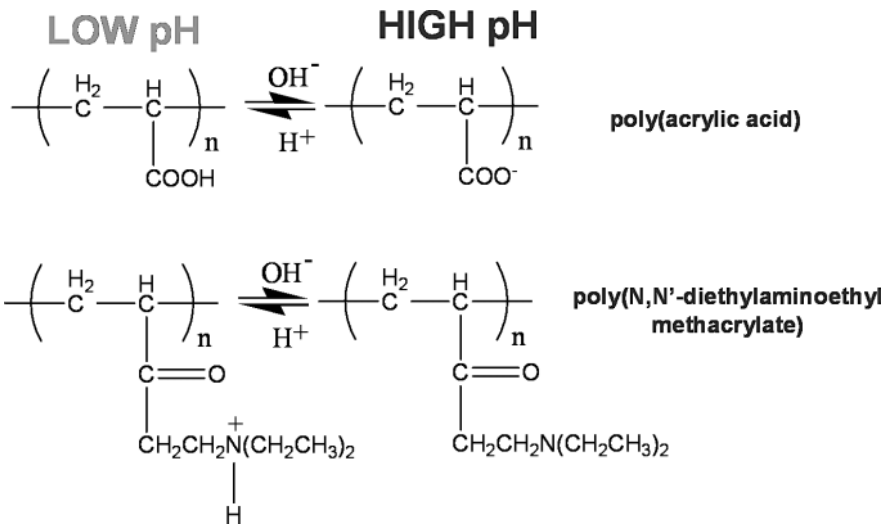

Figure 7 *A weak polyacid (top), exhibiting shrunk network at acid pH and an swollen conformation at basic pH (soluble in aqueous solution); A weak polybasic (bottom) that presents an opposite behaviour. [28]*

pH responsive hydrogels have found widespread application in the biomedical field, especially to incorporate and deliver drugs and bioactive agents through a controlled way. These technologies can be applied because pH differences among the different compartments of the body. For instance, along the gastrointestinal tract the pH is extremely different: acidic in the stomach region and basic in the intestine one. In this context lots of pH sensitive systems have been designed to deliver therapeutic molecules in the stomach [25]. A. Siegel et al. designed a pH-sensitive hydrogel based on copolymers of methyl-methacrylate and N,N'-diethylaminomethyl (DMEAM) methacrylate to design novel formulations suitable for oral administration. Being a polycationic hydrogel, no swelling occurred at pH 7.4, thus minimizing the release of drug into the mouth. In fact, the payload was released at pH 3-5 (condition available into the stomach) where DMEAM became ionized [28]. In another work, Ghandehari et al. developed a PAA-based hydrogel crosslinked with azo-aromatic crosslinkers. PAA as polyanion induced an increase in hydrogel swelling into the intestine where the increased pH allows carboxylic pendent groups to ionize. The drug was released at pH 7-8 into the colon where the effect of swelling due to PAA pH responsiveness was summed up with the degradation of azo-aromatic crosslinkers due to azo-reductase produced by microbial flora of the colon [27]. Another interesting feature of pH-sensitive hydrogels concerns their application in cancer drug targeting exploiting the differences existing in pH between tumour and healthy tissues [25].

In the last few years pH sensitive polymers have been largely used also in non-viral gene therapy. This technology is based on the transport of naked DNA into cells in order to substitute genes that are missing or not working or to modulate gene expression. DNA is negatively charged so cationic

polymer can be applied to incorporate and transfer it into the cell nuclei. Then, the DNA should be released from the endosome, which is the first cellular complex formed upon DNA-polycation system endocytosis, into the cytosol. This process is made possible by the so-called proton sponge effect: polycations absorb protons available as a consequence of endosomes acidification during the internalization, so vesicles containing DNA are disrupted and able to release their content. In this context chitosan is extremely applied, not only because of its charge but also thanks to its low cytotoxicity [29].

Recently, pH sensitive hydrogels have been also investigated for the release of insulin in the treatment of diabetes. Indeed, the conversion of glucose into gluconic acid by glucose oxidase in the presence of oxygen induced a reduction of the local pH. This acidification can cause the swelling of insulin-loaded gels and thus, the release *in situ* of their payload. This kind of concept has also been applied to develop glucose sensors [25]. Beside sensors and drug delivery systems, pH sensitive gels can also be exploited for microfluidic applications to design valves able to reversibly change their size as a consequence of pH changes [26].

Among the hydrogel constructs that can respond to specific biological events, the most common are **antigen responsive hydrogels.** They are designed by grafting antibodies and the corresponding antigens on the polymeric chains, thus introducing crosslinks into the newly formed network thanks to antibody-antigen binding. In an environment containing free competitive antigens, hydrogels can undergo swelling as a consequence of the decreased amount of crosslinks (**Figure 8**). This may be useful to develop antigen-sensing devices which can release biomolecules, proteins or drugs to desired target sites [30].

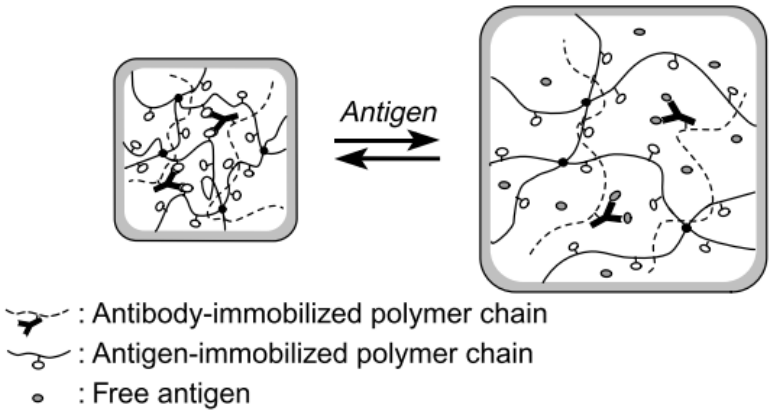

Figure 8 *Swelling of an antigen-antibody hydrogel in the presence of free antigen molecules in the surrounding environment [30].*

1.3 Thermosensitive hydrogels

Among physically responsive hydrogels, temperature sensitive gels are considered the most exploited for biomedical applications, due to their capability to swell and shrink as a consequence of temperature changes in the surrounding environment, without the need of any other external factor.

Temperature-sensitive hydrogels can be classified into *negatively thermosensitive, positively thermosensitive* and *thermally reversible gels*. In the first two classes the formation of covalent and permanent bonds occur between polymeric chains, while hydrogels belonging to the last class are physically cross-linked. Indeed, thermally reversible gels undergo a sol-gel transition upon temperature changes instead of a swelling-shrinking phase transition. Nevertheless, they all have the same structure [9].

Therefore, exploiting their responsiveness to temperature, these systems can be effectively exploited as delivery systems of properly selected drugs/biomolecules. Negatively thermosensitive drug release systems are characterized by a critical parameter, called low critical solution temperature (LCST), that is the temperature below which the hydrogel swell. Conversely, positively thermosensitive hydrogels possess an upper critical solution temperature (UCST) above which they swell [31]. This concept is schematized in **Figure 9** [32].

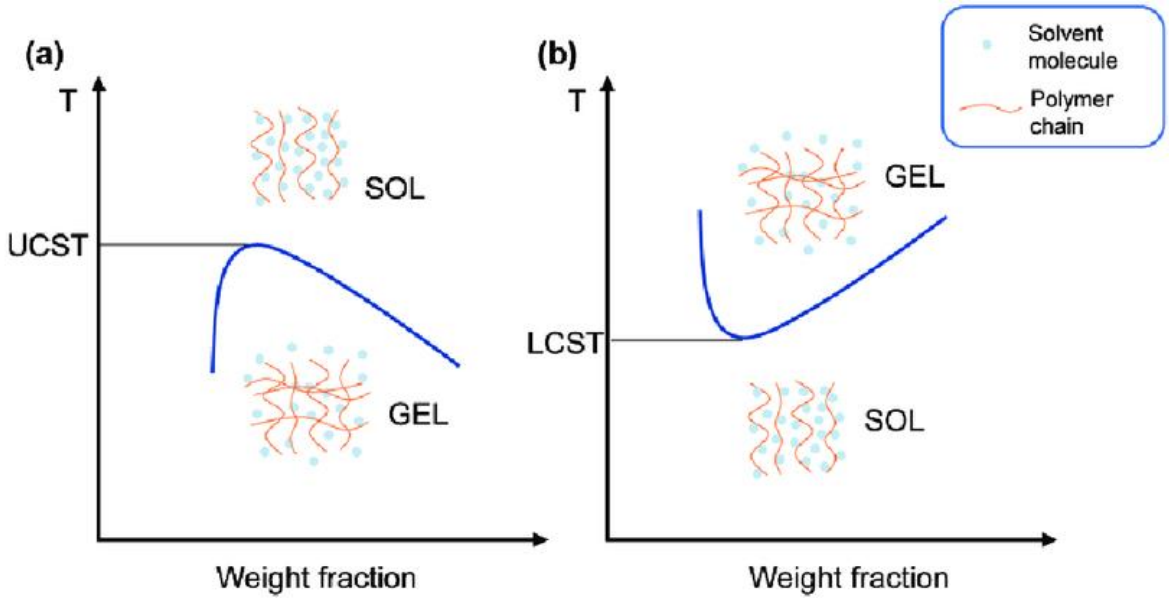

Figure 9 *Sol-gel transition in thermo-responsive hydrogels:*
a) positively thermosensitive hydrogels, b) negatively thermosensitive hydrogels [32]

To what concerns thermo-reversible hydrogels, polymers forming this kind of networks are generally amphiphilic copolymers, i.e., polymer composed by the alternation of hydrophilic and hydrophobic segments. These amphiphiles are usually water soluble at low temperature, while upon temperature increase, system entropy increases and the hydrophobic domains aggregate into organized structures (i.e., micelles). This organization at the nanoscale results in a sol to gel transition at the macroscale [9][33].

As in crosslinked hydrogels, also thermo-reversible gels exhibit a phase transition from sol to gel above or below a specific temperature value defined as lower critical gelation temperature (LCGT) and upper critical gelation temperature (UCGT), respectively. Furthermore, the micellar conformation occurs not only at a proper temperature but also when the polymeric system exceeds a specific concentration, known as critical gelation concentration (CGC) [34].
Hydrogels with LCGT behaviour, also known as inverse thermo-responsive hydrogels, are preferable to UCGT hydrogels as injectable systems for biomedical applications because they can entrap therapeutic molecules or cells at low temperature (e.g., room temperature), be easily injected in the body in the sol or same gel state and finally undergo a rapid sol-to-gel transition at body temperature.

Figure 10 shows the typical phase diagram of a thermo-reversible hydrogels with a LCGT behaviour. These systems are usually in the gel state above their LCGT for a range of temperature called gel window (i.e., temperatures higher than LCGT and lower then UCGT) [34]. Upon a further temperature increase (i.e., T higher than UCGT), the gel undergoes a reverse transition from the gel to the sol state or precipitate as a consequence of syneresis phenomena.

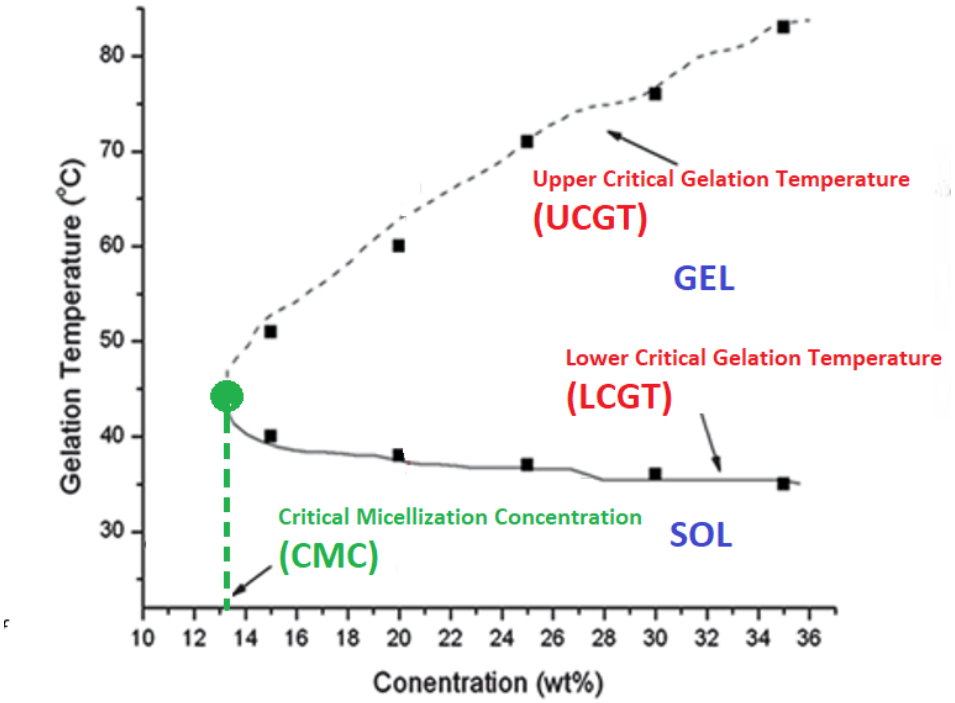

Figure 10 *Phase diagram of thermo-reversible hydrogel with LCGT behaviour [34]*

For what concerns the materials used for the design of thermo-reversible hydrogels, synthetic polymers can offer many advantages with respect to natural ones in terms of higher resistance to enzymatic degradation, which ensures a longer residence time *in vivo* and the opportunity to modulate their chemical properties according to the final demands. For this reason, in the following paragraph synthetic thermo-responsive hydrogels will receive greater emphasis.

1.3.1 Thermo-reversible hydrogels: Emerging materials

- *N-isopropylacrylamide copolymers*

Hydrogels based on N-Isopropylacrylamide homopolymer (poly(NiPAAM) (**Figure 11**) are one of the most studied thermo-reversible systems for drug release or cell encapsulation. pNiPAAm responsiveness to temperature is due to the existence of a LCST at about 32°C (for 1%w/w aqueous solution of pNiPAAm [35]), above which a reversable transition occurs from the sol to the gel state. [36]

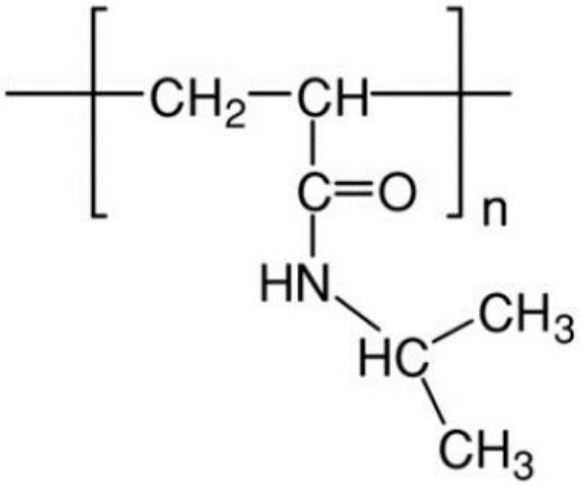

Figure 11 *The chemical structure of poly (N-isopropylacrylamide) [36].*

The LCST of NiPAAM polymers can be finely tuned by copolymerizing them with other monomers [37]. Combining pNiPAAm with a more hydrophilic monomer results in increasing both polymer hydrophilicity and consequently LCST, while its combination with a more hydrophobic block leads to a decreased LCST with respect to the starting polymer. One example of these kinds of hydrogel has been developed by Lin and Cheng [38] , who designed a copolymer consisting of a central hydrophilic polyethylene oxide (PEO) block and thermo-responsive pNiPAAm as terminal segments. This copolymer forms liquid solutions at room temperature that turn into gel upon heating.

- *PEO/PPO block copolymers and their derivatives* [39]

Widely exploited polymers for the development of thermo-sensitive drug releasing hydrogels are block-copolymers composed of polyethylene oxide (PEO) and polypropylene oxide (PPO) segments grafted at different weight ratio and able to undergo sol-to-gel transition in a wide concentration range. Furthermore, these copolymers are also FDA approved [40]. **Figure 12** reports the structure of the PEO-PPO block-copolymers mainly used in biomedical applications.

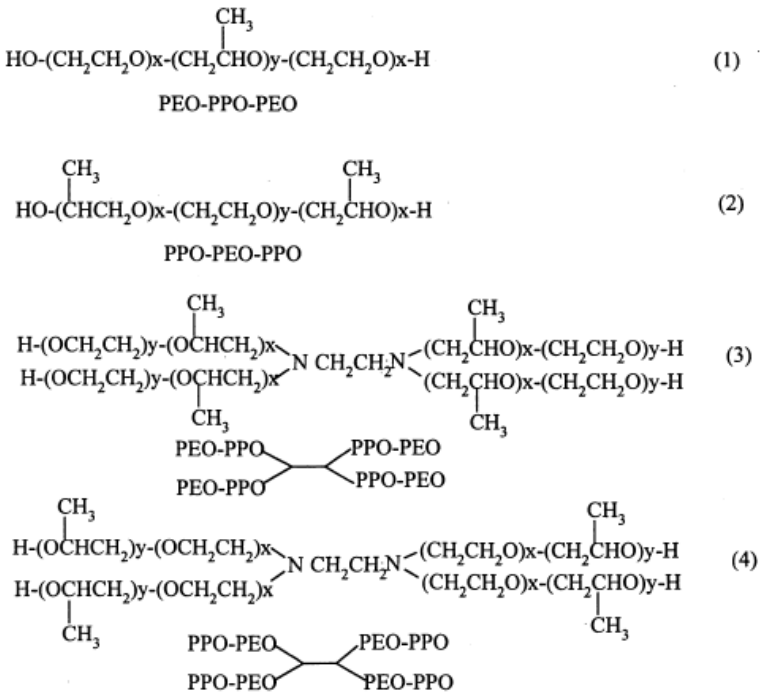

Figure 12: *Commercial name of PEO-PPO block copolymers: 1) Pluronic ®; 2) Pluronic ®R; 3) Tetronic ®; 4) Tetronic ®R [40].*

Among PEO-PPO block copolymers, Pluronics®, also known as Poloxamers®, are the most common and studied amphiphilic copolymers in biomedical field. Pluronics® are triblock copolymers (PEO-PPO-PEO) which can show different ratios of hydrophilic/hydrophobic segments and different resultant molecular weights. As previously mentioned, these commercial polymers are widely used to obtain thermo-reversible hydrogels by exploiting their micellar chain organization during gelation [40]. In fact, Pluronics gelation mechanism is based on chain arrangement into micelles and micelle nucleation, which depend on both polymer content and temperature (**Figure 13**). Below the critical micellization concentration (CMC), only unimers are present within the samples. Upon an increase in polymer concentration at a value higher than CMC, the chains start to aggregate into micelles with a hydrophobic core and a hydrophilic shell (**Figure 13a**). Once micelles are formed, further temperature changes let micelles to aggregate (as shown in **Figure 13c**) macroscopically resulting in a sol-to-gel transition.

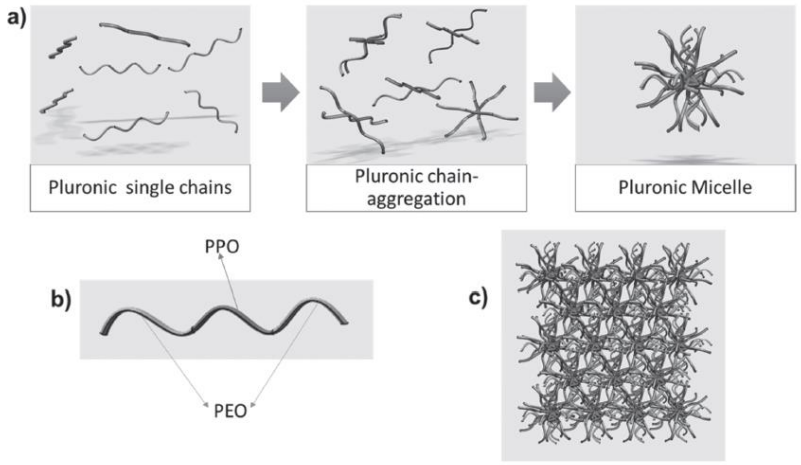

***Figure 13**: a) Pluronic micelles formation during gelation, b) Pluronic single chain, c) Pluronic micelles aggregation [40].*

The most commonly used PEO-PPO-PEO triblock copolymer for biomedical applications, is Pluronic® F127 (also known as Poloxamer® 407). It has been largely investigated in the biomedical field because of its low toxicity, which makes it well tolerated by the human body, and its sol-gel transition at about room temperature for 30%w/V concentrated solutions [41], thus making it a suitable system to design injectable hydrogels. Indeed, at room temperature (<25°C) it behaves as a liquid solution, while it turns into a gel at body temperature (37°C) [42][43].

Potential drawbacks of Poloxamer-based hydrogels are associated with their poor mechanical properties and stability in aqueous environment. In order to overcome these issues two different approaches have been proposed in the literature. The first one is based on Poloxamer chain extension through a diisocyanate used as a linker between this macrodiol and a shorter diol or diamine, leading to the synthesis of a poly(ether urethane) with high molecular weight, while the other one involves the copolymerization of poly(ethylene glycol) and poly(propylene glycol) chains, using phosgene as bridge. In this way, Cohn et al. reported a 15 times higher viscosity and better stability of the new synthesised copolymer with respect to Poloxamer 407 as such [44]. The first approach has been exploited by Boffito et al. to develop novel thermo-responsive hydrogels based on a poly(ether urethane) (NHP407) synthesized by chain extending Poloxamer 407 with an aliphatic diisocyanate and an amino acid-based diol. NHP407-based hydrogels overcame many drawbacks associated to Poloxamer-based gels, and turned out to be suitable for drug delivery application or bioprinting of scaffolds [45].

- Poly (ethylene oxide)/poly (D, L-lactic acid-co-glycolic acid) block copolymers

Poly (ethylene oxide) (PEO) has been widely investigated to design hydrogels because of its hydrophilicity and biocompatibility. PEO has been also used to synthesise triblock copolymers with the hydrophobic poly (D, L-lactic acid-co-glycolic acid) (PLGA). Therefore, due to the presence of both hydrophobic and hydrophilic segments, this copolymer shows high thermo-responsiveness similarly to PEO-PPO-PEO copolymers.

PEO-PLGA-PEO polymers (**Figure 14**) exhibit a sol-to-gel transition in aqueous medium at optimized concentrations via a micellar aggregation mechanism due to the self-assembling nature of the amphiphilic chains. The gels formed by this copolymer exhibit good mechanical stability, mostly due to the presence of the hydrophobic lactic acid moieties, and the gel residence time in aqueous enviroment is up to one month. This property can be related to the micellar aggregation mechanism: with increasing temperature, PEO units increase their interactions with PLGA core, leading to the formation of new interconnections between the two phases constituting the micelles. The gels thus form as a consequence of micelle connections, created by PEO chains interpenetration [46].

The balance between hydrophobic PLGA and hydrophilic PEO units influences the thermo-responsive behaviour of the hydrogel: the more hydrophilic is the polymer, the higher are the temperature and the polymer concentration needed to achieve a sol-gel transition at 37 °C [47]. In particular, sol-gel transition temperature can vary between 21 and 40 °C, based on polymer concentration.

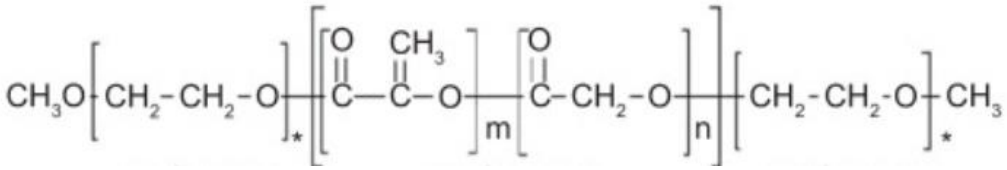

***Figure 14**: Structure of PEO-PLGA-PEO triblock copolymer [47].*

Alternatively, PLGA-PEO-PLGA copolymers (**Figure 15**), commercially known as Regel®, has been developed, aiming at offering good performances when exploited as thermo-sensitive drug delivery systems. Moreover, they are easier and faster to synthesize rather than the previous ones.

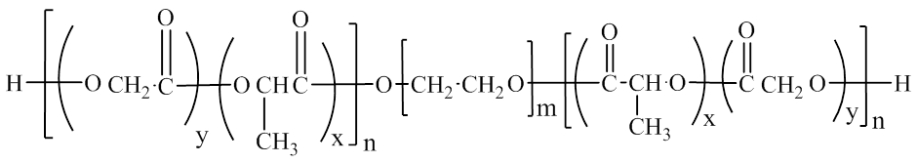

***Figure 15:** Structure of PLGA-PEO-PLGA triblock copolymer [47].*

Because of the presence of both hydrophilic and hydrophobic segments, the gelation of these systems results from both micelle formation and packing and hydrophobic interactions as shown in **Figure 16**. As previously explained, micelles originate by looping hydrophilic and hydrophobic chains and then they are connected together and interact more and more as a consequence of temperature increase.

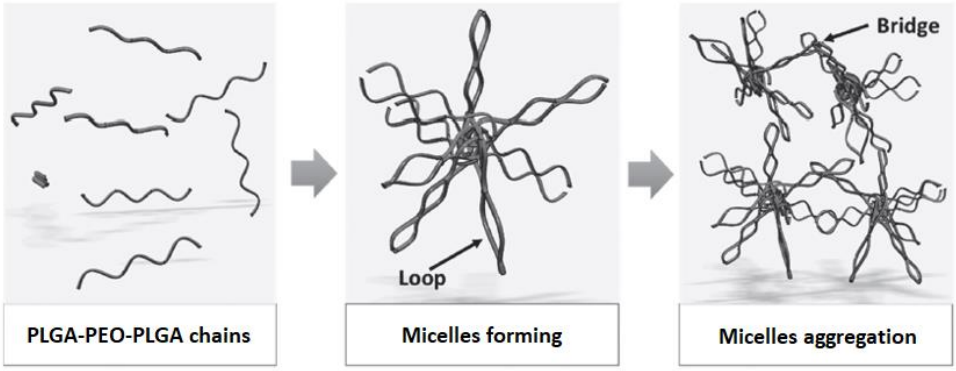

Figure 16: PLGA-PEO-PLGA micelles gelation mechanism [47].

1.4 Photo-curable hydrogels

As previously described, thermo-sensitive hydrogels are characterized by low stability in a watery environment as a consequence of the weak interactions occurring between the constituent polymeric chains. Conversely, chemical hydrogels are characterized by the presence of covalent bonds, resulting in a higher residence time in aqueous media and improved mechanical properties. Among chemical hydrogels, photo-curable gels are widely exploited due to the possibility to precisely control the crosslinking reactions through UV/Vis light photo-irradiation. Many works have been reported in literature on the improvement of thermosensitive hydrogel mechanical properties through the addition of a photo-sensitive component. Specifically, two strategies can be followed to achieve this purpose: (i) the blending of a thermo-sensitive component (physical crosslink) with a photo-responsive one (chemical crosslink) to overcome the lack of mechanical properties and the poor stability while keeping the advantages of physical gels [48] or (ii) the design of polymers simultaneously responsive to temperature and photo-irradiation [49] and thus, able to undergo a physical sol-to-gel transition followed by a chemical crosslinking.

Photo-curable hydrogels can be polymerized *in vivo* or *in vitro* using visible or UV light. The use of UV light brings with it several advantages mainly related to the transport of a higher amount of energy, and thus the capability to form a higher number of covalent bonds upon shorter irradiation

time. For this reason, UV-irradiated crosslinking has been more investigated and studied till now. However, UV light may be not ideal for biomedical applications because cells can be damaged by this high energy. Conversely, visible light (λ = 400-700 nm) is a more cell-friendly source to initiate hydrogel photo-crosslinking reaction [50][51].

Based on the exposed photo-sensitive moieties along polymer chains, covalent-crosslinked hydrogels can be obtained with three different photo-polymerization mechanisms, including chain-growth, step-growth and a combination of the above two methods (**Figure 17**) In the first photo-polymerization mechanism (i.e., chain-growth), light sources interact with photo-sensitive molecules, called photo-initiators, to form free radicals which can propagate across specific vinyl moieties on macromers resulting in “chain growth” polymer networks (homo-polymerization process) [52]. In the second one (i.e., step-growth mechanism) multifunctional macromers exposing mutually photoreactive groups are crosslinked under light irradiation, with or without a photo-initiator. For example, Greene et al. designed a novel gelatin-poly-(ethylene glycol) (PEG) hybrid hydrogel exploiting step-growth photo-polymerization. They functionalized gelatin and PEG with norbornene molecules and thiol-groups, respectively, allowing the resulting polymers to crosslink under light exposure through thiol-ene reaction [50]. These “step growth” photo-polymerized networks are not as spatial-temporally controlled as the “chain-growth” ones, although they have the benefit of forming more homogeneous crosslinks with a better control over crosslinking density and, as a consequence, over material properties [53]. The mixed-mode mechanism, which combines the benefits of both chain and step growth photo-polymerizations, has been developed to obtain highly uniform hydrogel networks with better controlled mechanical properties as reported by E. Rydholm et al. [53]. However, the presence of specific vinyl groups (i.e. thiol and acrylate groups) on the starting monomers should be considered to proceed with this kind of photo-polymerization. Specifically, this mixed mode mechanism involves three reactions, the first two correspond to the conventional step growth thiol-ene photo-polymerization, where propagation and chain transmission happen consecutively, while the third is an additional propagation step that can occur in thiol-acrylate polymerizations as a consequence of acrylate reactivity towards carbon-based radicals. This third reaction ends up in acrylate homo-polymerization, which is a mechanism analogous to chain-growth polymerization of acrylates.

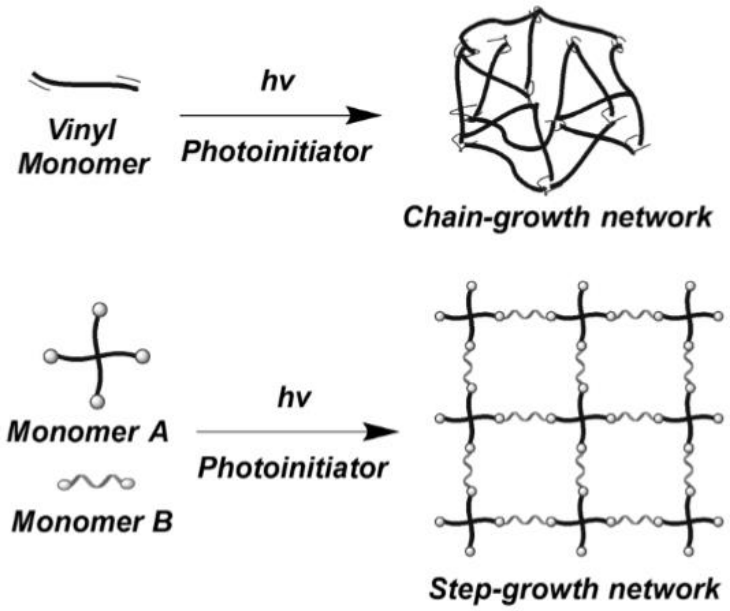

Figure 17 *Schematic representation of hydrogels formed by: (top) chain-growth photo-polymerization using linear homo-bifunctional macromer to produce heterogenous network; (bottom) step-growth photopolymerization of multifunctional monomers in which idealized network structure is produce using a stoichiometric molar ratio of the two functional groups [52].*

1.4.1 Photo-curable hydrogels: Photo-initiators

Photo-polymerization starts when photo-initiators are exposed to a light source, namely UV or visible light. Two kinds of photo-initiators can be distinguished. Type I or cleavage-type photo-initiators absorb photons and decompose into two primary radicals to start hydrogel polymerization, while Type II photo-initiators subtract a hydrogen from a co-initiator to form secondary radicals and start the cross-linking reaction.

Adequate solubility of a photo-initiator in an aqueous solution and sufficiently high molar absorptivity at cytocompatible wavelengths are major factors concerning the suitability of a photo-initiator for the preparation of biocompatible hydrogels. Only a few photo-initiators fulfil these requirements, such as type I initiators Irgacure-2959 (I-2959) and lithium arylphosphanate (LAP), as well as type II initiator eosin-Y, Rose Bengal, Riboflavin. However, the commercially available I-2959 is characterized by a poor solubility in water (< 0.5% w/w) and low molar absorptivity at wavelengths considered cyto-compatible ($\varepsilon < 10\ M^{-1}cm^{-1}$ at 365 nm). In addition, I-2959 cannot be adopted in Vis-light initiated photo-crosslinking because of its molar absorptivity that it is close to zero at wavelengths higher than 400 nm. Among Type I photo-initiators, LAP is characterized by high water solubility (> 5% w/w) and absorbance at 365 nm ($\varepsilon \sim 200\ M^{-1}cm^{-1}$), while its capacity to be excited by Vis light is restricted ($\varepsilon \sim 30\ M^{-1}cm^{-1}$ at 405 nm) [54]. Differently, type II photo-initiators, such as

eosin-Y, are soluble in water and can be easily excited by Vis light (ε > 100000 $M^{-1}cm^{-1}$ at 515 nm).For instance, Eosin-Y has been used to initiate the gelation by chain-growth polymerization of poly(ethylene glycol) diacrylate (PEGDA) hydrogels. However, a co-initiator (e.g., triethanolamine, TEOA) and a co-monomer (e.g., 1-vinyl-2pyrrolidinone, NVP) are generally required to generate enough radicals and succeed in obtaining a high and fast functional group conversion, respectively. The selection of the different components required to achieve photo-polymerization can be so difficult, and this is perhaps why UV-mediated photopolymerization is still a preferred method to prepare hydrogels, despite the associated biosafety risks [55].

1.4.2 Photo-curable hydrogels: Emerging materials

As already pointed out in previous paragraphs, multifunctional macromers can be subjected to chain or step growth photo-polymerization depending on the specific photo-responsive groups exposed along the polymer backbone.

- ***Chain-growth networks***

In general, any hydrophilic macromer with terminal or internal vinyl groups can be crosslinked into a hydrogel via chain-growth polymerization, as long as the vinyl groups are capable of undergoing homo-polymerization.

Polyethylene glycol (PEG) acrylate derivatives, PEG methacrylate derivatives (**Figure 18A**), polyvinyl alcohol (PVA) derivatives (**Figure 18B**), and modified polysaccharides (e.g., hyaluronic acid derivatives (**Figure 18C**) and dextran methacrylate (**Figure 18D**)) are among the most commonly used macromers to prepare chain-growth hydrogels [52].

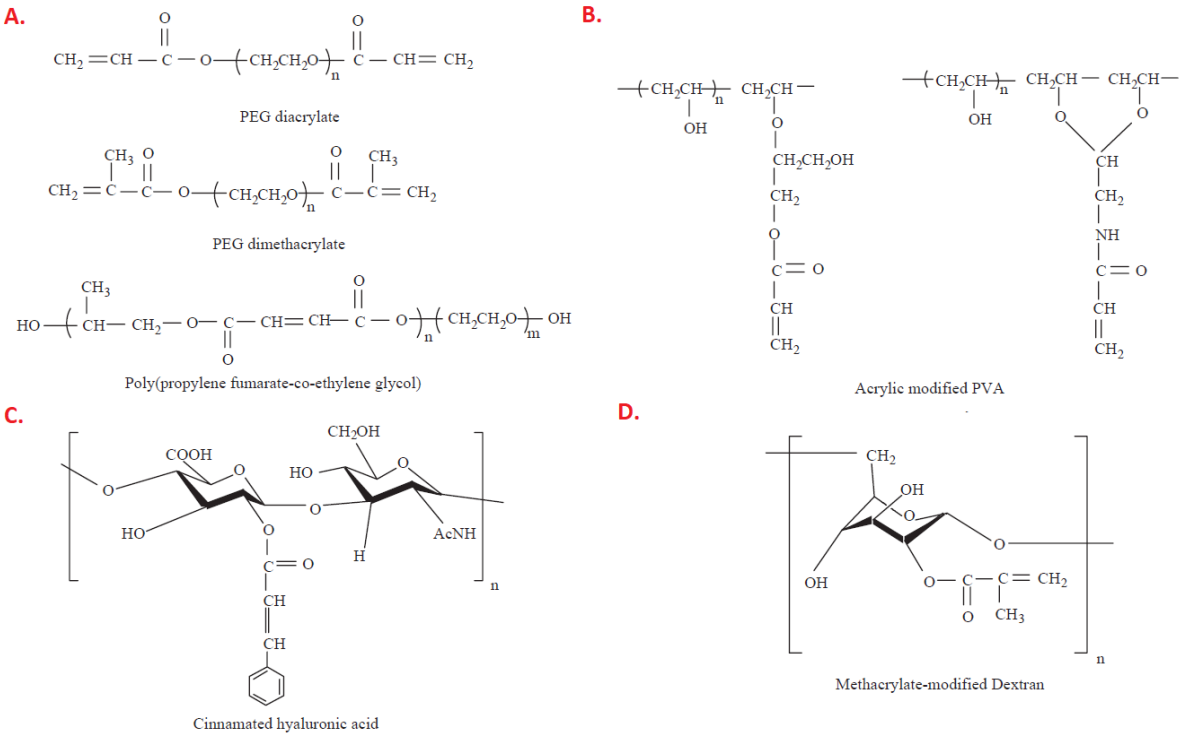

Figure 18 *Chemical structures of photopolymerizable biomaterials suitable for creating crosslinked hydrogel networks: (A) PEG diacrylate, methacrylate, and propylene fumarate derivatives, (B) Crosslinkable PVA derivatives, (C) Hyaluronic acid derivatives, (D) Dextran-methacrylate. [52]*

In this context, Sawhney et al. synthesized a bio-erodible hydrogel using macromers having a central block made of PEG, extended with oligomers of α-hydroxy acid and terminated with acrylate groups. The special feature of this hydrogel relies on the possibility to be photo-polymerized after or before its application in contact with tissues. In the first case the resulting gel adheres to the surrounding tissues, maybe by interpenetration, while in the second one the gel appears to be non-adhesive, because of the encapsulation of a huge amount of free water that is not involved in H-bonds with the ether bonds of PEG. Additionally, these gels can degrade upon hydrolysis due to the presence of oligomers of α-hydroxy acid. By a proper selection of the α-hydroxy acid moiety, gel degradation kinetics can be finely taylored, making them well-suited for drug release applications [56]. In another work, Kim an coworkers designed hydrogel nanoparticles through radical polymerization of glycidyl methacrylate dextran (GMD) and dimethacrylate poly(ethylene glycol) (DMP) in the presence of ammonium peroxydisulfate (APS) as initiator and UV-light irradiation. Different drug delivery studies were performed incorporating into the hydrogel network a hydrophobic drug, called clonazepam (CNZ), which release resulted to be dependent on pH variation and enzyme dextranase presence [57]. Martens et al. modified PVA macromers with pendent acrylate groups to make them photo-cross-linkable by chain growth photo-polymerization with the aim of studying the

correlation existing between photocuring protocol and the resulting properties of the hydrogel network [58].

Since homo-polymerization, which is typical of acrylate monomers, lead to heterogeneities in crosslink-density and thus weaker network structures, Cramer and Bowman showed the possibility to mix multifunctional thiols and acrylates to couple the acrylate chain growth polymerization with the thiol-acrylate crosslinking (step-growth mechanism) in order to form more uniform network[59].

- ***Step growth thiol-ene networks***

In addition to chain-growth photopolymerized networks, hydrogels can also be prepared via a radical mediated step-growth photopolymerization. As shown in **Figure 19**, light-activated photo-initiators cause hydrogen subtraction from a thiol moiety, forming thiyl radicals. These reactive species interact with the norbornene compound creating an orthogonal thiol-ether bond [50].

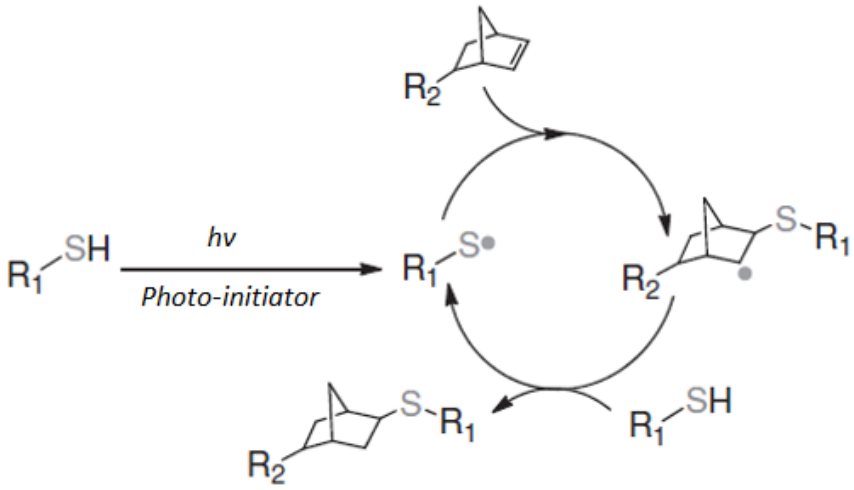

Figure 19 *Schematic representation of step-growth hydrogel system formed by light-mediated thiol-ene reaction. [50]*

This “click” process, based on thiol-ene crosslinking, offers several advantages not only related to process parameters, such as fast reaction and high conversion rates, but also linked to the resulting network in terms of hydrogel mechanical properties and biocompatibility [60].

Anseth et al. developed a new platform of PEG-based hydrogels synthesized by radical-mediated orthogonal thiol-ene photo-click reaction. UV light at 365 nm and intensity within the range 5 – 10 mW/cm^2 were applied to induced the formation of thiyl radicals from thiol-containing molecules

(bis-cysteine-containing oligopeptides). These thiyl radicals react with -ene moieties on norbornene-grafted multi-arm PEG to create orthogonal thiol-ether linkages and consequently a step-growth network. The thiol-ene hydrogels obtained from this thiol-ene photoclick chemistry can be degraded by hydrolysis of their ester bonds if PEG-ester-norbornene (PEGeNB) is used to form thiol-ene hydrogels (**Figure 20A**). Conversely, the gels remain hydrolytically stable when PEGamide-norbornene (PEGaNB) is used (**Figure 20B**).

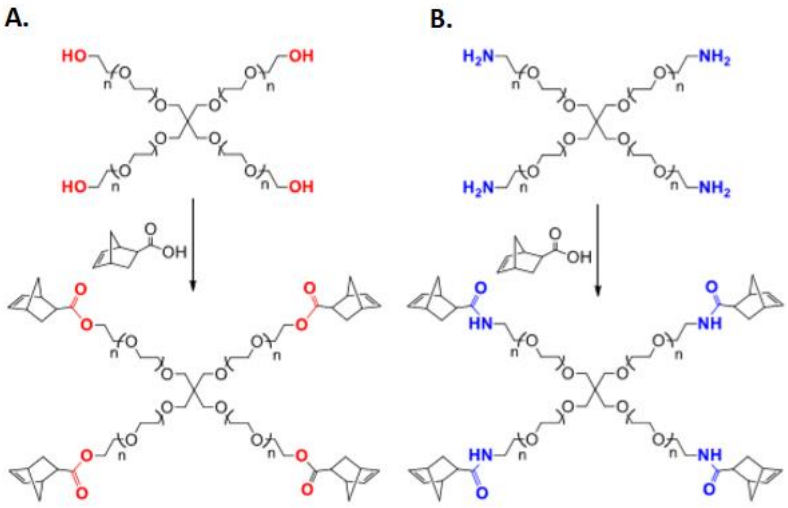

Figure 20 *(A) Synthesis route of PEG-tetra-ester-norbornene (PEG4eNB); (B) Synthesis route of PEG-tetra-amide-norbornene (PEG4aNB); [60]*

The majority of thiol-ene based hydrogels are prepared using PEG as macromer, functionalized with both thiol and norbornene, obtaining strong and elastic hydrogels suitable for many biomedical applications [61][62]. However, natural polymers have been also employed, in particular hyaluronan-based thiol-norbornene hydrogels and gelatin-based thiol-norbornene hydrogels, in order to create systems able to support cell adhesion, spreading and migration. [50]

Early works on thiol-ene gelation have focused on the exploitation of UV light and cleavage-type initiators. Recently, Lin et al. developed Vis-light mediated thiol-ene gelation using the type II photosensitizer eosin-Y as the sole photo-initiator. In this case, thiol-ene chemistry can be exploited to create stable and resistant step-growth hydrogels [54]. Radicals formation and thiol-norbornene coupling proceed in stoichiometric ratio until all the involved moieties, both thiol and norbornene, are processed. It is remarkable that only orthogonal crosslinks can be found in thiol-ene hydrogels. Indeed, differently from acrylate-based hydrogels, no homo-polymerization between norbornene molecules take place [48].

Although one of the major benefits of visible-light thiol-ene crosslinking is related to the possibility to avoid the use of toxic co-initiators and other catalysts, the addition of soluble tyrosine amino-acid has been investigated to evaluate cytocompatibility improvements for cell-encapsulation applications and enhancements in gelation efficiency [63].

2. Polyurethanes

Polyurethanes (PUs) are synthetic polymers containing the urethane bond (**Figure 20**) in their backbone as a consequence of the reaction occurring between the –OH and NCO functional groups.

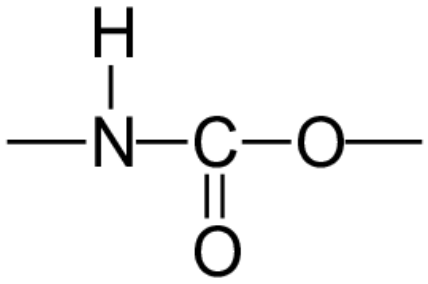

Figure 21: *Urethane functional group [63]*

Compared to other polymeric class of materials, polyurethanes are characterized by more complex structures. They are the result of the reaction between three building blocks: a diisocyanate, a macrodiol and a chain extender (i.e., low molecular weight diol or diamine). By selecting the proper starting reagents it is possible to ideally create an infinite number of materials with tuneable physical, chemical and mechanical characteristics. Because of their versatility, they have been used in many technological and industrial fields, such as in the biomedical one, where they stand out thanks to their excellent characteristics in terms of strength, elongation and hardness [64].

2.1 Synthesis of Polyurethanes

The characteristic ***urethane bond*** in polyurethanes is the result of the polyaddition reaction shown in **Figure 22**.

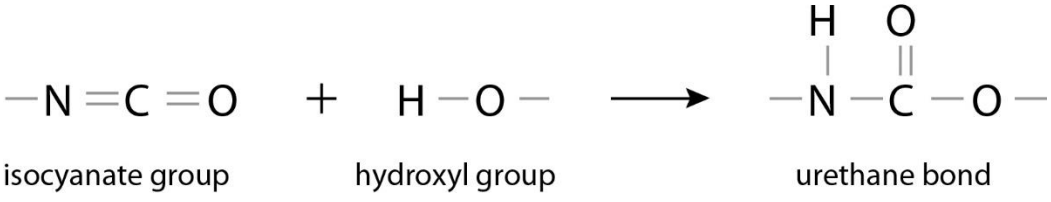

Figure 22: *Urethane linkage formation*

Specifically, a diisocyanate and a polyol with hydroxyl terminal groups are required to synthesize a polyurethane. Diisocyanates and diols are generally utilized to obtain linear chains, while

multifunctional polyols or polyisocyanates can be used to create side branching in the resulting polymer [65]. Additionally, another reagent, known as chain extender, is usually used to chain extend the prepolymer and thus, to obtain high molecular weight polyurethanes.

Generally, two different methods can be employed to synthesise polyurethanes: the one-step or the two-step procedure [64]. In the first method, all the reagents (i.e., macrodiol, diisocyanate and chain extender) are mixed simultaneously giving directly a high molecular weight polymer; in the latter method polyurethane synthesis is carried out in two different steps, as suggested by the name. Specifically, in the first step, a macrodiol reacts with a diisocyanate giving an isocyanate-terminated prepolymer with low molecular weight; then, in the second step, this prepolymer reacts with the chain extender, that can be either a diol or a diamine, leading to the formation of a high molecular weight polyurethane or a polyurethane urea, respectively.

The two-step procedure is generally preferred because it allows a better control over the reaction, resulting in greater features of the final product.

Figure 23 shows the most common two-step synthesis method for polyurethanes, also known as "prepolymer method".

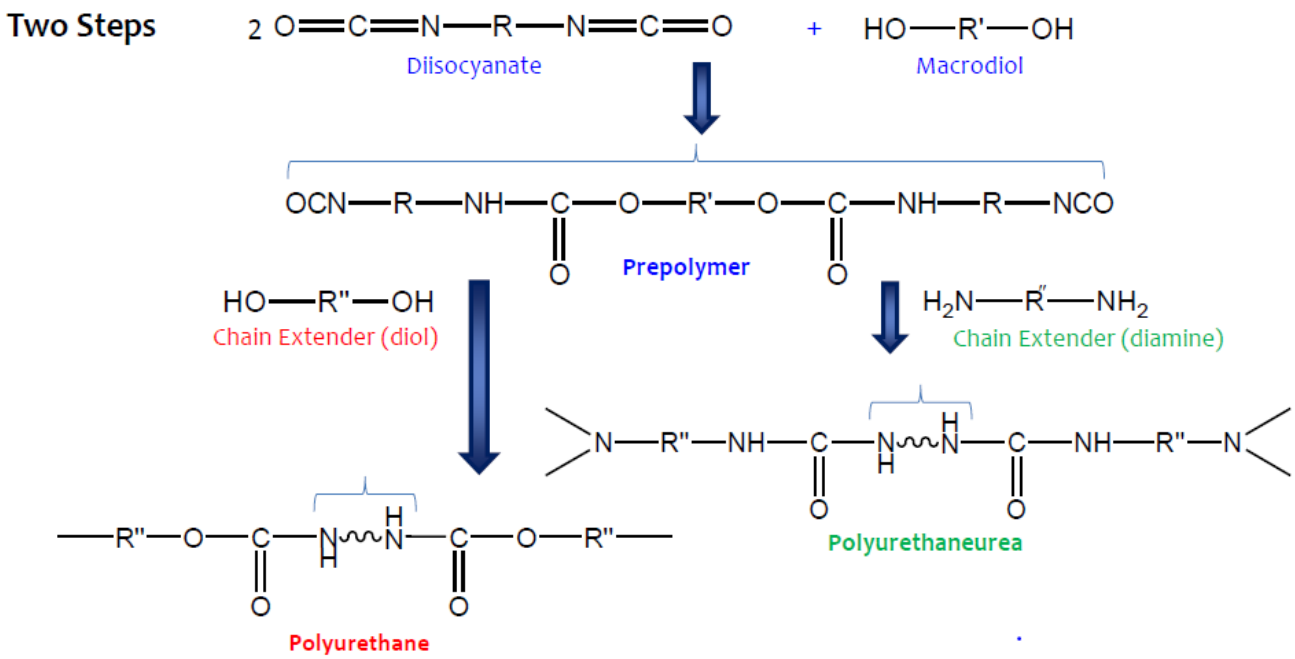

Figure 23 Two-step synthesis of polyurethanes. In the first step, an isocyanate-terminated prepolymer is obtained by reacting a macrodiol and a diisocyanate (1:2 molar ratio); the second step leads to a polyurethane or a polyurethane-urea through chain extension

In conclusion, the polyurethane synthesis process is characterized by the following features [65]:

- a large number of different reagents are available;
- the reaction is exothermic and can occur at room temperature;
- the reaction rate can be controlled by a wide range of catalysts;
- the selected stoichiometric ratio between reagents influences the molecular mass of the polymer and its structural properties;
- the composition can be selected to obtain products able to match different requirements, such as flexibility or stiffness.

2.1.1 Polyurethane synthesis reagents

- Isocyanate

The monomer isocyanate [OCN – R – NCO] may have two, three or more groups (-NCO) capable of reacting with hydroxyl groups. R-groups may be composed of aromatic or aliphatic segments. Many polyurethanes are synthesised starting from aromatic isocyanates which have a high reactivity towards hydroxyl compounds. In addition, in the presence of aromatic diisocyanate the final polyurethanes show higher mechanical properties with those containing aliphatic diisocyanates [65]. Among aromatic isocyanates, the most commonly used are methylene bis-phenyl isocyanate (MDI) and toluene diisocyanate (TDI). However, in the biomedical field, the most used is 4,4'-diphenylmethane diisocyanate (4,4'-MDI), which is aromatic and more reactive than an aliphatic isocyanate, thanks to the electronic configuration of the constituting benzene rings [64]. However, aromatic chains tend to be more sensitive to light and their degradation products are toxic and potentially cancerogeni, so their use has been limited for biomedical applications during the last years [65][66].

Concerning aliphatic isocyanates, the most commonly used are 1,6-hexamethylene diisocyanate (HDI), 1,4-butane diisocyanate (BDI) and 4,4'-di-cyclo-hexyl methane diisocyanate. PUs based on aliphatic diisocyanates usually show lower mechanical properties with respect to those containing aromatic diisocyanates. However, aliphatic diisocyanate-based poly(urethane)s are less sensitive to hydrolytic and thermal degradation [65]. **Figure 24** shows the most commonly used diisocyanates in the design of polyurethanes biomaterials.

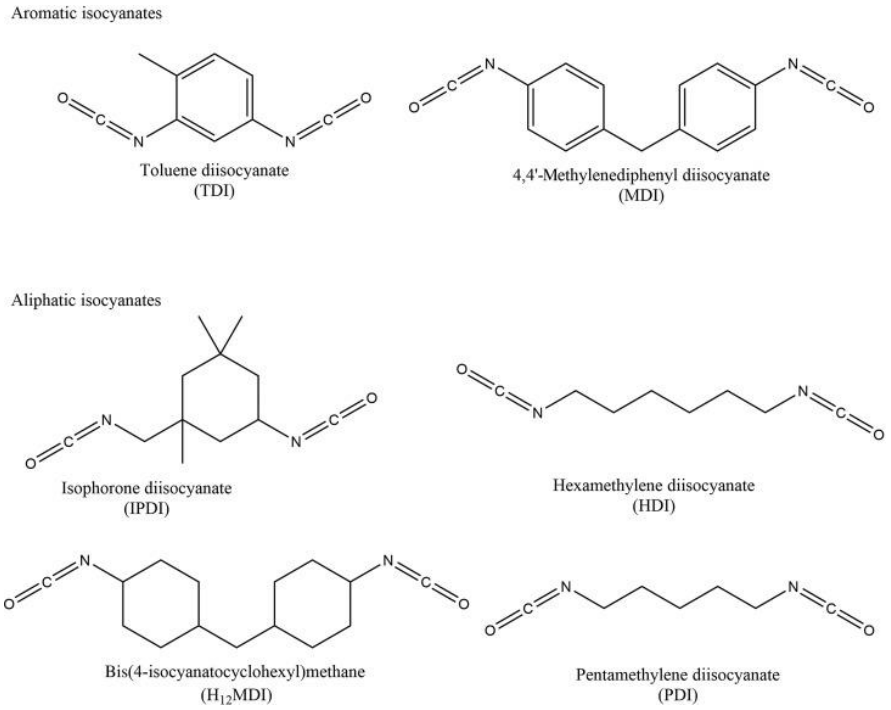

Figure 24: *Diisocyanates used as precursors for biomedical polyurethanes [65]*

- Macrodiols

The most commonly used macrodiols belong to two main families, i.e., polyesters (-R-COO-R'- repeating structure) and polyethers (-R-O-R'- repeating structure), which can influence the physico-chemical and mechanical characteristics of the obtained polyurethanes.

- *Polyesters* are used to synthesise polyurethanes both rigid and flexible, in compact or expanded form, with excellent chemical resistance, physical abrasion, bending resistance and good elastomeric properties. However, they can be degraded by hydrolysis.
- *Polyethers* are exploited to synthesise flexible polyurethanes. They are more resistant to hydrolysis than polyesters, but they can easily undergo oxidation.

The macrodiols can be also categorized depending on their molecular weight: high molecular weight macrodiols (ranging from 2000 to 1000 g/mol) are commonly used to synthesise flexible PUs, whereas more rigid materials can be obtained starting from low molecular weight polyols [64]. **Figure 25** shows macrodiols employed to synthesize poly(ether urethane)s or poly(ester urethane)s for biomedical applications.

Chemical Name	Code	Chemical Structure of the Repeating Unit
Poly(ethylene oxide)	PEO	(CH_2CH_2O)
Poly(pro pylene oxide)	PPO	(CH_2CHO) with CH_3
Poly(tetramethylene oxide)	PTMO	$(CH_2CH_2CH_2CH_2O)$
Poly(butylene adipate)	PBA	$(O(CH_2)_4OC(CH_2)_4C)$ with O, O
Polycaprolactone	PCL	$(CH_2CH_2CH_2CH_2CH_2CO)$ with O
Polydimethylsiloxane	PDMS	$(Si—O)$ with CH_3, CH_3
Polyisobutylene	PIB	$CH_2—C$ with CH_3, CH_3
Poly(ethylene butylene)	PEB	$(CH_2CH)(CH_2CH)$ with CH_2CH_3

***Figure 25**: Macrodiols used to synthesize polyurethanes for biomedical applications [64]*

-Chain Extender

The chain extender is a low molecular weight diol or diamine exploited to bind two prepolymers in order to obtain a high molecular weight polymer. Hence, they show amines or hydroxyl groups as end-functionalities able to react with the isocyanate groups of the prepolymer. 1,4-butanediol (BDO), 1,4-cyclohexanedimethanol, ethylene glycol, hydroquinone bis (2-hydroxyethyl) ether (HQEE) and 1,6-hexanediol are examples of chain extenders used to synthesise poly(urethane) biomaterials [64].

2.2 Structure of Polyurethanes

Polyurethanes generally exhibit a two-phase separation in which hard domains are dispersed into a soft matrix, as shown in **Figure 26**. Hard domains are constituted by diisocyanates and chain extenders, while soft segments are based on the macrodiols. For this particular molecular architecture, polyurethanes belong to the wide family of segmented block copolymers. Both the molecular structure of the synthesised polyurethanes and the properties of each constituent block, contribute to the unique features of these polymer respect to other materials [67].

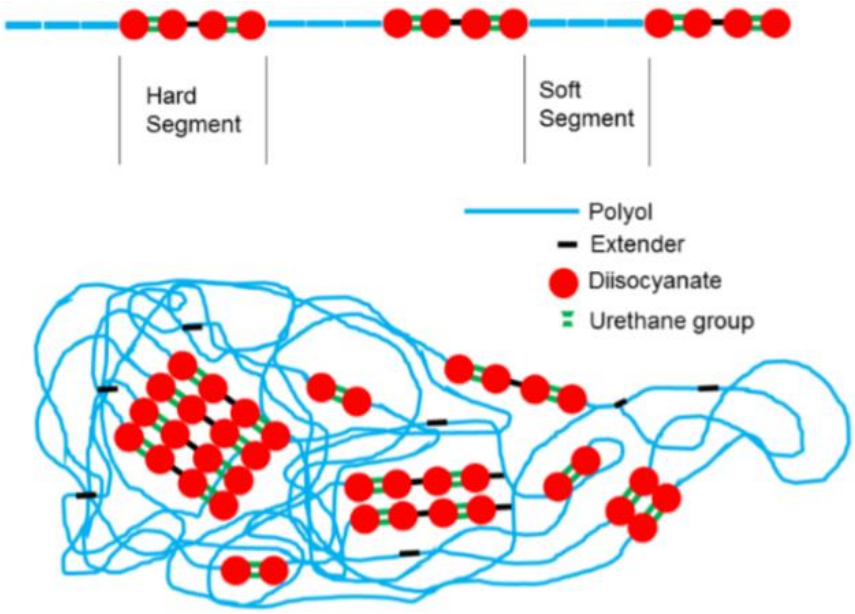

***Figure 26**: PU typical structure highlighting hard and soft domains (top) and their organization into chain aligned isocyanate/chain extender domains and non-aligned, long-chained polyol domains (bottom) [67].*

Soft segments derive from long-chained polyols which make the polymer elastic and resistant to low temperature, while hard ones, formed by the reaction between the chain extender and the diisocyanate, create hydrogen and dipole-dipole bonding involving urethane bonds, which are used as reinforcing fillers for the soft domains [68]. This structure gives polyurethanes excellent mechanical properties as well as biocompatibility [65].

2.3 Properties and biomedical applications of polyurethanes

Polyurethanes have been largely investigated in the biomedical field because of their well-known biocompatibility, chemical versatility and capability of coupling in a sole material elasticity toughness and durability. These mechanical and physical properties, which appear to be comparable to biological tissues, make polyurethanes suitable materials for cardiovascular devices (e.g., vascular prostheses, cardiac valves, stents, pacemakers), breast implants and dialysis membranes [68]. However, all the polyurethanes used for long-term devices are not biodegradable, so they cannot be used as materials for tissue regeneration because of their inability to be replaced with newly formed tissue. In this context, new resorbable and biodegradable polyurethanes have been

developed by the introduction of specific labile units, in most cases degradable by hydrolysis, used as soft segments or as chain extenders. Hence, beside traditional applications, the introduction of biodegradable polyurethanes in literature and into the market has opened the way to the possibility to wide the potential applications of the materials, including temporary scaffolds and carriers for localized drug/biomolecule release.

Poly(ε-caprolactone) (PCL) has been widely investigated as building block constituting the soft domains of degradable polyurethanes due to the low toxicity of its degradation products, which allowed it to get FDA-approval, and to the good mechanical properties, in terms of elasticity, tensile and yield strength [68].

Poly(ethylene glycol) (PEG) is another polyol suitable as component of degradable PU soft domains. It has always been used in biomedical applications for tissue engineering, drug delivery and surface functionalization. Indeed, thanks to its anti-fouling effect, which is related to its hydrophilicity, PEG has been incorporated into polyurethane structure in order to obtain materials, able to exert an anti-fouling activity against proteins and cells and, at the same time, to provide functionalization with biomolecules to promote the adhesion of specific cell types [68]. For instance, Silver et al. synthesized different polyurethanes containing poly(ethylene oxide) as macrodiol to study the influence of the molecular weight of the macrodiol on the physical properties and hemocompatibility of the resulting PUs. The material based on PEG with the lowest investigated molecular weight (i.e., PEG 600 Da) was found to be thrombogenic, while the others showed blood compatibility due to PEG hydrophilicity, which was able to avoid protein absorption and platelet adhesion [69].

Recent studies also reported the use of polyurethane hydrogels as ideal systems for the design of wound dressings due to the versatility of PU chemistry which allows the synthesis of polymers with optimal properties for the final application. For instance, Yoo et al. synthesized a waterborne polyurethane (WBPU) using PEG as component of soft domains to design a hydrogel-based wound dressing. Then, the wound healing capability was tested in rat models by covering the wound with this hydrogel. Results showed the formation of a new epithelium in about two weeks without adverse reactions, as shown in **Figure 27** [70].

***Figure 27**: Wound healing process using WBPU hydrogel-based dressings [70]*

Exploiting their chemical versatility, polyurethanes have been used in many other biomedical applications, such as for the design of *stimuli-responsive hydrogels*.

Zhou et al. designed biodegradable and pH-responsive PCL-based polyurethanes, suitable for drug delivery applications. Briefly, these novel polyurethanes were successfully synthesized using the pH-sensitive macro-glycol poly(ε-caprolactone)-hydrazone-poly-(ethylene glycol)-hydrazone-poly(ε-caprolactone) diol (PCL-Hyd-PEG-Hyd-PCL), lysine-based diisocyanate (LDI) and a new type of tripeptide chain extender. Their capability to undergo micellization in aqueous solutions and to be degraded in acidic environment (pH∼ 4-6) made these PUs suitable candidates as carriers for active intracellular drug release [71]. pH-responsiveness was also exploited to develop hydrogels for novel strategies of targeted drug delivery: anticancer drugs can be encapsulated in polyurethane pH-sensitive systems and then *in situ* delivered as a result of polymer pH-dependent degradation. In another work the same authors investigated the potential application of these systems for the release of antitumor drugs [72].

Concerning stimuli-responsive polyurethanes, injectable thermo-sensitive hydrogels have been widely explored for application in the biomedical field due to their rapid sol-gel transition *in situ*. For example, Boffito et al. developed an amphiphilic poly(ether urethane) starting from FDA-approved poly(ethylene oxide)/poly(propylene oxide)/poly(ethylene oxide) (PEO-PPO-PEO) triblock copolymer as macrodiol, 1,6-hexandiisocyanate (HDI) and N-Boc serinol as chain extender [45]. Hydrogels based on this material resulted to be biocompatible, injectable and able to undergo gelation at about body temperature. Additionally, the use of a chain extender containing Boc-protected amino groups opens the possibility to further functionalize the material with bioactive molecules upon Boc protecting group removal. The possibility to tune their properties, based on polyurethane building blocks, makes thermosensitive polyurethane-based hydrogels suitable systems for cell delivery/encapsulation and to design bio-printed scaffolds for tissue engineering.

Liu et al. provided poly(urethane) hydrogels with antibacterial properties in addition to thermo-responsiveness. To this aim, they grafted temperature sensitive poly(N-isopropylacrylamide/polyurethane (PNIPAAm/PU) hydrogel to cellulose unwoven fabrics, and then they functionalized this system with chitosan, exploiting carbodiimide chemistry, as shown in **Figure 28**. After functionalization with chitosan, the developed structs showed antibacterial activity towards S. aureus. and E. coli (efficiency approx. 80%) [73].

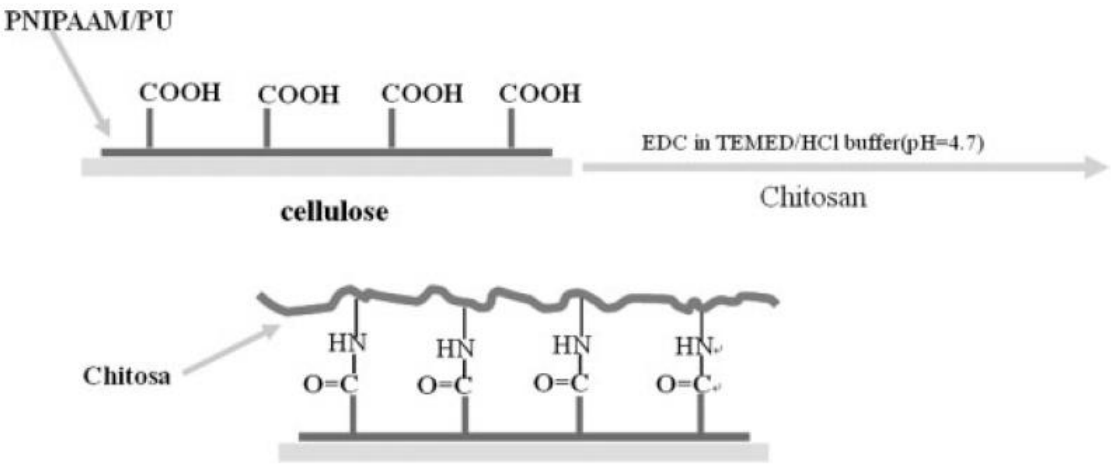

Figure 28 *Schematic picture of surface modification with chitosan [73]*

3. RAPID PROTOTYPING TECHNIQUES

As an alternative to conventional scaffold fabrication methods (e.g., electrospinning, phase separation, solvent casting), *rapid prototyping techniques (RP) are gaining increasing interest in the biomedical field* due to the possibility to more precisely control the scaffold geometrical structure, especially in terms of pore dimension and distribution [74].

RP technologies create three dimensional (3D) scaffolds with a computer-controlled layer by layer process: models, derived from patient-defect images, are generated using Computer Aided Design (CAD) softwares; the model is then processed by a software, which slices the 3D-model into 2D-layers, printable sequentially one over the other [75]. **Figure 29** shows the main steps of rapid prototyping techniques.

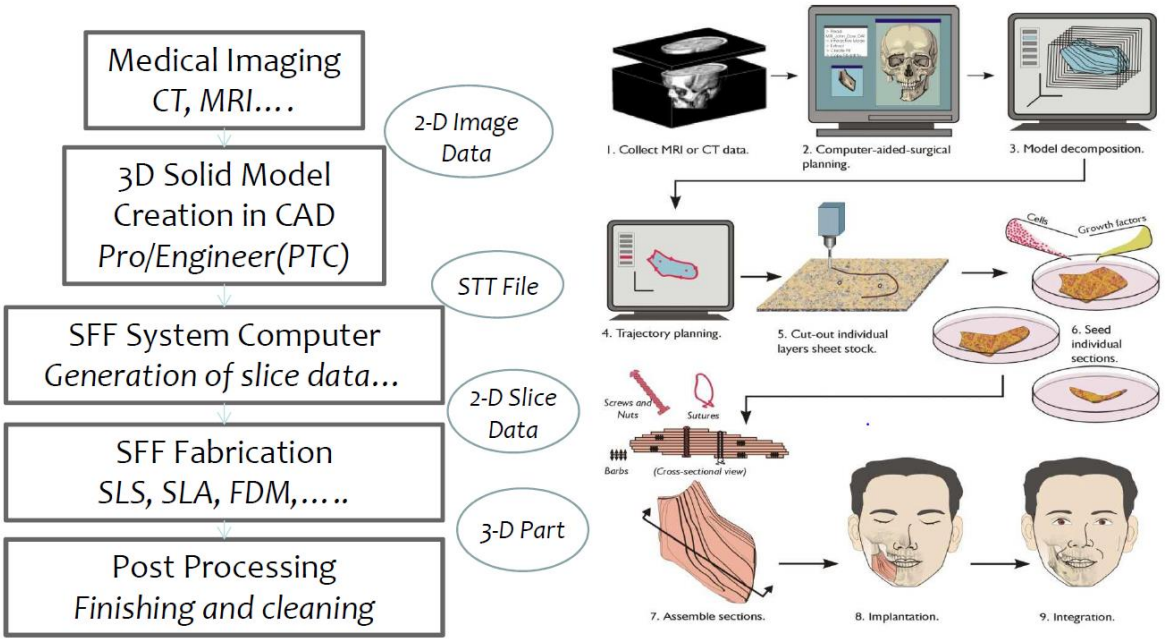

Figure 29 *Schematic representation of RP techniques steps.*

RP techniques involve many systems that can be classified in three different categories based on the working principle (**Figure 30**):

- Laser - based systems
- Nozzle - based systems
- Printer-based systems

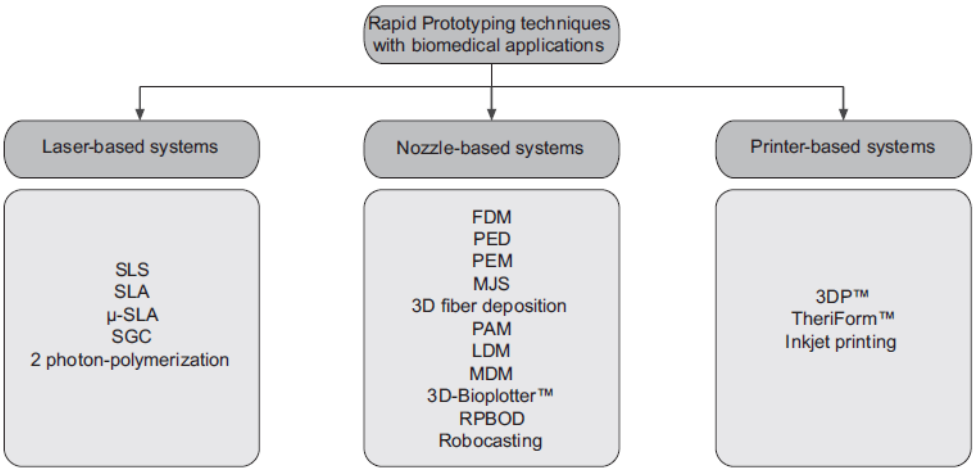

Figure 30: *RP techniques classified into laser-, nozzle- and printer-based systems [73]*

Technologies belonging to the first class use a laser source to photo-polymerize powder-material, thus fabricating crosslinked-polymeric structures suitable for biomedical applications. On the other hand, nozzle-based systems involve a large variety of different extrusion methods; among them the most commonly used are based on the extrusion of melted material (e.g., Fuse Deposition Modelling (FDM) technique). However, the latter technology has the big limitation of not being suitable for cell applications; for this reason, systems based on dissolution instead of melting, such as Low-Temperature Deposition Modelling (LDM) and Pressure Assisted Micro-syringe (PAM), have been widely investigated. Finally, printer-based systems can be continuous or drop-on-demand. In the first case the ink is extruded continuously under pressure, while in the second one single ink droplets are ejected under electrical signal control.[76]

Figure 31 shows a schematic representation of the three different categories of RP systems:

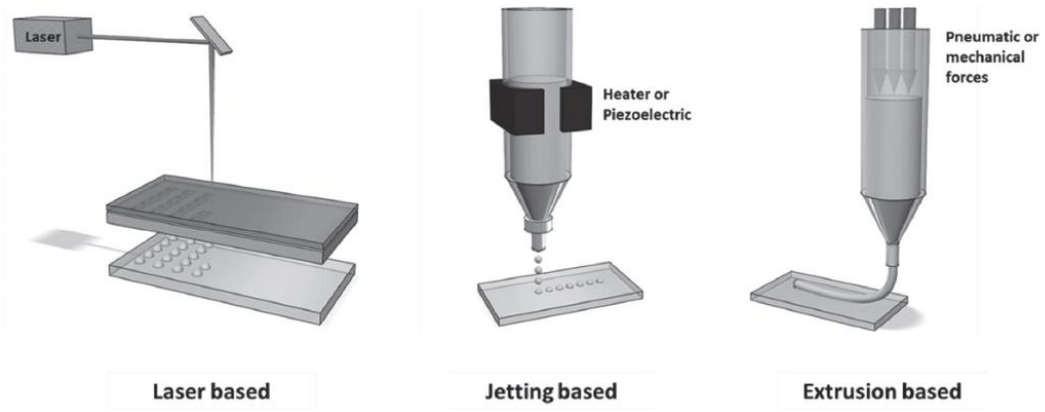

Figure 31: *Sketch of three different RP technology systems [75]*

3.1 RP techniques used for biomedical applications: 3D-bioprinting

Originally used only to create three-dimensional models and prototypes, 3D printing is widening its horizons, finding application in many different fields, including the biomedical one. It is emerging as a powerful tool to realize structures with custom-designed geometries, mainly applied as substitutes of damaged tissues in biomedical and tissue engineering (TE) applications. A large variety of materials can be used for 3D printing. In the case of biological materials this technique is also known as ***3D bio-printing***. In this context, *hydrogels* are attracting interest as promising systems, mainly because of their high and well-known biocompatibility and the possibility to tune their viscosity as a consequence of external stimuli changes.

The three main components of 3D bioprinting are (**Figure 32**):

- Living cells which have to populate the resulting printed structures;
- Bioinks made of hydrogels eventually enriched with growth factors to promote cell adhesion and vitality;
- The bioprinter and the software used to generate the CAD-file in order to create the tissue construct.

These three elements are strictly related: cells are supported by the bioink during the printing process, reason why it must be biocompatible and able to ensure cells growth after the deposition. Additionally, the bioprinter has to ensure a proper cellular viability and density in order to promote the right tissue formation. In conclusion, bioinks should provide high printability and ensure good resolution for the final printed structures [75].

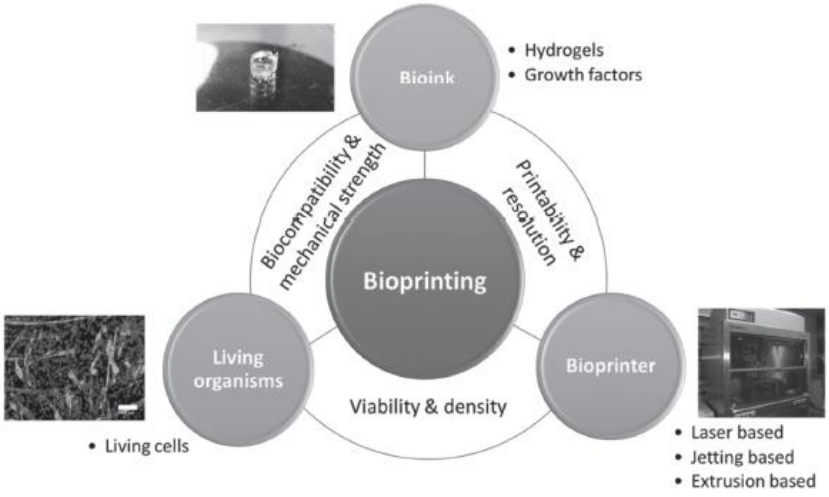

***Figure 32**: Three main components of 3D-bioprinting and their relationship [74]*

3.1.1 Bioink requirements for extrusion bioprinting

Although bioprinting offers a great potential in TE applications, the main challenge is to evaluate the key parameters of 3D printing process, in terms of extrusion rate, printing speed, and resolution and, at the same time, the suitability of the printable hydrogel-based bioinks to optimize the reproduction of artificial tissue constructs, as summarized in **Figure 33** [77].

The ideal hydrogel-based inks must possess several key properties:

- suitable consistency and viscosity to allow the ink to be extruded through the needle with no clogging phenomena;
- suitable consistency and viscosity to keep their shape upon printing;
- good mechanical properties in term of stiffness, to ensure self-support of the printed filaments, in order to realize fabrication of constructs with high shape fidelity, avoiding self-gravity problems.

In addition, as previously mentioned, also printing parameters are crucial to obtain an ideal 3D scaffold, with uniform filaments and a regular structure. Printing pressure and speed, feeding rate, and the needle-printing bed distance should be optimized. Hence, the combination of ink properties and processing parameters affect both printing resolution and cell viability.

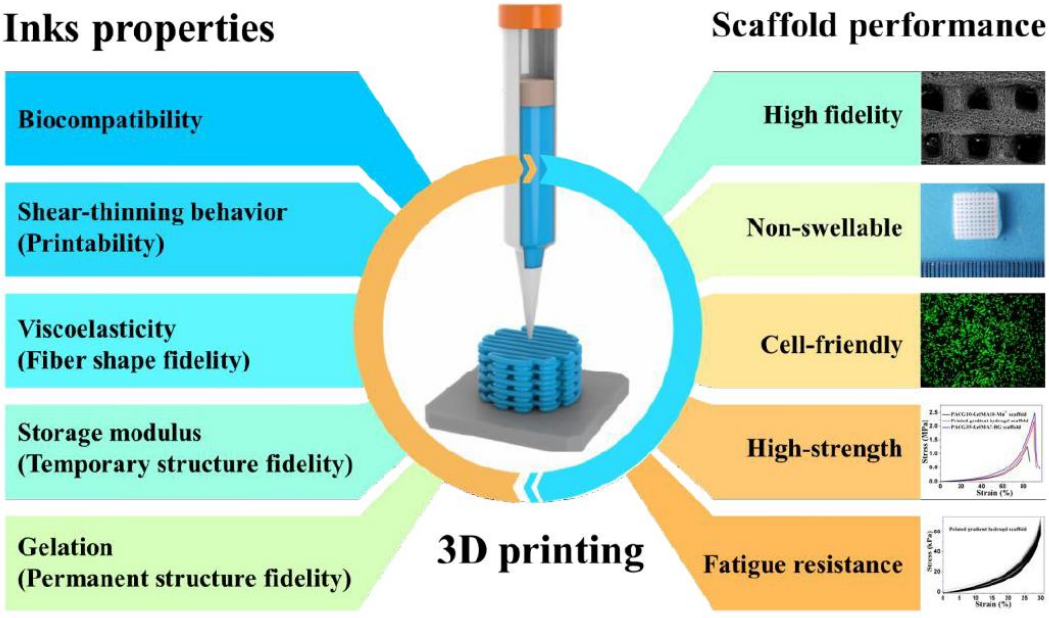

Figure 33 *Requirements a hydrogel should comply with to be used as bioink for 3D printing [76.]*

3.1.2 Hydrogel gelation mechanism in 3D-printing

Crosslinking of the printed material is necessary for the constructs to retain their shapes. As explained in previous paragraphs, hydrogels could be physically or chemically crosslinked upon application of external stimuli, such as light, temperature, or ion concentration [78].

Physical crosslinking mechanisms rely on non-covalent interactions, such as ionic interactions, hydrogen bonds, hydrophobic interactions, and thermal response. Physically crosslinked hydrogels are not stable since the reactions are reversible and can change their state in response to changes in pH, temperature, and ion concentration. However, physically crosslinked hydrogels are the dominant biomaterials used for bio-extrusion. One of the reasons is related to the absence of extra chemical agents, which could bring toxic issues. For instance, He et al. designed a new bioink based on sodium alginate (SA) and gelatin, blended at a proper weight ratio to exploit gelatin thermosensitivity in the printing process and the possibility of SA to be ionically crosslinked (using a calcium chloride enrich medium) after the deposition (**Figure 34**) [79].

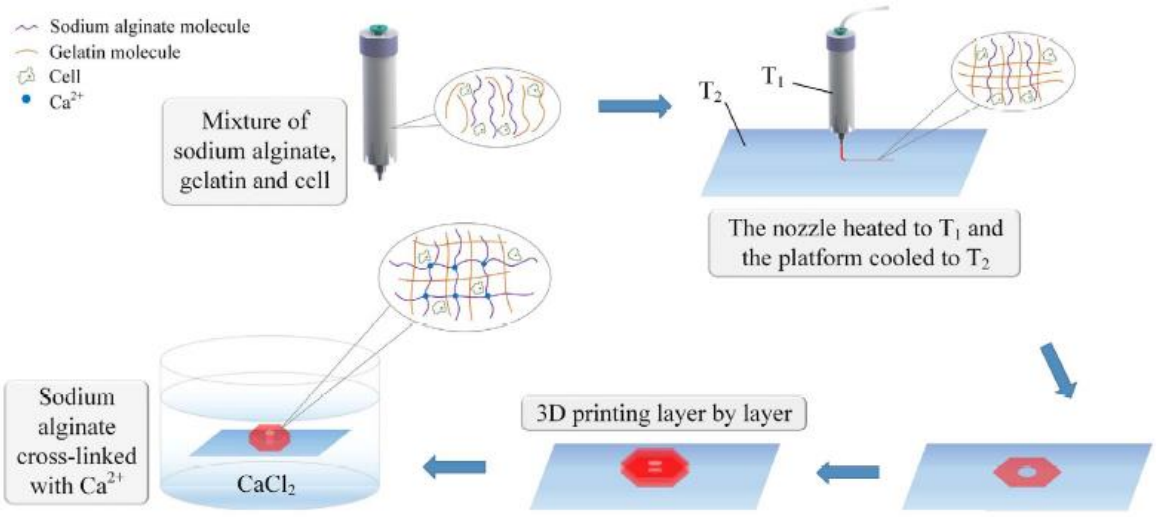

Figure 34 *Schematic representation of the printing process: layer-by-layer deposition of the ink followed by structure immersion in a calcium chloride solution allowing ionic crosslinking. [79]*

In recent years, the electrostatics interactions between opposite charged particles in hydrogels have been exploited too. Rapid gelation occurs upon mixing but the resulting structure liquefies over a certain shear stress, at which the interactions between oppositely charged particles are broken [78].

Chemical crosslinking mechanisms depend on the formation of covalent bonds. The resultant chemically crosslinked hydrogels are stable for a longer period compared to physically crosslinked

hydrogels. Moreover, the mechanical strength of chemically crosslinked hydrogels can be finely tailored working on the crosslinking density. The most commonly used method cross-link 3D printed structures is photopolymerization. However, cell viability could decrease upon exposure to UV light and free radicals. In addition, the pre-gel solution could clog the nozzle during printing if it is exposed to light.

Considering the advantages and disadvantages of physically and chemically crosslinked methods, attention should be focused on *hydrogels* that can interact through weak physical interactions and then further crosslinked through chemical interactions [80]. The purpose of the first physical crosslink process is to tune the viscoelastic properties and primary shape retention. Then, chemical interactions help post-processing fixation and stabilization of printed constructs.

3.1.3 Thermosensitive and photocurable hydrogels for 3D printing

As stated above, it is a great challenge to develop hydrogels as bioink for 3D printing process, mainly because, if properly treated, they can couple the main advantages of both chemical and physical gelation mechanisms.

The simplest possibility is to use *thermosensitive hydrogels* because they possess an excellent control over their properties by changing their chemical composition. Additionally, they can be printed in a semi-gel state and undergo a complete sol-to-gel transition after bioink extrusion [81]. However, thermo-sensitivity does not provide a long-term stability. Indeed, printing the hydrogel solution on a temperature-controlled plate makes it possible to create a solid network but then, a further step is required to eliminate the structure temperature dependence at the end of the process. In this regard, a good strategy is represented by *photocurable hydrogels,* which can be blended with the thermosensitive component.

For example, recent studies have reported bioinks based on a blend of methacrylated hyaluronic acid (HA-MA) with GelMA, which were first extruded exploiting gelatin thermo-sensitivity and then crosslinked under UV-light exposure to obtain a structure suitable for hepatic regeneration [82]. Among synthetic polymers, PEG is one of the most commonly used materials for the preparation of bioinks due to its hydrophilicity and the possibility to be easily modified with photosensitive moieties. One example refers to the production of an aortic valve formed by PEGDA and alginate as a result of extrusion and then photo-polymerization procedure. This device is essential to restore

the efficiency of the valve biomechanical functions [83]. In another work Muller et al. described the nano-structuring approach to improve the biocompatibility of Pluronic gels at concentrations suitable for 3D-printing. In detail, the authors combined the printability of Pluronic gels with the possibility to stabilize the printed structures through UV irradiation upon the grafting of acrylate photo-sensitive moieties to the starting polymer (**Figure 35**). In particular, modified Pluronic was mixed with cells and blended with hyaluronic acid modified with methacrylate groups. Then, the gelation process was carried out exploiting the temperature-driven micelle formation of Pluronic copolymer, while photo-crosslinking led to an improvement in hydrogel mechanical stability. Finally, the hydrogel was washed to remove not-crosslinked Pluronic, thus forming nanostructures which could enhance the long term viability of the encapsulated cells [84].

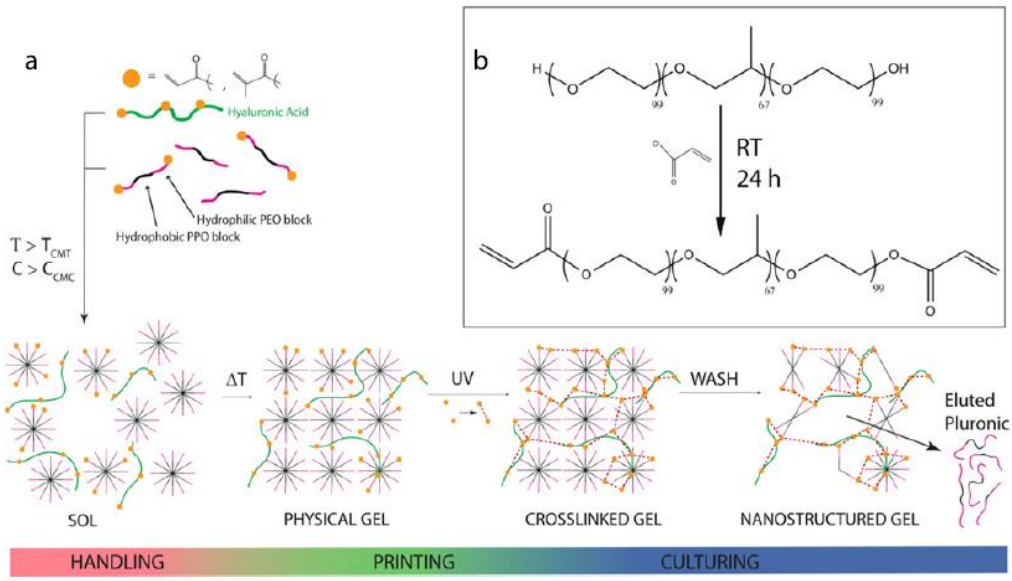

Figure 35: *Schematic representation of nano-structured Pluronic [83]*

Thesis Goal

The aim of this thesis work is the design of a smart hydrogel with responsiveness to a double external stimulus, i.e. temperature and visible light, and suitable to be used as bioink in the fabrication of scaffolds through an additive manufacturing technology (i.e., 3D-printing). The main polymeric component will belong to the polyurethane family as the versatility of this chemistry allows the synthesis of materials with tuneable physico-chemical and mechanical properties by simply changing their building blocks (i.e., the macrodiol, the diisocyanate and the chain extender). Specifically, in this work an amphiphilic poly(ether urethane) (PEU) will be synthesised starting from a commercial triblock copolymer (i.e., Poloxamer® 407) as macrodiol, an aliphatic diisocyanate (1,6-hexamethylene diisocyanate) and an amino group-containing chain extender (N-Boc diethanolamine). Due to its amphiphilic nature, the selected macrodiol will ensure hydrogel thermo-responsiveness through polymeric chain arrangement into organized micelles upon temperature increase. On the other hand, exploiting the presence of secondary amino groups along PEU backbone, hydrogel visible-light sensitivity will be provided through the grafting of photo-responsive moieties (i.e., thiol and norbornene groups) to PEU-NH via carbodiimide chemistry, thus obtaining PEU-SH and PEU-NB. Complete chemical characterization of PEU, PEU-SH and PEU-NB will be carried out through infrared and nuclear magnetic resonance spectroscopy, size exclusion chromatography and colorimetric assays (e.g., Ellman's test, Orange II sodium salt assay). Then, polyurethane-based aqueous solutions will be analysed by Dynamic Light Scattering to assess their thermosensitivity. Photo-crosslinking protocol will be optimised in terms of photoinitiator (eosin Y) and co-initiator (tyrosine) concentration through UV-Vis spectroscopic analyses conducted on aqueous solutions containing photo-sensitive molecules (i.e., thioglycolic acid, 5-norbornene-2-carboxilic acid) and subjected to visible-light irradiation at 525 nm. Hydrogels will be then designed by blending PEU-SH and PEU-NB at SH-NB molar ratio of 1:1 and final polymer concentration of 18% w/v. The success of hydrogel photo-crosslinking with green light will be assessed through rheological characterization and nuclear magnetic resonance spectroscopy. Finally, the developed bioink will be 3D-printed according to different CAD models (e.g., square grids, honeycomb structures) through its layer-by-layer deposition in the semi-gel state followed by its stabilization through visible-light irradiation. Specifically, hydrogel thermo-sensitivity will be exploited to tune bioink viscosity, while hydrogel photo-responsiveness will be exploited for the formation of photo-induced covalent bonds in the printed structure, thus ensuring higher shape fidelity and improved mechanical properties.

Materials and Methods

1. Synthesis of Poloxamer-based poly(ether urethane) (PEU)

1.1 Synthesis Reagents and Solvents

Kolliphor® P407 (P407, poly(ethylene oxide)-poly(propylene oxide)-poly(ethylene oxide) PEO-PPO-PEO triblock copolymer, M_n=12600 Da, 70% w/w PEO), 1,6-hexanediisocyanate (HDI), dibutyltin dilaurate (DBTDL) and N-Boc diethanolamine were purchased from Sigma Aldrich, Italy. Before the synthesis, P407 was dried under dynamic vacuum at 100 °C for 8 hours to remove residual water and then cooled down at 30 °C at approx. 200 mbar, while N-Boc diethanolamine was anhydrified under vacuum at room temperature. HDI was distilled under vacuum and stored in a dessicator before use. All solvents were purchased from CarloErba Reagents, Italy in the analytical grade. 1,2-dichloroethane (DCE) was anhydrified by pouring the solvent over activated (at 120 °C for 8 hours) molecular sieves and under nitrogen flux. All glassware required for the synthesis was dried overnight in an oven at 120 °C.

1.2 Synthesis procedure

The synthesis of the Poloxamer-based polyurethane used in this work was carried out through a two step process under inert atmosphere.

The starting reagents were:

- Macrodiol: Kolliphor P407;
- Diisocyanate: 1,6-hexamethilene diisocyanate;
- Chain Extender: N-Boc-diethanolamine.

The first step was carried out by reacting P407, dissolved at 15% w/v in DCE, with HDI, in 1:2 molar ratio with respect to P407. The pre-polymerization reaction was conducted for 45 minutes at 80 °C in the presence of the catalyst dibutyltin dilaurate (DBTDL), at 0.1% w/w with respect to P407. In the second step, N-Boc-diethanolamine (5% w/v in DCE and 1:1 molar ratio with respect to P407) was added to the mixture in order to obtain a high molecular weight poly(ether urethane). This

reaction took place for 2 hours at 60 °C under N_2. Finally, the reaction was stopped by adding methanol (6 mL of methanol each 16 g of polymer produced considering a 100% reaction yield). The polymer solution was precipitated in petroleum ether (4:1 volume ratio with respect to DCE) and, after supernatant removal, was dried overnight. Then, the polymer was purified by dissolution in DCE (16%w/v), followed by precipitation in diethyl ether and methanol at 98:2 volume ratio (5:1 volume ratio with respect to the DCE used for PEU solubilization). The polymer was collected by centrifugation at 6000 rpm and 0 °C for 20 minutes and dried overnight at room temperature under the fume hood. Finally, the synthesised polymer was stored under nitrogen atmosphere at 4 °C to prevent oxidative degradation.

The synthesized PEU has acronym DHP407, where D indicates the chain extender, H corresponds to HDI and P407 refers to Kolliphor P407.

1.3 Boc-deprotection of DHP407 to expose secondary amino groups

The polyurethane DHP407 shows the possibility to expose free secondary amines upon Boc group removal, which can be exploited for further functionalization of the polyurethane.

In order to expose amino groups along DHP407 polymeric chains, the PEU was treated in a mixture of chloroform and trifluoracetic acid (TFA) at 90:10 volume ratio according to Laurano et al [85]. Briefly, DHP407 was first dissolved in chloroform for 2 hours at room temperature and 250 rpm. Afterwards, trifluoroacetic acid was added to obtain a final polymer concentration of 4% w/v and the deprotection reaction lasted for 1 h. Subsequently, the solution was evaporated under controlled pressure (Buchi, Switzerland) to remove solvents. Then, after the first evaporation, the sample was washed in 100 mL of chloroform and the solvent was evaporated with the rotary evaporator. This washing process was repeated twice. The resulting material was solubilized in distilled water (5% w/v) and stirred overnight at 4 °C to avoid micellization. The solution was dialyzed (cut-off 10-12 kDa) against distilled water for 48 hours at 4 °C (dialysis medium refresh 3 times/day) and then the dialysed solution was freeze dried for 2 days. To wash out residual TFA traces, the freeze-dried polyurethane was washed in diethyl ether (DEE, 30 mL of DEE for each gram of polymer) through overnight stirring at room temperature. The PEU dispersion in DEE was then filtered using a Buchner system and then dried under a fume hood. The obtained polymer was called D-DHP407 (from deprotected-DHP407) and stored under nitrogen atmosphere at 4 °C.

2. PEU Chemical Characterization

Attenuated Total Reflectance-Fourier Transform Infrared (ATR-FTIR) spectroscopy and Size Exclusion Chromatography (SEC) were exploited to assess the success of PEU synthesis and, at the same time, to verify the integrity of urethane bonds after Boc-deprotection procedure.

2.1 Attenuated Total Reflectance Fourier Transform Infrared (ATR-FTIR) spectroscopy

ATR-FTIR spectroscopy is a widely exploited characterization technique to investigate the formation of new bonds in synthesised materials. In this work, a Perkin Elmer (Waltham, MA, USA) Spectrometer 100 equipped with an ATR diamond crystal (UATR KRS5) was used to record ATR-FTIR spectra of the commercial P407 and the synthesized DHP407 and D-DHP407 within the spectral range 4000-600 cm^{-1} at room temperature. Each spectrum resulted from 32 scans with a resolution of 4 cm^{-1} and was analysed using the Perkin Elmer Spectrum software.

2.2 Size Exclusion Chromatography (SEC)

SEC (Agilent Technologies 1200 Series, CA, USA) was used to estimate the number average and weight average molecular weights ($\overline{M_n}$ and $\overline{M_w}$, respectively) of P407, DHP407 and D-DHP407 to assess both the success of the PEU synthesis and the preservation of the urethane bonds after the Boc-removal procedure. The instrument was equipped with a refractive index (RI) detector and two Waters Styragel columns conditioned at 55 °C. N,N-dimethyl-formamide (DMF, HPLC grade) added with 0.1% w/v lithium bromide (LiBr) was used as eluent at a flow rate of 0.5 ml/min. The estimation of $\overline{M_n}$ and $\overline{M_w}$ was performed with the Aligent ChemStation Software by referring to a calibration curve based on 10 narrow PEO standards with $\overline{M_n}$ ranging from 4000 to 200000 g/mol. Samples (2 mg/ml) were prepared through polymer solubilization in the mobile phase followed by filtration through a 0.45 µm syringe filter (poly(tetrafluoro ethylene), PTFE).

2.3 UV-Visible spectroscopy to quantify exposed amino groups on D-DHP407

2.3.1 Ninhydrin Assay (Kaiser Test)

The amount of exposed amino groups after Boc removal procedure was quantified through ninhydrin assay (Kaiser test kit, Sigma Aldrich, Italy). The reaction of ninhydrin molecules with free amines induces a blue-purple colour, while in the absence of free amines the solution is characterized by a yellow colour. Therefore, by measuring the absorbance at 570 nm through a UV-Vis spectrophotometer (PerkinElmer Lambda 365 UV/VIS spectrometer), it is possible to quantity the exposed free amines by applying the Lambert-Beer law. Specifically, the amino group concentration can be calculated by measuring the absorbance and then results converted in mol/g of material.

To this aim, D-DHP407 samples (20 mg) were dissolved in a mixture of 75 µL of Phenol solution (80% in ethanol), 100 µL of KCN in H_2O/pyridine and 75 µL of Ninhydrin (6% in ethanol). Then, samples were incubated at 120 °C for 10 minutes and finally 200 µL were taken and mixed with 600 µL of an ethanol/distilled water mixture (60/40 v/v). Finally, the obtained solutions were analysed with an UV-Vis spectrophotometer to obtain the molar concentration of free -NH groups. DHP407 samples were also subjected to the same assay and used as control.

Analyses were performed in triplicate and results are reported as mean ± standard deviation.

2.3.1 Orange II Sodium Salt Assay

The quantification of amino groups on D-DHP407 was also conducted through Orange II Sodium Salt colorimetric assay (Sigma Aldrich, Italy). In detail, 30 mg of D-DHP407 were dissolved into 50 mL of dye solution (Orange II Sodium Salt solubilized at 0.263 mg/ml concentration in double demineralized water -ddH2O- adjusted to pH 3). Control samples were prepared with DHP407 following the same protocol. The formation of electrostatic interactions between exposed amino groups (protonated in acidic aqueous solution) and the anionic dye was carried out for 18 hours at room temperature. Then, to wash out unreacted orange dye, samples were put into Vivaspin 20 centrifugal concentrators with 10 kDa cut-off and polyether-sulfone (PES) membrane (Sigma Aldrich) and centrifuged at 6000 rpm, at 15 °C for 20 minutes. This process was repeated until clear solutions (i.e., not-containing free dye) were collected on the lower compartment of the centrifugal concentrators. Subsequently, samples were freeze-dried for 48 hours. Bonded Orange dye was

desorbed after incubation of 10 mg of samples in 1 mL of alkaline solution (ddH2O adjusted to pH 12) for 2 hours at room temperature. Then, the absorbance at 485 nm was measured by UV-vis spectrophotometer (PerkinElmer, Lambda 25). The quantification of amino groups was conducted by referring to a specific calibration curve based on orange/ ddH2O (at pH 12) solutions with defined concentrations in the range 0.002 – 0.02 mg/ml. Analyses were performed in triplicate on samples belonging to three different deprotection batches. Results are reported as mean ± standard deviation.

3. Functionalization of D-DHP407

The exposed amino groups along D-DHP407 polymeric chains after the Boc-removal procedure were exploited to provide the designed material with additional responsiveness to other stimuli through the grafting of specific molecules containing pendant functional groups via carbodiimide chemistry.

3.1 Norbornene modified D-DHP407 – NB-DHP407

3.1.1 Synthesis of NB-DHP407

Norbornene-functionalized D-DHP407 (NB-DHP407) was synthesized by reacting deprotected-DHP407 with 5-norbornene-2-carboxylic acid (NBE, Sigma Aldrich, Italy) upon the addition of 1-ethyl-3-(3-dimethylaminopropyl) carbodiimide/N-hydroxysuccinimide (EDC/NHS, TCI and Sigma Aldrich, receptively) coupling reagents, thus allowing the formation of amide bonds between the amino groups exposed on deprotected-DHP407 and carboxylic groups on NBE molecules. First, the carboxylic groups available on NBE molecules (20:1 molar ratio with respect to amino groups) were activated upon addition of an EDC and NHS solution (2:1 molar ratio with respect to the carboxylic groups). Briefly, the carboxylated norbornene molecules were added to a 15.3 ml aqueous solution of EDC (50 mg/ml) and NHS (25 mg/ml), the pH was adjusted to 5 and the activation reaction was carried out for 1 hours at 4°C under stirring. Then, D-DHP407 (500 mg), previously solubilized in 4.7 mL of ddH2O, was added to the solution containing EDC/NHS and the activated carboxylic groups of the NBE molecules. The grafting reaction was carried on for 6 hours at room temperature under stirring at three different pH conditions (pH 5, 7 and 9) to investigate the best grafting condition. Then, samples were dialyzed (cut-off 10-12 kDa) against ddH2O in the dark at room temperature

for 2 days to wash out unreacted reagents (dialysis medium refresh 3 times/day). Subsequently, samples were freeze-dried for 48 hours.

3.1.2 Chemical characterization of NB-DHP407

3.1.2.1 ATR-FTIR spectroscopy

The previously explained ATR-FTIR analysis was performed also on NB-DHP407 samples to investigate the presence of the absorption bands indicative of the formation of amide bonds and differences induced by the different pH conditions adopted in the grafting step. D-DHP407 samples were analysed as control condition. Analyses were conducted according to the protocol described in paragraph 2.1.

3.1.2.2 Size Exclusion Chromatography (SEC)

SEC analyses were performed on NB-DHP407 samples obtained at three different grafting pH conditions to estimate the number average and weight average molecular weights ($\overline{M_n}$ and $\overline{M_w}$, respectively). Samples were prepared as described in the previous paragraph. Results were compared to D-DHP407 to verify that no-degradation occurred during the functionalization procedure.

3.1.2.3 Proton Nuclear Magnetic Resonance Spectroscopy (^{1}H NMR)

^{1}H NMR analyses were performed on norbornene-functionalized D-DHP407 samples prepared at the three different pH conditions. To this aim, 30 mg of samples were dissolved in anhydrous deuterated dimethyl sulfoxide (DMSO-d6, 99.8% D with 0.03% TMS, Sigma Aldrich, Italy). Tests were performed by means of an Avance III Bruker spectrometer equipped with a 11.75 T superconductor magnet (500 MHz 1H Larmor frequency). The spectra were obtained by the average of 32 runs, with 10 s of relaxation time. The residual d6-DMSO proton signal at 2.5 ppm was used for ^{1}H chemical shift scale. The degree of norbornene substitution was found out through the integration of the signal peaks of norbornene double bonds (at 6 and 6.2 ppm) and results compared to non-functionalized polymer (D-DHP407).

3.2 Thiol modified D-DHP407 – S-DHP407

3.2.1 Synthesis of S-DHP407

Thiol-functionalized D-DHP407 (S-DHP407) was synthesized by reacting deprotected-DHP407 with thioglycolic acid (TGA) upon the addition of 1-ethyl-3-(3-dimethylaminopropyl) carbodiimide/N-hydroxysuccinimide (EDC/NHS) coupling reagents, thus allowing the formation of amide bonds between the amino groups exposed on D-DHP407 and carboxylic acid groups on TGA molecules [85]. First the carboxylic groups available on TGA molecules (20:1 molar ratio with respect to amino groups) were activated upon the addition of an EDC and NHS aqueous solution (1:1 molar ratio with respect to the carboxylic groups). Briefly, the carboxylated thiol molecules were added to a 17.2 ml aqueous solution of EDC (100 mg/ml) and NHS (50 mg/mL), the pH was adjusted to 5 and the activation reaction was carried out for 1 hours at 4 °C under stirring. Then, D-DHP407 (500 mg), previously solubilized in 2.8 mL of ddH2O, was added to the solution containing EDC/NHS and the activated carboxylic groups of the TGA molecules. The grafting reaction was carried out 6 hours at 4 °C and pH 4, under continuous mixing. Then, samples were dialyzed (cut-off 10-12 kDa) in the dark at 4° C for 2 days against ddH2O adjusted to pH 4 (dialysis medium refresh 3 times/day) to wash out unreacted reagents. Subsequently, samples were freeze dried for 2 days and stored under nitrogen before use to avoid disulphide bond formation.

3.2.2 Chemical characterization of S-DHP407

3.1.2.1 ATR-FTIR spectroscopy

The previously explained ATR-FTIR analysis was performed also on S-DHP407 samples to investigate the presence of the absorption bands ascribable to the formation of amide linkages. D-DHP407 samples were analysed as control condition. Analyses were conducted according to the previously described protocol.

3.1.2.2 Size Exclusion Chromatography (SEC)

SEC analyses were performed on S-DHP407 samples to estimate the number average and weight average molecular weights ($\overline{M_n}$ and $\overline{M_w}$, respectively). Samples were prepared as described in the

previous paragraph. Results were compared to D-DHP407 to verify that no-degradation occurred during the functionalization procedure.

3.1.2.3 UV-visible spectroscopy to quantify thiol-groups on S-DHP407 – Ellman's test

The quantification of thiol groups exposed on S-DHP407 was carried out using the Ellman's method, which is based on the reaction of Ellman's reagent (5,5-dithiolbis-(2-nitrobenzoic acid) - DTNB) with sulfhydryl compounds. Ellman's reagent is a water-soluble composite useful to quantify free sulfhydryl groups in solution.

Specifically, thiol groups available on S-DHP407 chains react with Ellman's reagents, cleaving the disulphide bond to give 2-nitro-5-thiobenzoate (TNB^-), which ionizes to the TNB^{2-} dianion in water at alkaline pH (**Figure 36**). TNB^{2-} ions give a yellow-coloured solution, which can be analysed using UV-visible spectroscopy. Then, thiol groups can be easily estimated by referring to a calibration curve based on standards of known concentrations of thiol-containing compounds such as thioglycolic acid (TGA). Briefly, 2.5 mg S-DHP407 were solubilized in 250 µl of ddH2O. Then, 250 µl of 0.5 M phosphate buffer (pH 8) and 500 µL Ellman's reagent (1.5 mM in phosphate buffer pH 8, in excess respect to thiol-groups) were added to the samples. The reaction was allowed to proceed at room temperature for 2 hours, then the absorbance peak was measured at a wavelength of 415 nm. Analyses were performed in triplicate on samples belonging to three different batches. The same analysis was also performed on not-functionalized D-DHP407 as control condition. The quantification of thiol groups was calculated from the corresponding standard curve based on TGA solutions prepared in ddH2O at a concentration within the range 0.02 - 0.25 mM.

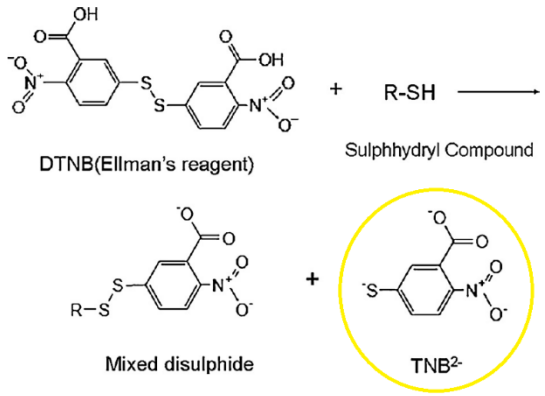

Figure 36 *Ellman's method scheme. The coloured specie produced in the reaction is circled in yellow.*

4. Characterization of polyurethane-based aqueous solutions

Aqueous solutions based on the newly synthesized polyurethanes (i.e., NB-DHP407 and S-DHP407) were first analysed through Dynamic Light Scattering (DLS) in order to study their thermo-sensibility and to verify that the functionalization reactions did not alter polymer responsiveness. Furthermore, solutions were analysed with UV-visible spectroscopy to optimize photo-crosslinking parameters.

4.1 Dynamic Light Scattering (DLS)

Dynamic Light Scattering (DLS, Zetasizer Nano S90, Malvern Instruments, Worcestershire, UK) was used to estimate the average hydrodynamic diameter of micelles/clusters formed in 0.5 % w/v PEU concentrated aqueous solutions at different temperatures (25 °C, 30 °C, 37 °C and 45 °C). Since DLS requires non-turbid solutions, only very diluted solutions that are unable to form gels could be used to study the polymeric structure formation at different temperatures. Specifically, the effects of PEU functionalization on chain capability to arrange into organized structures were investigated by comparing the estimated average hydrodynamic diameters of micelles based on D-DHP407, NB-DHP407 and S-DHP407. The solutions were prepared and incubated overnight at the test temperature (25, 30, 37, 45°C); then, before each analysis samples were equilibrated for 900 seconds. The micelle diameter was then estimated by the average of three measurements belonging to three different samples.

4.2 UV-visible spectroscopy to optimize photo-crosslinking parameters

To investigate the reaction mechanism which occurs between thiol groups and norbornene molecules upon visible-light irradiation and to elucidate the role exerted by tyrosine (TYR) as co-initiator of the reaction, UV-Vis spectroscopic analyses were performed on non-gelling solutions containing specific concentrations of photo-sensitive molecules, photo-initiator and co-initiator. Specifically, this study was made possible through the measurement of eosin-Y (EY) absorbance changes at 516 nm upon irradiation at 525 nm (green light), when mixed with thioglycolic acid (TGA), 5-norbornene-2-carboxilic acid (NBE) and TYR, alone or in combination.

Briefly, three different stock solutions of EY, TGA and NBE, at 2.2, 1.4 and 0.8 mM respectively, were prepared in phosphate-buffered saline (PBS) solution. Then, different amounts of these solutions were mixed in order to expose 1:1 molar ratio of functional groups. To each sample EY was added to achieve different concentrations (0.1 mM, 0.5 mM, 1 mM, 1.5mM, 2mM) and the resulting solutions were finally analysed using the UV-visible spectrophotometer PerkinElmer, Lambda 365. Spectra were recorded between 400 and 700 nm before and after irradiation (LED at the wavelength of 525 nm) at 80000 Lux for 10 minutes under stirring at 450 rpm. Results are reported as absorbance differences between pre- and post-irradiation.

On the other hand, to investigate the role exerted by tyrosine as co-initiator, TYR was added to the samples containing the optimized EY content at different concentrations (0.1 mM, 1 mM, 5 mM, 10 mM). Then, solutions were irradiated and analysed as previously described. Results are reported as absorbance differences between pre- and post-irradiation.

Before performing each UV-Vis analysis, solutions were diluted to reach a final EY concentration of 0.1 mM, in order to avoid saturation phenomena.

5. Step-growth thiol-ene polyurethane-based Hydrogels

5.1 Visible-light initiated photopolymerized hydrogel preparation

Step-growth thiol-ene hydrogels were prepared through visible light mediated photo-click reaction between polyurethanes functionalized with thiol groups (S-DHP407) and norbornene molecules (NB-DHP407). Stoichiometric ratio of thiol-ene moieties was adopted in all experiments. The photo-initiator EY was added to the PEU precursor solutions prepared by dissolving the polymer at a final concentration of 18% w/V. Then, the photo-crosslinking reaction was carried out by irradiating the solution at 525 nm (green light) for 10 minutes at 80000 Lux. Specifically, 200 µL of the prepared PEU solution were deposited in an appropriate toroidal mold to obtain samples with an approx. 10 mm diameter. The mold was placed on a slide that was used as support for the sample after the mold removal. The polymeric solution was then irradiated as described above. The same procedure was adopted also for the crosslinking of tyrosine containing thiol-norbornene hydrogels. Photo-initiator and co-initiator concentrations were chosen according to studies performed through UV-visible spectroscopy analysis, as described in the previous paragraph.

5.2 Hydrogel Characterization

5.2.1 ATR-FTIR spectroscopy

The previously explained ATR-FTIR analysis was performed also on NB-DHP407/S-DHP407 samples before and after light exposure to investigate the presence of the absorption bands indicative of the bonds that should form between norbornene molecules and thiol groups (i.e. C-S or S-S bonds), as well as to verify whether the bands characteristic of urethane bonds remained unchanged upon irradiation. Analyses were conducted according to the protocol described in paragraph 2.1.

5.2.2 Size Exclusion Chromatography (SEC)

SEC analyses were performed to estimate the number average and weight average molecular weights ($\overline{\mathrm{M_n}}$ and $\overline{\mathrm{M_w}}$, respectively) and the polydispersity index D=$\overline{M_w}/\overline{M_n}$ of NB-DHP407/S-DHP407-system before and after light exposure. Samples were prepared as described in the previous paragraph. Results were compared to evaluate if the molar mass values were higher after light exposure, suggesting new bonds formation between thiol and norbornene functional groups.

5.2.3 Dynamic Light Scattering (DLS)

To investigate the effect of visible light irradiation on micelle dimension, Dynamic Light Scattering (DLS) measurements were performed following the protocol previously described in paragraph 4.1. Specifically, DLS measurements were used to estimate the average hydrodynamic diameter of micelles/clusters formed in 0.5 % w/v NB-DHP407/S-DHP407-system concentrated aqueous solutions at 37 °C with the addition of photo-initiator EY (0.5 mM) before and after light exposure.

5.2.4 Rheological Characterization

To investigate how photo-irradiation could improve hydrogel mechanical properties, a complete rheological characterization of the systems was carried out exploiting their resultant thermo-reversibility upon photo-crosslinking.
Measurements were performed on a stress-controlled rheometer (MCR302, Anton Paar GmbH) equipped with a Peltier system for temperature control, using a 25 mm parallel plate geometry.

Frequency sweep tests were performed to study the viscoelastic properties of the hydrogels (angular frequency 0.1 to 100 rad/s, strain=0.1 %, temperature=25 °C, 30 °C, 37 °C), while strain sweep tests (frequency=10 Hz, strain from 0.01 to 500 %, 37 °C) were conducted to evaluate gel resistance to applied deformation. For each test, the sample was poured on the lower plate of the rheometer at 0 °C and then equilibrate at the test temperature for 15 minutes.

These two different tests (i.e., frequency sweep test and strain sweep test) were performed on different PEU solutions, as described below, prepared in phosphate buffer solution (PBS) at 18 %w/V overall concentration (-SH/NBE 1:1 molar ratio):

-NB-DHP407/S-DHP407-based sol-gel systems with the addition of photo-initiator EY (0.5 mM), co-initiator TYR (5 mM) before and after light exposure;

-NB-DHP407/S-DHP407-based sol-gel systems with the addition of photo-initiator EY (0.5 mM) before and after light exposure.

To further investigate thiol-ene photo-crosslinking mechanism, the same rheological tests were also performed on a polyurethane based thiol-acrylate system (A-DHP407/S-DHP407) developed in a previous thesis work [86]. Specifically, frequency sweep tests and strain sweep tests were conducted on:

-A-DHP407/S-DHP407-based sol-gel systems with the addition of photo-initiator EY (1 mM) and co-initiator TEOA (7.5 mM) before and after light exposure;

-A-DHP407/S-DHP407-based sol-gel systems with the addition of photo-initiator EY (1 mM) before and after light exposure.

5.2.5 Proton and Carbon Nuclear Magnetic Resonance (^{1}H NMR - ^{13}C NMR) Spectroscopy

To verify the success of visible light-initiated photo-crosslinking and thus the formation of new bonds among the polymeric chains, ^{1}H NMR and ^{13}C NMR analyses were performed on photo-crosslinked NB-DHP407/S-DHP407 samples with the aim to quantify the residual norbornene and thiol groups. Specifically, samples were first prepared and irradiated as previously described; then, they were lyophilized, and 30 mg and 60 mg of polymer were dissolved in deuterated dimethyl sulfoxide (DMSO-d6, 99.8% D with 0.03% TMS, Sigma Aldrich, Italy) for ^{1}H NMR and ^{13}C NMR, respectively. The same amounts of NB-DHP407/S-DHP407 before irradiation were prepared according to the same protocol as control condition. Tests were performed by means of an Avance III Bruker spectrometer equipped with a 11.75 T superconductor magnet (500 MHz 1H Larmor frequency). ^{1}H NMR spectra were obtained by the average of 32 runs, with 10 s of relaxation time,

while ^{13}C NMR resulted from 1024 scans. The residual d6-DMSO proton signals at 2.5ppm and at 39.5 ppm were used for ^{1}H and ^{13}C chemical shift scale, respectively. Residual norbornene molecules and thiol groups were quantified through integration of the bands at 6-6.2 ppm (in ^{1}H NMR spectra) and 35.8-35.9 ppm (in ^{13}C NMR spectra) ascribed to the resonance of norbornene double bonds and thiol groups, respectively.

6. 3D Bioprinting

The photo-responsive materials (S-DHP407 and NB-DHP407) were dissolved in PBS at 1:1 norbornene-thiol molar ratio and final polymer of 18 % w/v concentration. Then, the optimized Eosin Y concentration was added and the solution was stored at 4 °C until use. Square meshed grids and honeycomb-like structures were optimized and then printed by micro-extrusion 3D using an Inkredible+ (Cellink) bio-printer. Briefly, CAD 3D models of different sizes and shapes were created using Solidworks as CAD software. The resulting 3D structures were first converted into STL files upon the application of a mesh and then converted into G-code files through Slice3r software. Then, the G-code files were analysed through Repetier-Host software to check the results of the slicing process. Finally, Inkredible+ 3D bioprinter was used to print the grids.

The following printing parameters were set:

- syringe temperature at 25 °C,

- print bed temperature at 30 °C,

Specifically, in order to select the proper pressure, feed-rate and nozzle diameter to obtain continuous filaments and regular structures, the pressure was varied in the range 70 - 130 kPa and the feed-rate 20 - 100%. In addition, different nozzle diameters were tested (G22 (0.7 mm), G25 (0.5mm) and G27 (0.4 mm).

Exploiting the possibility to provide the printer with a led at 525nm, the G-codes previously obtained were modified adding a step of photo-crosslinking after the deposition of each layer.

Firstly, the parameters were optimized for the square meshed grid to have a proof of concept of the bioink printability. More in detail, the grid was first printed exploiting only bioink thermo-sensibility, then a step of photo-crosslinking was added to evaluate the higher fidelity to the CAD model upon irradiation. Then, in order to investigate the possibility to print more complex geometries able to fit with irregular tissue defects, the honeycomb-like structures of different sizes (hexagon dimension

ranging from 2 to 5 mm) were printed and photo-crosslinked. Successively, for each printed structure, ten microscope images were taken to measure the mean diameter of the printed filament. Results are reported as mean ± standard deviation.

Results and Discussion

1. Chemical Characterization of the synthesised poly(ether urethane) (PEU)

1.1. Attenuated Total Reflectance Fourier Transform Infrared (ATR-FTIR) spectroscopy

Attenuated Total Reflectance Fourier Transform Infrared (ATR-FTIR) spectroscopy was performed to assess the success of the PEU synthesis and the preservation of urethane bonds after the Boc-removal procedure.

Figure 37 reports the ATR-FTIR spectra obtained for the synthesized polyurethane DHP407 and for the macrodiol P407.

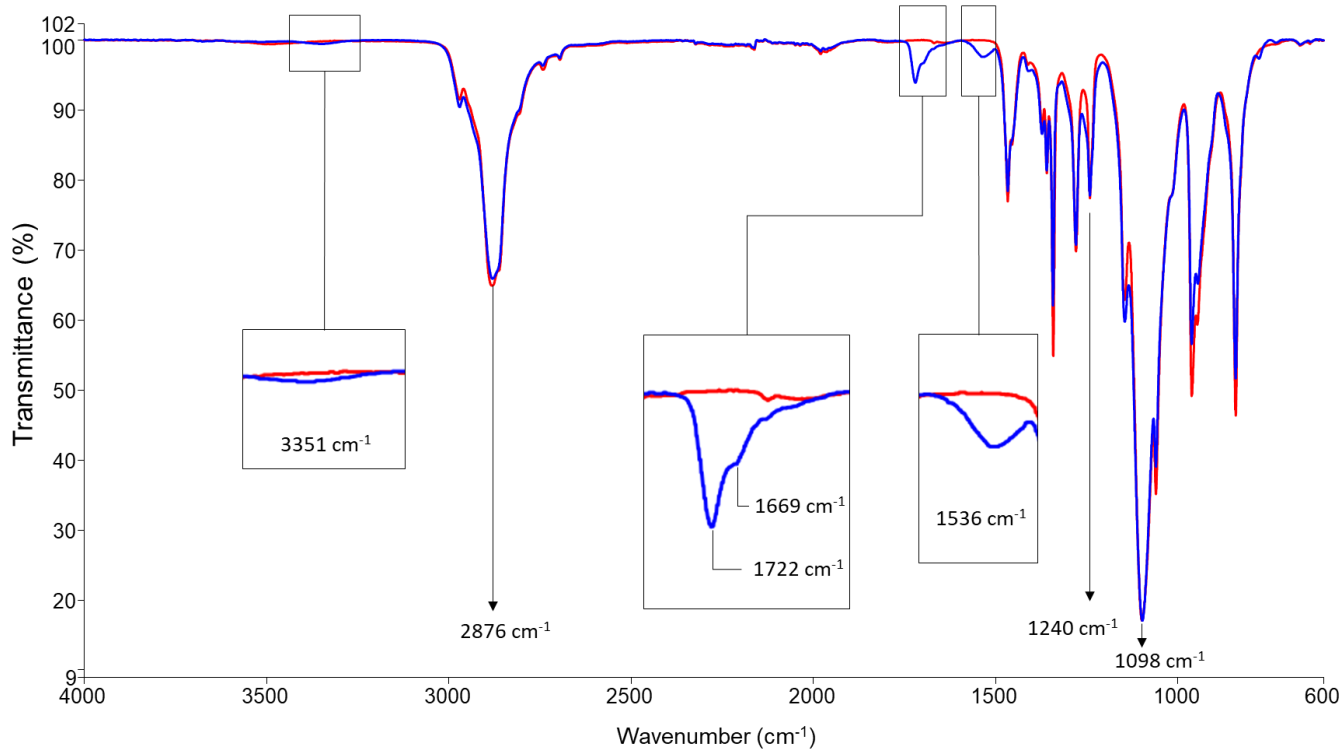

Figure 37 ATR-FTIR spectra of P407 (red) and DHP407 (blue). Inserts highlight differences between the spectra.

Poloxamer 407 ATR-FTIR spectrum showed the typical absorption peaks of CH_2 stretching vibrations (2876 cm^{-1}), CH_2 rocking and C-O-C stretching vibrations (1240 cm^{-1} and 1098 cm^{-1}, respectively), ascribed to the repetition of $-OCH_2CH_2$ units in PEO backbone. On the other hand, the comparison between P407 and DHP407 spectra demonstrated the success of PEU synthesis: two new bands

appeared at 1722 cm^{-1} and 1669 cm^{-1} which can be attributed to the stretching vibrations of the free and H-bound carbonyl groups (C=O), respectively, while the peak at 1536 cm^{-1} can be ascribed to the concurrent N-H bending and C-N stretching vibrations. Hence, the appearance of these new absorption bands proved urethane bond formation. Furthermore, the peak at 3351 cm^{-1} can be attributed to N-H stretching vibrations. Finally, the absence of peaks at 2200 cm^{-1} proved that the complete conversion of isocyanates groups during the synthesis.

Figure 38 shows the ATR-FTIR spectra of the as-synthesized polyurethane before (DHP407) and after Boc-removal procedure (D-DHP407) to expose functional secondary amino groups.

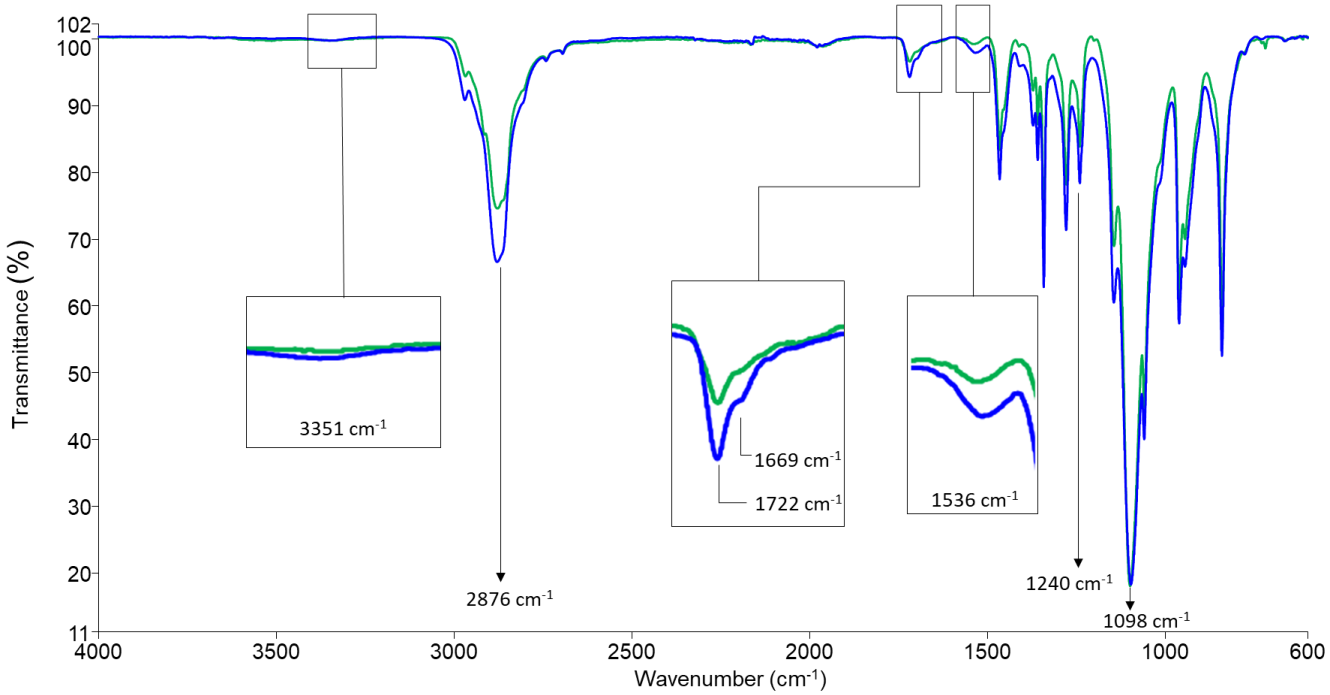

Figure 38 ATR-FTIR spectra of DHP407 (blue) and D-DHP407 (green). Inserts highlight differences between the spectra.

D-DHP407 ATR-FTIR spectrum showed that the typical urethane peaks remained unchanged with respect to DHP407 ATR-FTIR spectrum, proving that the acidic treatment carried out for Boc-removal on DHP407 was not detrimental for the urethane bonds. The slight differences between the two spectra could be attributed both to the nature of the analysis (ATR-FTIR spectroscopy is a qualitative analysis) and to the nature of the samples (i.e., DHP407 was analysed in the form of small pieces of polymer, while D-DHP407 appeared as a thin film of polymeric material).

1.2. Size Exclusion Chromatography (SEC)

Size Exclusion Chromatography (SEC) was performed to estimate the number and the weight average molecular weight ($\overline{M_n}$ and $\overline{M_w}$, respectively) as well as the polydispersity index D=$\overline{M_w}/\overline{M_n}$

of P407, DHP407 and D-DHP407. Weight average molecular weight $\overline{M_w}$ was estimated to be approx. 7000 Da for Poloxamer 407 with a polydispersity index of 1.2, while it was found to be approx. 30000 Da, with a polydispersity index of 1.5, for both the as-synthesized polyurethane (DHP407) and its deprotected form (D-DHP407). These results were a further confirmation of the successful PEU synthesis as well as a validation that the treatment performed on the native polymer to remove Boc-caging groups was not degradative.

1.3. UV-Vis spectroscopy to quantify exposed amino groups on D-DHP407

The exposed functional secondary amino groups along PEU backbone were quantified through two colorimetric assays differing for the coupling reaction mechanism: the Ninhydrin Assay (also called Kaiser test) in based on the formation of covalent bonds between primary amino groups and Kaiser reagents, while the Orange II Sodium Salt assay works through electrostatic interactions occurring between the anionic orange dye and cationic amino groups. Therefore, while this second assay can be successfully exploited to quantify secondary amino groups, the Ninhydrin Assay was adapted to estimate the number of secondary amines.

1.3.1 Kaiser test

Kaiser test allowed the quantification of exposed secondary amino groups through the measurement of the absorbance at 570 nm of samples subjected to the colorimetric assay. Indeed, upon a successful reaction between functional groups and Kaiser reagents, the yellow-coloured solution becomes purple. Hence, a first evidence of the successful exposure of amine functionalities was immediately obtained by visual inspection: upon treatment with Kaiser reagents, DHP407 solution remained yellow, while D-DHP407 one became purple, as shown in **Figure 39**.

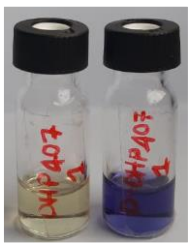

Figure 39 *DHP407 (yellow) and D-DHP407 (purple) solutions upon reaction with Kaiser reagents*

Then, the concentration of free secondary amino groups was estimated by measuring sample absorbance through an UV-VIS spectrophotometer and, by referring to the volume of the sample, it

was possible to obtain the moles of functional groups per gram of polymer. **Figure 40** reports the UV-Vis absorption spectra of DHP407 and D-DHP407 within the spectral range between 700 and 400 nm.

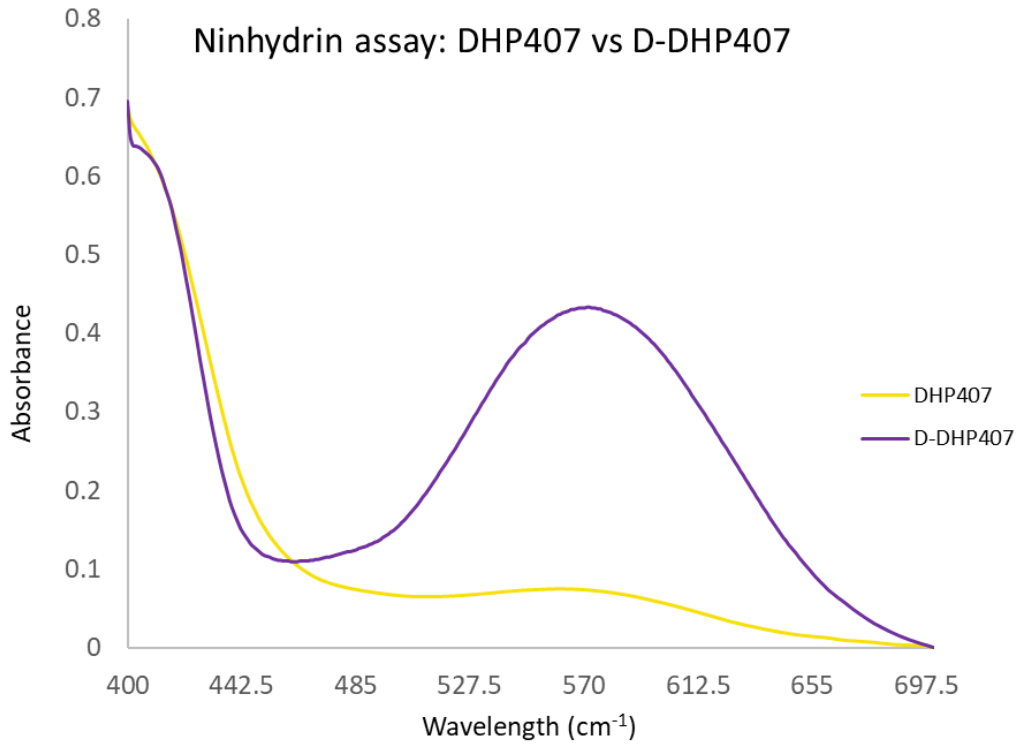

Figure 40 *UV-Vis absorption spectra of DHP407 (yellow) and D-DHP407 (purple) within the spectral range between 700 and 400 nm*

The quantified secondary amino groups exposed on D-DHP407 polymer chains upon Boc group removal (reported as mean ± standard deviation) turned out to be $2.2 \cdot 10^{17} \pm 2.4 \cdot 10^{16}$ units/$g_{D\text{-}DHP407}$ (the absorbance contribution at 570 nm of DHP407 has been subtracted to that of D-DHP407).

1.3.2 Orange II Sodium Salt test

The colorimetric Orange II Sodium Salt assay was also used to quantify the amount of secondary amino groups exposed after the treatment used to remove Boc-caging groups. In this case, the solution containing free secondary amines should exhibit a more intense orange intensity with respect to the control (which colour can be ascribed to dye absorption phenomena to the polymer chains), as a consequence of the electrostatic interaction occurring between the exposed functional groups and the cationic dye. Indeed, a visible difference in the intensity was immediately observed between D-DHP407 and control (DHP407) solutions. **Figure 41** reports photos of DHP407 and D-DHP407 solutions after the centrifugation procedure: D-DHP407 samples showed increased orange colour intensity than the controls (DHP407), thus proving the presence of secondary amino groups

bonded to Orange molecules. However, also DHP407 samples showed a light orange colour. This evidence can be justify considering the partial absorption of dye molecules to the polymer chains and not to the presence of -NH groups.

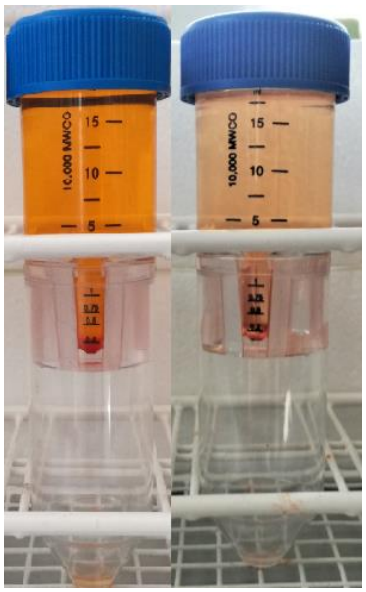

Figure 41 D-DHP407 (dark orange) and control DHP407 (light orange) solutions

Figure 42 reports the absorbance profiles of DHP407 and D-DHP407 samples subjected to Orange II Sodium Salt assay within the spectral range 630-350 nm.

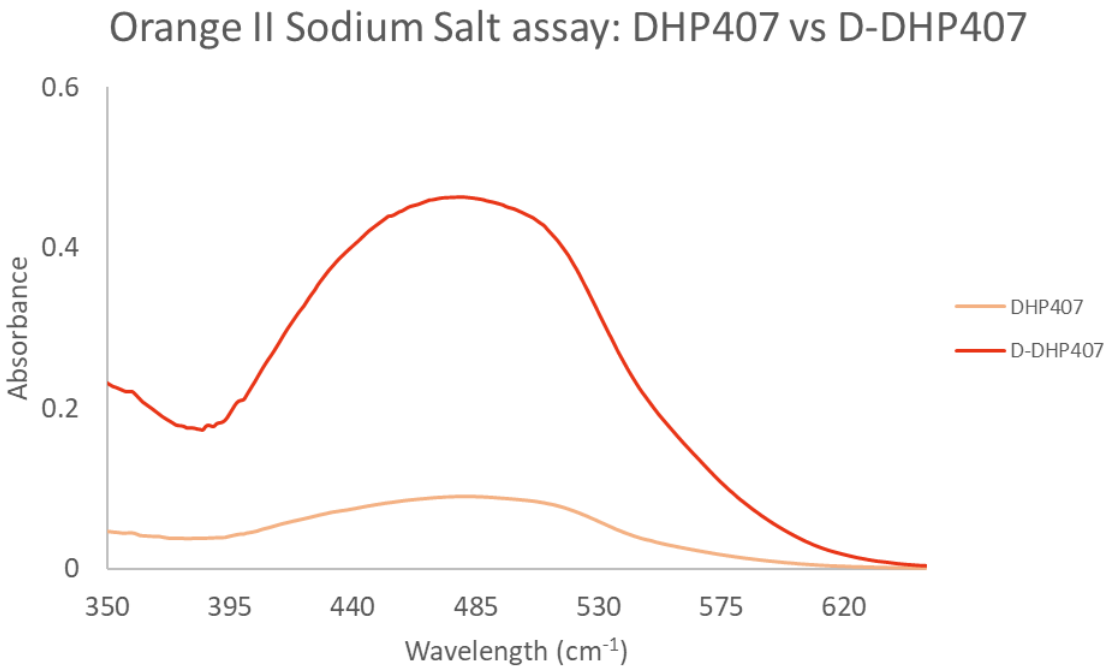

Figure 42 Absorbance profiles of DHP407 (light orange) and D-DHP407 (dark orange) samples subjected to Orange II Sodium Salt assay within the spectral range 630-350 nm

The amount of amino groups was calculated by referring to a specific calibration curve based on orange/ddH2O (pH 12) solutions with defined concentrations in the range 0.002 – 0.02 mg/ml.

The quantified secondary amino groups exposed on D-DHP407 polymer chains upon Boc group removal (reported as mean ± standard deviation) turned out to be $1.6 \cdot 10^{19} \pm 1.3 \cdot 10^{18}$ units/$g_{D\text{-}DHP407}$ (the absorbance contribution at 485 nm of DHP407 has been subtracted to that of D-DHP407 to eliminate the contribution of absorption phenomena).

By *comparing the results obtained from the two colorimetric assays on three different D-DHP407 batches* (**Figure 43**), a difference of two orders of magnitude in the quantification of -NH groups was observed. These results can be explained by considering that both tests, usually exploited for the quantification of primary amino groups, were adapted in this work to the quantification of secondary amines. Specifically, the ninhydrin assay requires the formation of covalent bonds and thus, in the presence of secondary amines different reaction mechanisms could occur, resulting in an underestimation of the exposed functional groups. On the other hand, the Orange II Sodium Salt assay works through electrostatic interactions both in the presence of –NH and $–NH_2$ groups. Indeed, the amount of free amino groups calculated through Orange II Sodium Salt test resulted to be in accordance with the value obtained through Proton Nuclear Magnetic Resonance (^{1}H-NMR) spectroscopy, as recently reported by Laurano et al. [85]. Therefore, Orange II Sodium Salt assay turned out to be a more reliable test for the quantification of secondary amino groups.

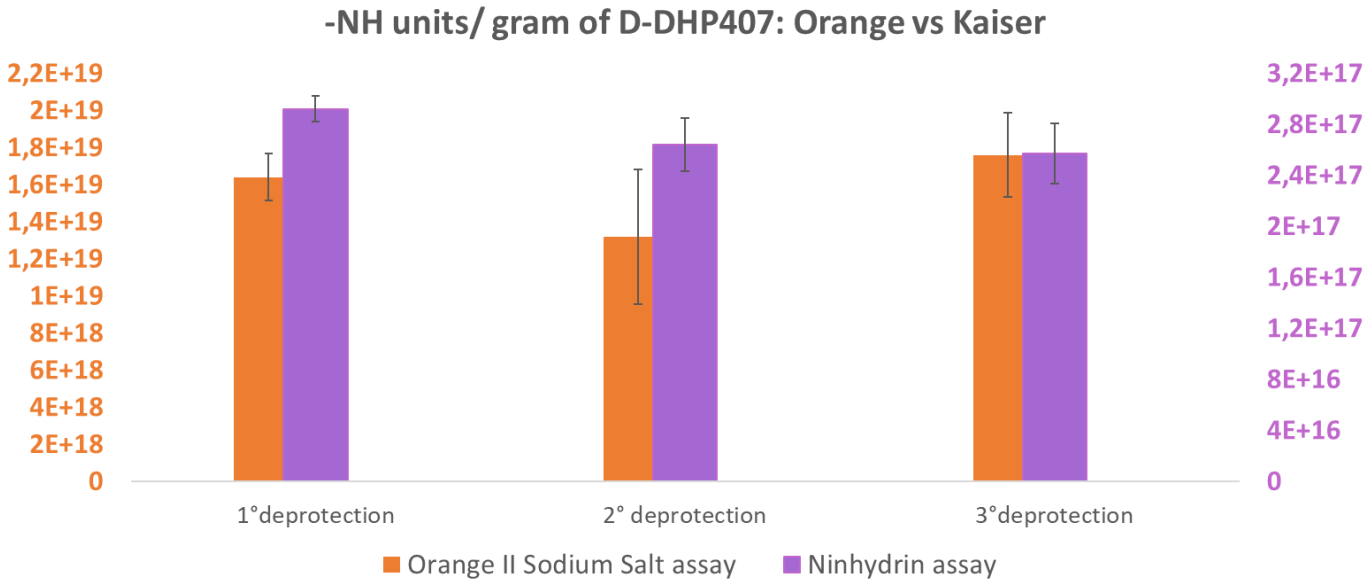

Figure 43 *Comparison between Orange II Sodium Salt assay and Ninhydrin assay in the quantification of -NH groups*

2. Functionalization of D-DHP407

The exposed secondary amino groups along D-DHP407 polymeric chains were then exploited to graft photosensitive moieties, thus providing the resulting polymer with responsiveness to UV/Vis light irradiation. Specifically, thioglycolic acid (TGA) and 5-norbornene-2-carboxylic acid (NBE) were grafted to PEU-NH through carbodiimide chemistry to expose thiols (S-DHP407) and norbornene (NB-DHP407) moieties, respectively.

2.1. Chemical Characterization of NB-DHP407

NB-DHP407 was chemically characterized to verify the success of D-DHP407 functionalization with NBE molecules as well as to define the best grafting reaction parameters in terms of pH condition.

2.1.1 Attenuated Total Reflectance Fourier Transform (ATR-FTIR) spectroscopy

Attenuated Total Reflectance Fourier Transform Infrared (ATR-FTIR) spectroscopy was used as a first qualitative method to verify the success of the functionalization with NBE molecules.

Figure 44 reports the comparison between the spectrum of D-DHP407 and the three spectra of NB-DHP407 obtained using different pH conditions (pH 5, 7 and 9, respectively) for the grafting step.

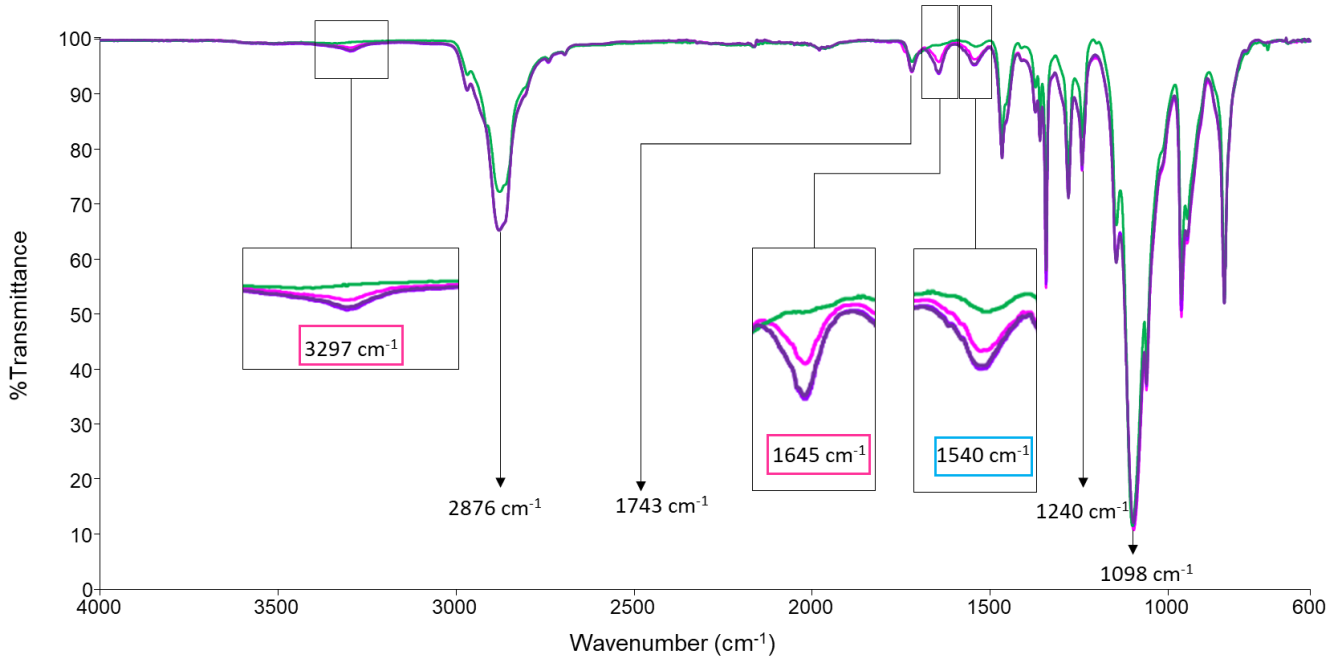

Figure 44 *ATR-FTIR spectra of NB-DHP407 polyurethanes obtained using three different pH condition for the grafting step (NB-DHP407 pH 5 (fuchsia), pH 7 (light purple), pH 9 (dark purple). D-DHP407 (green)is also reported as control condition.*

Irrespective of the pH adopted during the grafting step, all NB-DHP407 spectra showed an intensification of the bands ascribed to amide bond formation between PEU-NH and NBE-COOH as

schematically reported in **Figure 45**. Specifically, NB-DHP407 spectra showed increased intensity at 1540 cm^{-1} and 1645 cm^{-1} attributed to the stretching vibrations of C-N and C=O groups belonging to the newly formed amide bonds, respectively. Furthermore, it was also possible to notice an increase of the absorbance peak at 3297 cm^{-1} attributed to the overtone of C=O stretching vibration. Therefore, ATR-FTIR analyses proved the successful grafting of NBE molecules to the synthesised PEU in all the tested pH conditions for the grafting step. However, among the tested parameters for the grating step, the condition which was supposed to give the best grafting was pH=9, as the increase in the absorption bands resulted to be higher. Nevertheless, being ATR-FTIR spectroscopy a qualitative analysis, further analyses were performed to confirm this hypothesis and to quantify the grafted functional groups.

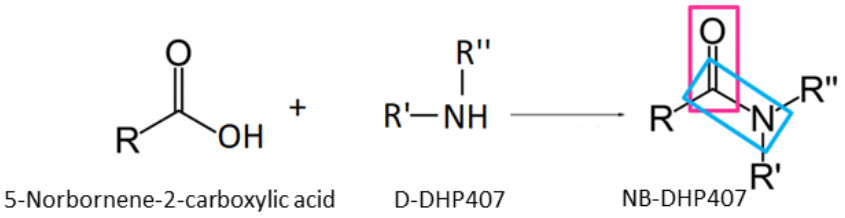

Figure 45 *Schematic representation of amide bond formation.*

2.1.2 Size Exclusion Chromatography (SEC)

Size Exclusion Chromatography (SEC) analyses were performed to estimate the number and the weight average molecular weights ($\overline{M_n}$ and $\overline{M_w}$, respectively) and the polydispersity index D=$\overline{M_w}/\overline{M_n}$ of NB-DHP407 at the three different pH conditions tested. Molecular weights $\overline{M_n}$ and $\overline{M_w}$ of all NB-DHP407 samples were measured to be approx. 20000 and 30000 Da with a polydispersity index of 1.5. Hence, the pH of the grafting step turned out not to affect the molecular weight of the resulting polymers. Additionally, no differences were observed between NB-DHP407 samples and the starting D-DHP407. These findings were a further confirmation that the treatment used to functionalize D-DHP407 with NBE molecules, i.e. carbodiimide chemistry, was not degradative for the urethane bonds.

2.1.3 Proton Nuclear Magnetic Resonance (^{1}H NMR) Spectroscopy: quantification of exposed NBE groups

Proton Nuclear Magnetic Resonance (^{1}H NMR) spectroscopic analyses were performed on both modified and un-modified materials to further confirm the success of the functionalization reactions carried out at different pH conditions and to quantify the exposed norbornene groups.

Figure 46 shows the spectra of NB-DHP407 polymers obtained by conducting the grafting step at pH 5, 7 and 9. The appearance of new peaks at 6 and 6.23 ppm and at 2.05, 2.02 and 2 ppm in the spectrum of NB-DHP407 obtained upon a grafting step at pH 9 definitely proved the success of the functionalization reaction as they were ascribed to the NBE protons involved in C=C double bond and to the aliphatic protons of NBE, respectively. However, despite evidences from the ATR-FTIR spectra, pH 5 and pH 7 as grafting conditions did not allow the exposure of a detectable amount of functional groups.

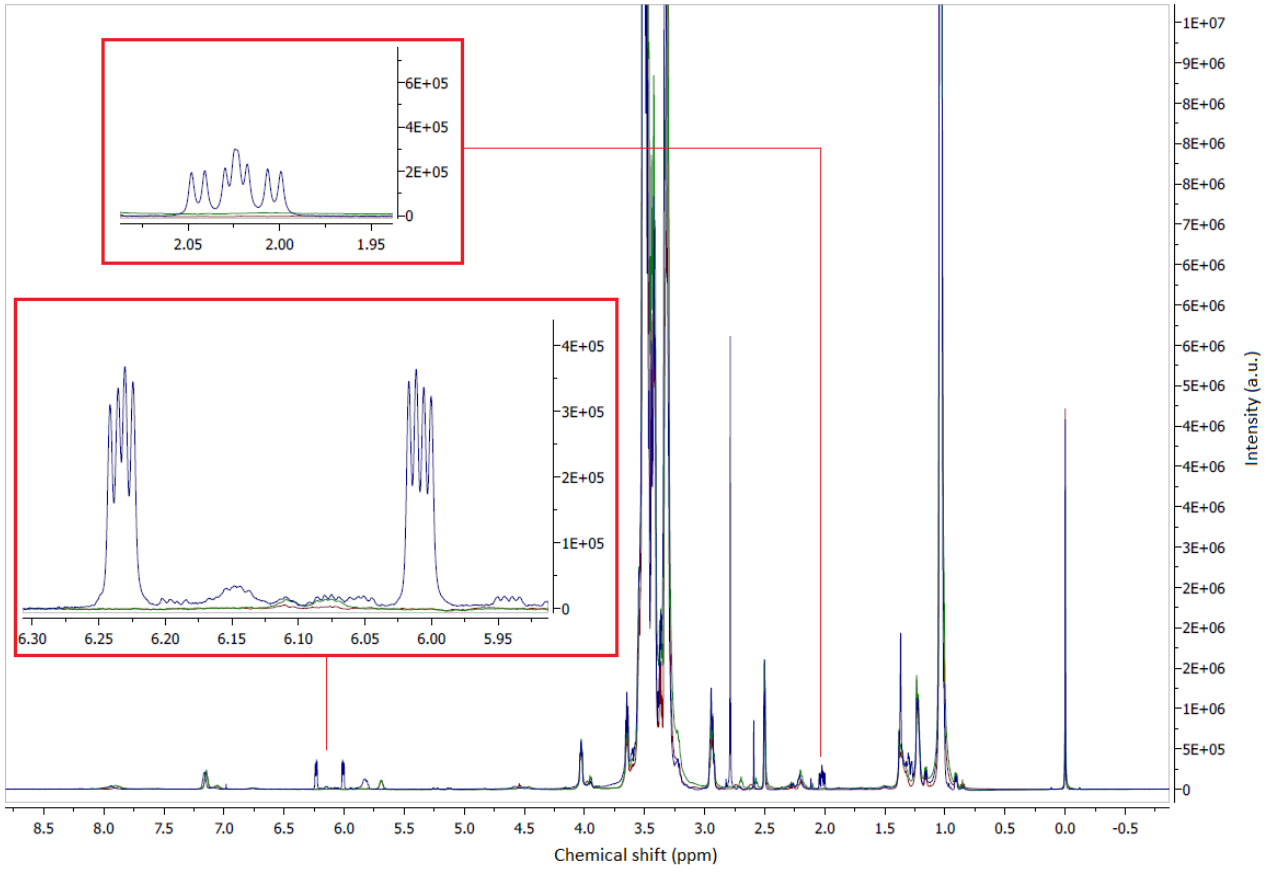

Figure 46 *1H NMR spectra of NB-DHP407 obtained by conducting the grafting step at three different pH values (pH 5, 7 and 9, respectively in red, green and blue). The grafting was confirmed by the appearance of new peaks at 6 and 6.23 ppm and at 2.05, 2.02 and 2 ppm in the NB-DHP407 spectrum obtained by conducting the grafting step at pH 9.*

The number of NBE molecules grafted in 1 g of NB-DHP407 obtained by conducting the grafting step at pH 9 was calculated through the integration of the peaks and it was measured to be $2 \cdot 10^{-4}$ moles/$g_{NB\text{-}DHP407}$

This result confirmed the possibility to functionalize D-DHP407 with norbornene moieties through carbodiimide chemistry. Moreover, the selection of an alkaline pH for the grafting step was in accordance with previous published works [87] [88].

2.2. Chemical Characterization of S-DHP407

S-DHP407 was chemically characterized to verify the success of D-DHP407 functionalization through carbodiimide chemistry with TGA molecules. Specifically, the reaction was carried out by setting the pH at 4 during the grafting phase, in accordance with the optimization of the grafting protocol recently published by Laurano et al. [85].

2.2.1 Attenuated Total Reflectance Fourier Transform (ATR-FTIR) spectroscopy

Attenuated Total Reflectance Fourier Transform Infrared (ATR-FTIR) spectroscopy was exploited as a qualitative method to verify the success of D-DHP407 functionalization with TGA molecules. **Figure 47** shows the comparison between D-DHP407 and S-DHP407 ATR-FTIR spectra. S-DHP407 spectra showed an intensification of the bands attributed to amide bond formation. The reaction leading to amide bond formation and the subsequent grafting of –SH moieties to the polymer backbone is schematically reported in **Figure 48**. As previously pointed out for NB-DHP407 samples, the increased intensity of the two peaks at 1535 cm^{-1} and 1637 cm^{-1} can be ascribed to the stretching vibration of C-N and C=O groups of the newly formed amide bonds, respectively. Furthermore, the increased intensity of the absorbance peak at 3306 cm^{-1} and at 2879 cm^{-1} can be ascribed to the overtone of C=O stretching vibration belonged to the amide bonds and to the CH_2 stretching vibration of TGA molecules, respectively. However, the characteristic peak of thiol groups at 1250 cm^{-1} was not clearly detectable because of the presence of an intense peak at 1240 cm^{-1} relative to CH_2 rocking vibration of the polyurethane.

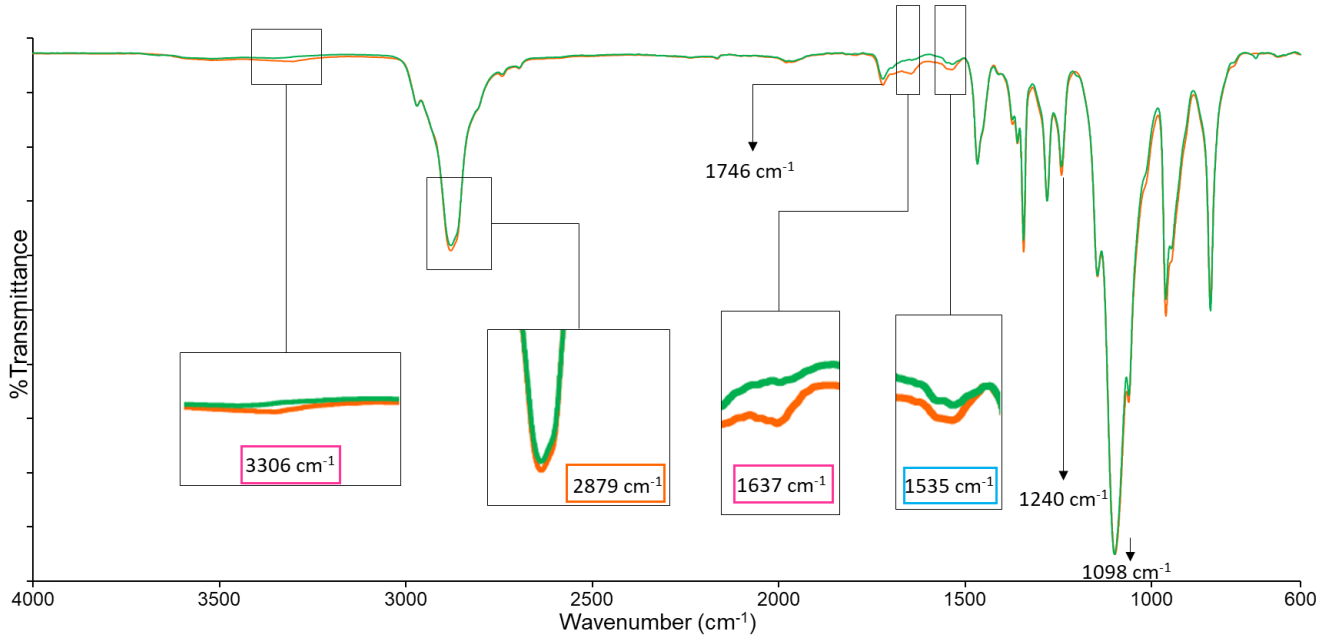

Figure 47 *ATR-FTIR spectra of S-DHP407 (orange) and D-DHP407 (green), used as control.*

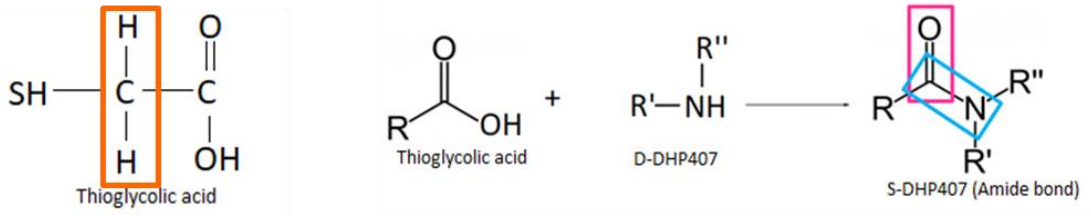

Figure 48 *Schematic representation of amide bond formation reaction (right) and TGA molecule (left).*

2.2.2 Size Exclusion Chromatography

Size Exclusion Chromatography (SEC) was exploited to estimate the number and the weight average molecular weights ($\overline{M_n}$ and $\overline{M_w}$, respectively) and the polydispersity index D=$\overline{M_w}/\overline{M_n}$ of S-DHP407. $\overline{M_n}$ and $\overline{M_w}$ were measured to be approx. 20000 and 30000 Da (polydispersity index of 1.5), respectively, with no differences with respect to D-DHP407.These findings were a further confirmation that the treatment used to functionalize D-DHP407 with thiol groups, i.e. carbodiimide chemistry, was not degradative for the urethane bonds.

2.1.3 UV-Vis spectroscopy: quantification of -SH groups

A colorimetric assay, i.e. the ***Ellman's test,*** was used to quantify the amount of thiol groups grafted to PEU-NH (D-DHP407) through carbodiimide chemistry. Indeed, the reaction between Ellman's reagents and the exposed thiol groups turned out to give a yellow-coloured solution. **Figure 49**

reports a photo showing the colour acquired by D-DHP407 (control) and S-DHP407 samples at the end of the colorimetric assay: S-DHP407 samples showed a higher yellow colour intensity than D-DHP407 ones because of the presence of thiol groups bonded to the polyurethane backbone which, reacting with Ellman's reagents (5,5-dithiolbis-(2-nitrobenzoic acid) or DTNB), cleave DTNB disulphide bond to obtain TNB^-, which ionizes to TNB^{2-}, giving to the solution a yellow colour.

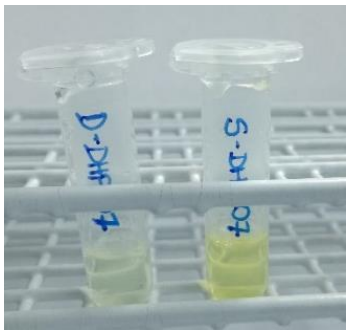

Figure 49 *S-DHP407 (yellow) and control D-DHP407 (light yellow) solutions*

UV-Vis spectrophotometric analyses confirmed the change in absorbance at 415 nm suggested by visual inspection. **Figure 50** reports the absorbance profile of S-DHP407 (dilution factor 1:20) and D-DHP407 samples (not-diluted) registered within the spectral range 600-300 nm.

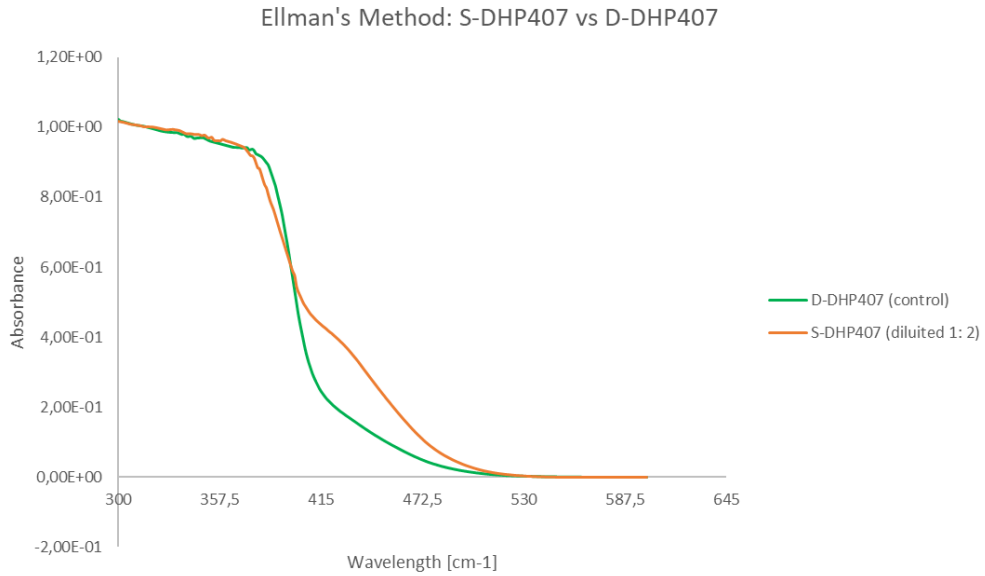

Figure 50 *Absorbance profile of S-DHP407 (dilution factor 1:20, orange) and D-DHP407 samples (not-diluted, green) registered within the spectral range 600-300 nm*

The amount of exposed thiol groups was calculated by referring to a specific calibration curve based on standards of thioglycolic acid in ddH2O with concentration in the range 0,02 - 0,25 mM subjected

to Ellman's test. The amount of grafted –SH moieties to D-DHP407 was measured to be $2.34 \cdot 10^{19} \pm 6.4 \cdot 10^{18}$ units/$g_{S\text{-}DHP407}$

Furthermore, to evaluate the repeatability of the grafting reaction, the Ellman's method was performed in triplicate on samples belonging to three different batches **Figure 51.**

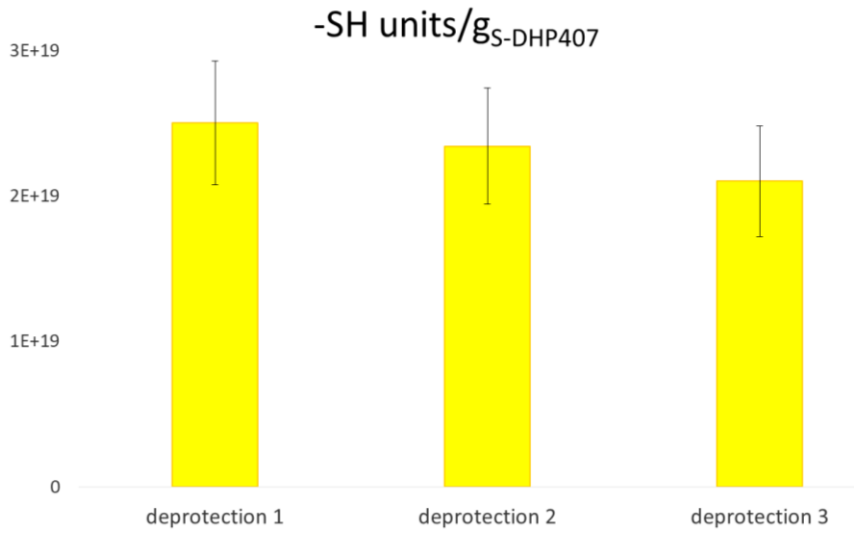

Figure 51 *Quantification of -SH groups grafted on S-DHP407 polyurethanes belonging to three different batches (i.e., grafting procedure performed on D-DHP407 of three different deprotection reactions).*

3. Characterization of non gelling solutions in terms of thermo- and photo-responsiveness

To investigate whether the functionalization procedure carried out to expose photo-sensitive moieties could bring detrimental effects on polymer thermosensitivity, non-gelling NB-DHP407 and S-DHP407 polyurethane-based solutions were first characterized through Dynamic Light Scattering. Then, to study the photo-crosslinking mechanism, functional group-based solutions added with different amounts of photo-initiator and co-initiator were analysed by UV/Vis spectrophotometry. Finally, to investigate if the photo-crosslinking could enhance the formation of bigger micelles/aggregates, Dynamic Light Scattering analyses were also performed on S-DHP407/NB-DHP407 samples upon irradiation at 525 nm.

3.1. Dynamic Light Scattering (DLS) analyses: measurement of the average micelle hydrodynamic diameter

Since the functionalized PEUs (NB-DHP407 and S-DHP407) have an amphiphilic nature due to the presence as P407 as macrodiol, their solutions in aqueous media are expected to form micelles with hydrophilic shells and hydrophobic cores. Therefore, these semi-spherical systems can be analysed by adapting the Dynamic Light Scattering (DLS) technique, which is usually exploited to measure the hydrodynamic diameter of spherical nanoparticles. Specifically, the hydrodynamic diameter of the structures formed by these polymers in physiological solution have been studied at different temperatures to evaluate the influence of temperature on micelle formation and aggregation. Results reported a bimodal size distribution: the first peak was relative to micelles while the second one to aggregates of micelles.

Table1 (data obtained from size distribution profiles by volume and represented as mean ± standard deviation) reports the mean hydrodynamic diameter of NB-DHP407 and S-DHP407 micelles measured at 25, 37 and 45 °C. Upon temperature increase, the mean hydrodynamic diameter of the micelles increased from 27 nm to 30 nm for S-DHP407, while it remained fairly constant to 30 nm over the three tested temperature for NB-DHP407.These results showed that the size distribution remained stable with increasing temperature for NB-DHP407 in contrast to S-DHP407. However, it must be pointed out that S-DHP407 hydrodynamic diameter measured at 25 °C showed a high variability (as clearly evidenced by the high standard deviation) as a consequence of the high instability of S-DHP407-based micelles at that temperature. Differently, NB-DHP407-based micelles turned out to be more stable than S-DHP407-based ones already at 25 °C.

Table 1 *Mean hydrodynamic diameter of NB-DHP407 and S-DHP407 micelles measured at 25, 37 and 45 °C .*

	Diameter (nm) at **25°C**	Diameter (nm) at **37°C**	Diameter (nm) **45°C**
NB-DHP407 0.5% w/v	**30.27** ± 0.5	**29.97** ± 0.7	**30.21** ± 0.5
S-DHP407 0.5% w/v	**27.53** ± 12.5	**30.13** ± 1.3	**30.34** ± 1.25

As matter of fact, DLS measurements performed on NB-DHP407 samples allowed to evaluate sample stability overtime and at a specific temperature.

Figure 52 shows, for each analysed temperature, the size distributions both by intensity and volume for NB-DHP407 solubilized in aqueous medium at 0.5% w/v concentration in *three successive measurements*. The results highlighted that the size distribution was stable overtime at 30 °C, 37 °C

and 45 °C (the three profiles are perfectly superimposed one to another), while at 25 °C the size distribution resulted to be a little bit unstable because of the presence of free chains that are not arranged into micelles yet. Specifically, with the increasing of time the intensity of the peak relative to micelle formation was always higher and more stable, differently from the peak relative to micelle aggregates, which showed great variability among the three measurements. This was because with the increasing of temperature, new micelle complexes formed with integration and breaking up of micelles leading to unstable hydrodynamic diameters of micelles aggregates.

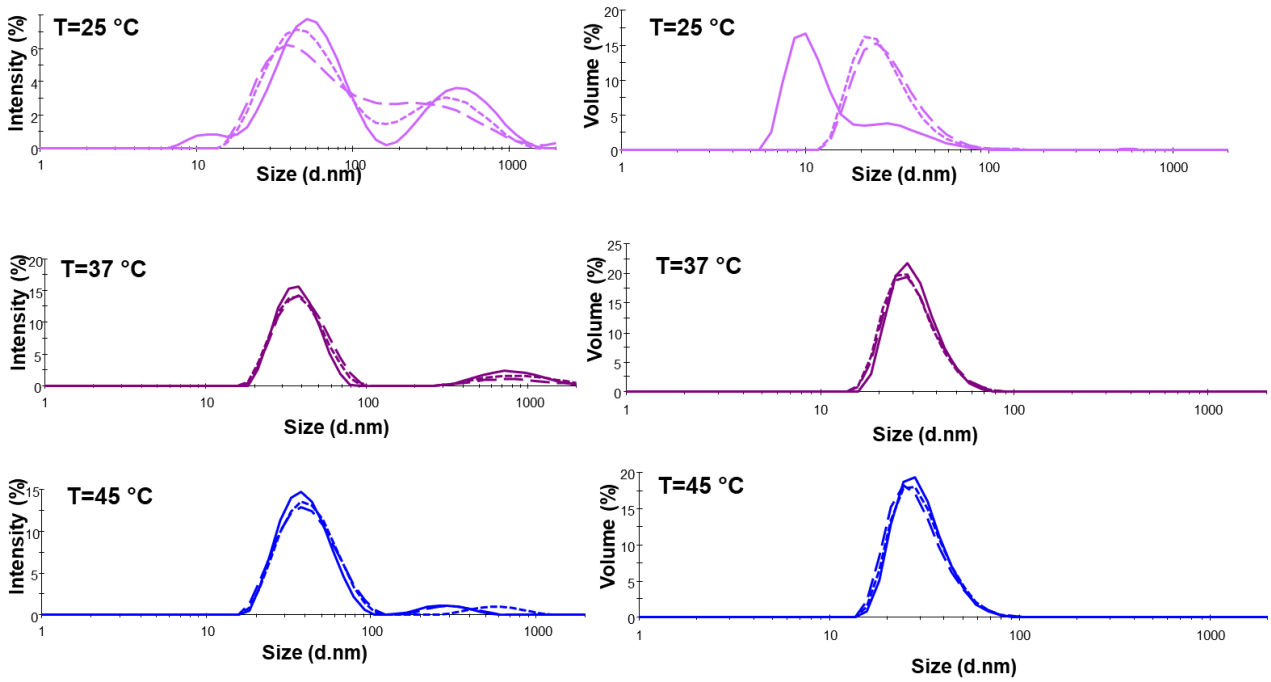

Figure 52 *Sample stability overtime investigated at 25 °C, 30°C, 37 °C and 45 °C. Profiles are reported by intensity (left column) and by volume (right colum).*

On the other hand, **Figure 53** shows the distribution patterns for *three different samples* of NB-DHP407 solubilized in aqueous medium at 0.5% w/v concentration at different temperatures. The results showed that the size distribution was stable at 30 °C, 37 °C and 45 °C (the three profiles are perfectly overlapped). On the contrary, at 25 °C the instability of the system, that stands out from three different size distribution profiles, was due to polymeric chains not yet arranged into micelles. Even in this case, it is possible to notice a great variability of the second peak upon temperature increase.

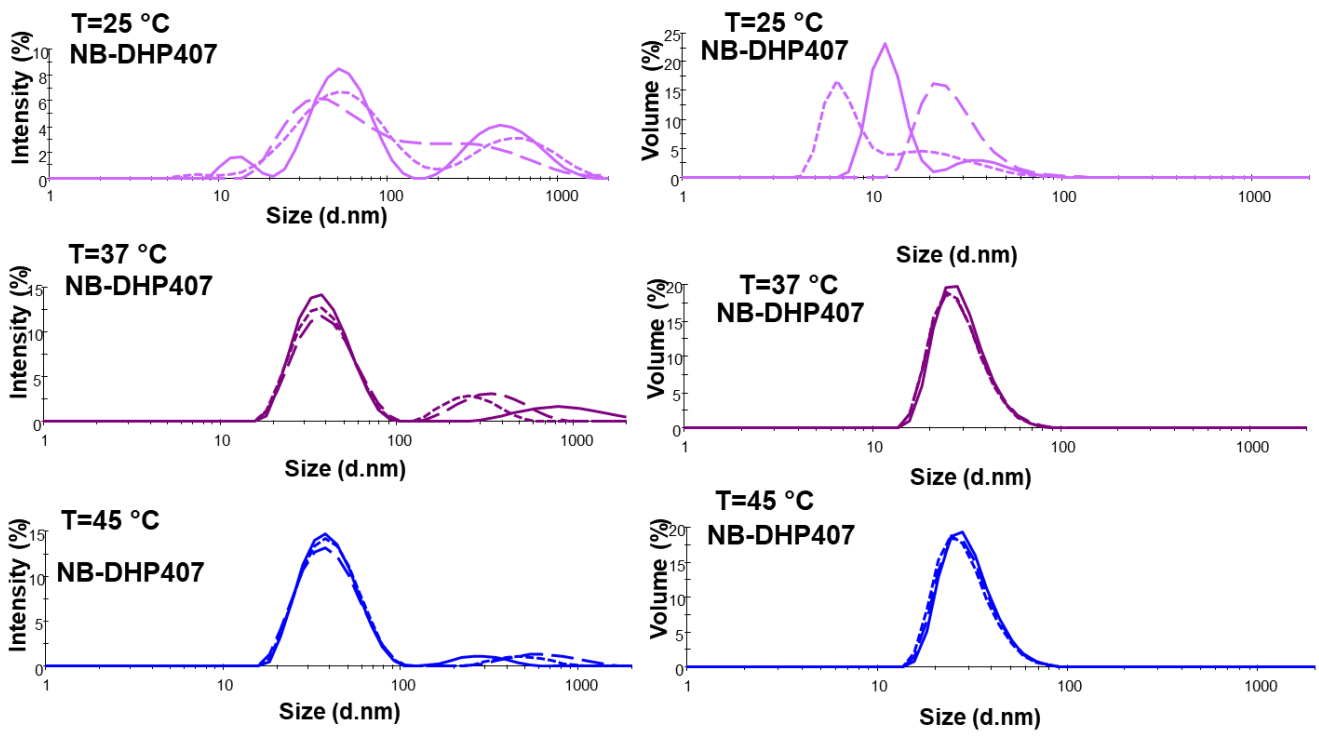

Figure 53 *DLS measurements carried out on three different samples to verify the repeatability of the system at 25 °C, 30°C, 37 °C and 45 °C. Profiles are reported by intensity (left column) and by volume (right colum).*

3.2. UV-Visible Spectroscopy to optimize photo-crosslinking parameters

UV-Vis spectroscopic analyses were performed on virgin molecules (i.e., TGA and NBE) to identify first the proper concentration of the photo-initiator (Eosin Y, EY, 0.1mM – 2mM).

Figure 54 shows that with increasing EY concentration from 0.1 to 2 mM, the absorbance changes upon irradiation at 525 nm increased both for samples with only EY and for the samples in which EY was mixed with TGA (EY+TGA). In this latter case, the intensification could be due to the role exerted by EY, which being a type II photo-initiator, interacted with TGA molecules generating a thyil radical after hydrogen abstraction. On the other hand, for each EY concentration tested, samples consisting of EY mixed with NBE (EY+NBE) had absorbance variations similar to samples made of only EY. Specifically, at low EY concentrations, the absorbance variations of EY+NBE systems resulted higher than EY sample. This could be probably due to EY interaction with carboxyl pendant groups of NBE molecules leading to hydrogen removal. Finally, for the samples containing both TGA and NBE (EY+TGA+NBE), the absorbance change at low EY concentrations appeared to be higher than for EY+TGA system. However, increasing EY concentration up to 1 mM the absorbance change became

lower. So, EY effect over TGA and NBE mixture seemed to decade in the presence of high EY concentration. This could be due to the effect of light attenuation and EY quenching at high EY concentrations, as reported in earlier articles [89]. For this reason, EY concentration of 0.5 mM resulted to be the proper concentration to have the highest absorbance change for EY+TGA+NBE system and so to be used for the subsequent photo-crosslinking tests.

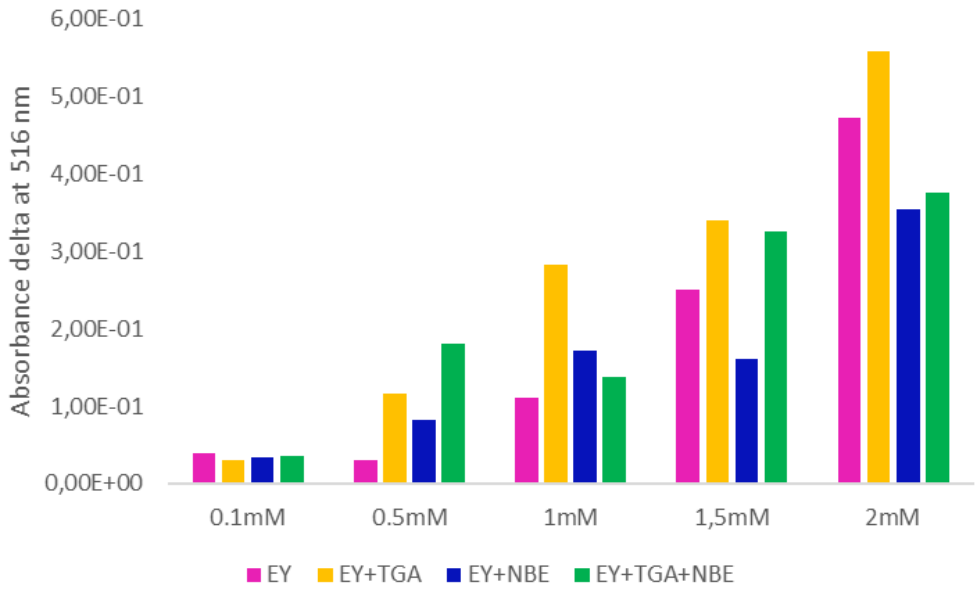

Figure 54 *UV-Vis spectroscopic analyses to investigate visible-light initiated photopolymerization by studying eosin-Y (EY) absorbance changes upon irradiation at 525 nm when mixed with thioglycolic acid (TGA) and 5-norbornene-2-carboxilic acid (NBE), alone or in combination.*

Then, by using the optimized EY concentration (0.5 mM), similar analyses were carried out to clarify the role exerted by the co-initiator tyrosine (TYR, 0.1mM – 10mM).

Figure 55 shows that increasing TYR concentration from 0.1 to 10 mM, the absorbance changes upon irradiation at 525 nm increased for the sample in which EY was used in combination with TYR with respect to EY containing system. This effect confirmed EY interaction with TYR. However, this interaction turned out to be more pronounced at low TYR concentrations. Concerning systems made of EY and TYR mixed with both TGA and NBE (EY+TYR+TGA+NBE), their absorbance changes appeared to be intermediate respect to those in which TGA and NBE were used alone (EY+TYR+TGA and EY+TYR+NBE, respectively) at low TYR concentrations. In contrast, at high TYR concentrations, the effect of EY+TYR+TGA and EY+TYR+NBE systems seemed to add up leading to a higher absorbance changes of EY+TYR+TGA+NBE system. So, 5 mM TYR concentration was selected, as it was the lowest concentration giving the best effect on the mixture.

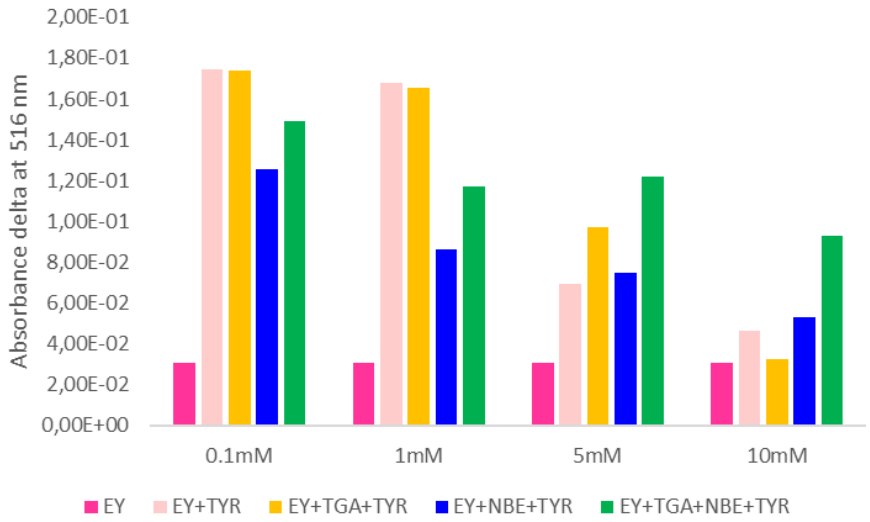

Figure 55 *UV-Vis spectroscopic analyses to investigate the role exerted by the co-initiator Tyrosine (TYR) in the thiol-ene system, adding different TYR concentrations to the previously optimized system*

Figure 56 compares the registered absorbance variation of the system in the presence and in the absence of TYR at 5 mM concentration. Interestingly, this latter condition showed the highest absorbance change for EY+TYR+TGA+NBE system. Therefore, these results suggested that no co-initiator is probably required to further improve thiol-norbornene reaction efficiency [54].

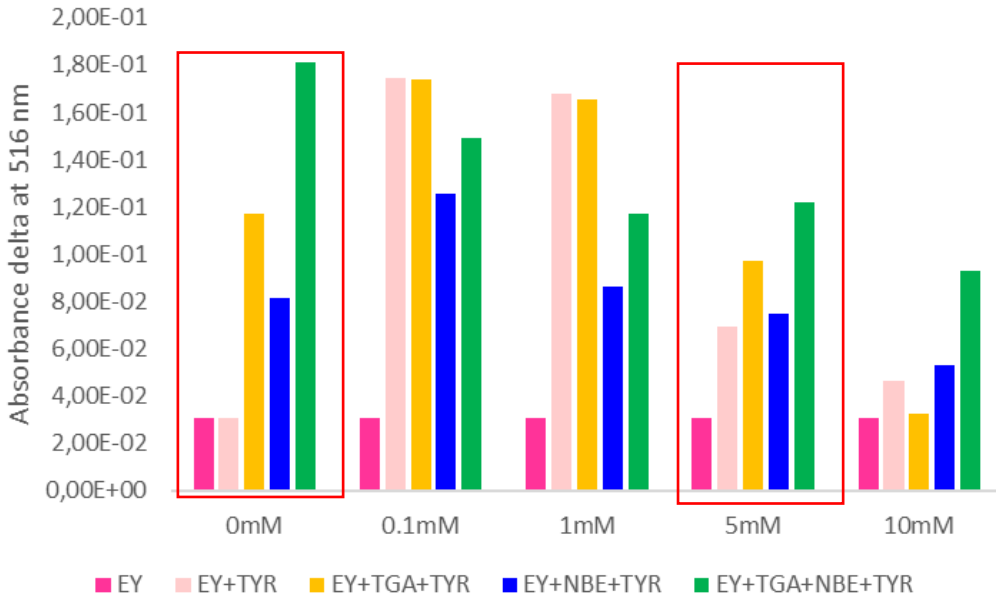

Figure 56 *Comparison between the optimized thiol-ene system with the addition of the optimized TYR concentration (5 mM) and without TYR (0 mM).*

4. Step-growth thiol-ene polyurethane-based hydrogels

4.1. Hydrogel formation

NB-DHP407/S-DHP407 hydrogels were prepared by dissolving the polymer at 18% w/v (1:1 molar ratio of functional groups) in phosphate saline buffer added with the previously optimized EY and TYR concentrations and then by irradiating at 525 nm, 80000Lux for 10 minutes. **Figure 57** shows an example of the final aspect of circular shaped hydrogels obtained after the photopolymerization. The colour of the PU solution is due to EY photo-initiator, characterized by a pink-red appearance. Specifically, NB-DHP407/S-DHP407 sol-gel system is shown before and after light exposure, respectively on the left and on the right side of the picture.

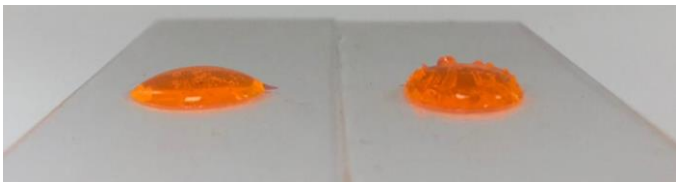

Figure 57 *NB-DHP407/S-DHP407 sol-gel system before (left) and after (right) light exposure*

4.2. Hydrogel Chemical Characterization

4.2.1 Attenuated Total Reflectance Fourier Transform Infrared (ATR-FTIR) spectroscopy

Attenuated Total Reflectance Fourier Transform Infrared (ATR-FTIR) spectroscopy was exploited as a qualitative method to verify the success of the visible light-induced photo-crosslinking between thiol and norbornene functional groups. **Figure 58** shows the comparison between NB-DHP407/S-DHP407-system spectra before and after light exposure. No evident differences were observed between the two spectra. Indeed, the bands attributed to the bonds that should form between norbornene molecules and thiol groups, i.e., the C-S or S-S bonds as by-products, were not detectable with the used instrument as they are out of the analysis range (600 - 4000 cm^{-1}). Indeed, the weak C-S and S-S stretching vibrations are reported to appear at 550-650 cm^{-1} and 500-600 cm^{-1}, respectively. Concerning the characteristic vibrational bands attributed to the urethane bonds, no differences were observed between the spectra, thus suggesting that the light intensity used in the photo-crosslinking process did not affect the integrity of polymer bonds.

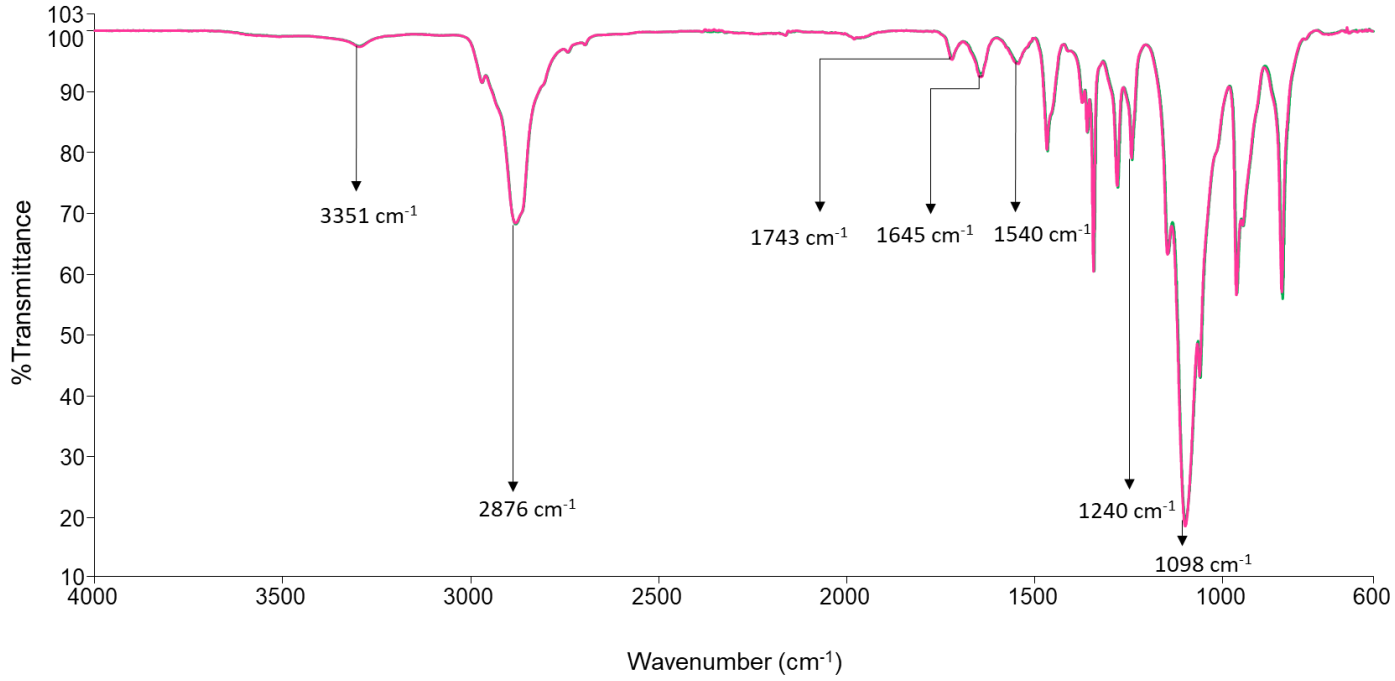

Figure 58 *ATR-FTIR spectra of NB-DHP407/S-DHP407-system before (green) and after (pink) light exposure. The characteristic vibrational bands of the poly(ether urethane)s are highlighted.*

4.2.2 Size Exclusion Chromatography (SEC)

Size Exclusion Chromatography (SEC) was used to estimate the number and the weight average molecular weights ($\overline{M_n}$ and $\overline{M_w}$, respectively) and the polydispersity index D=$\overline{M_w}/\overline{M_n}$ of NB-DHP407/S-DHP407-system before and after light exposure. $\overline{M_n}$ and $\overline{M_w}$ were measured to be approx. 20000 and 30000 Da, respectively, with a polydispersity index of 1.5 for both NB-DHP407/S-DHP407-systems before and after irradiation. **Figure 59** shows the molecular weight distribution profiles for both the analysed systems. No evident differences were observed for NB-DHP407/S-DHP407 system molar mass distributions before and after irradiation. However, a shift towards higher molar mass values was expected to occur after light exposure due to new bond formation between thiol and norbornene functional groups. The absence of differences between the two profiles could be probably due to the low increase in molecular weight that falls into the instrument error.

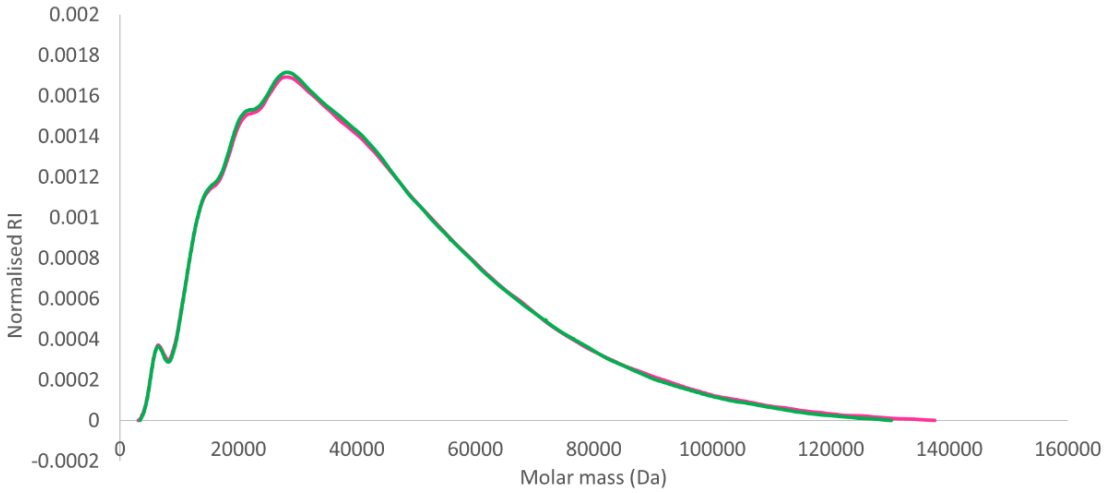

Figure 59 *Molecular weight distribution profiles before (green) and after (pink) light exposure*

4.2.3 Proton and Carbon Nuclear Magnetic Resonance (^{1}H NMR - ^{13}C NMR) Spectroscopy

To verify the success of visible light-initiated photo-crosslinking and, thus the formation of new bonds between the polymeric chains, ^{1}H NMR and ^{13}C NMR analyses were performed on photo-crosslinked NB-DHP407/S-DHP407 samples with the aim to quantify the residual norbornene and thiol groups.

Figure 60 shows ^{1}H NMR spectra of NB-DHP407/S-SHP407-system before and after light exposure. The reduction of the bands at 6-6.2 ppm and at 2-2.05 ppm, ascribed to the resonance of the hydrogen involved in the norbornene double bonds and to norbornene aliphatic protons, respectively, confirmed the successful photo-induced formation of a cross-linked network. However, there was not a total disappearance of the two NBE characteristic bands after irradiation. This could be ascribed to different issues: (i) to the higher weight amount of NB-DHP407 with respect to S-DHP407 one as a consequence of the different functionalization degree. Indeed, to keep a 1:1 molar ratio thiol-ene, NB-DHP407/S-DHP407 polymers were mixed at 99:1 weight ratio, thus limiting the probability of thiol groups to react with norbornene double bonds; (ii) to the norbornene hydrophobic nature which could affect their exposure in a watery environment, thus lowering their reactivity, and (iii) to the fact that thiol groups could react with themselves forming S-S disulphide bonds, thus lowering the amount of thiol groups available to react with norbornene moieties. However, to better clarify the reason of this un-complete double bond reaction and further supporting the hypothesis of disulphide bond formation, ^{13}C NMR analyses were also performed.

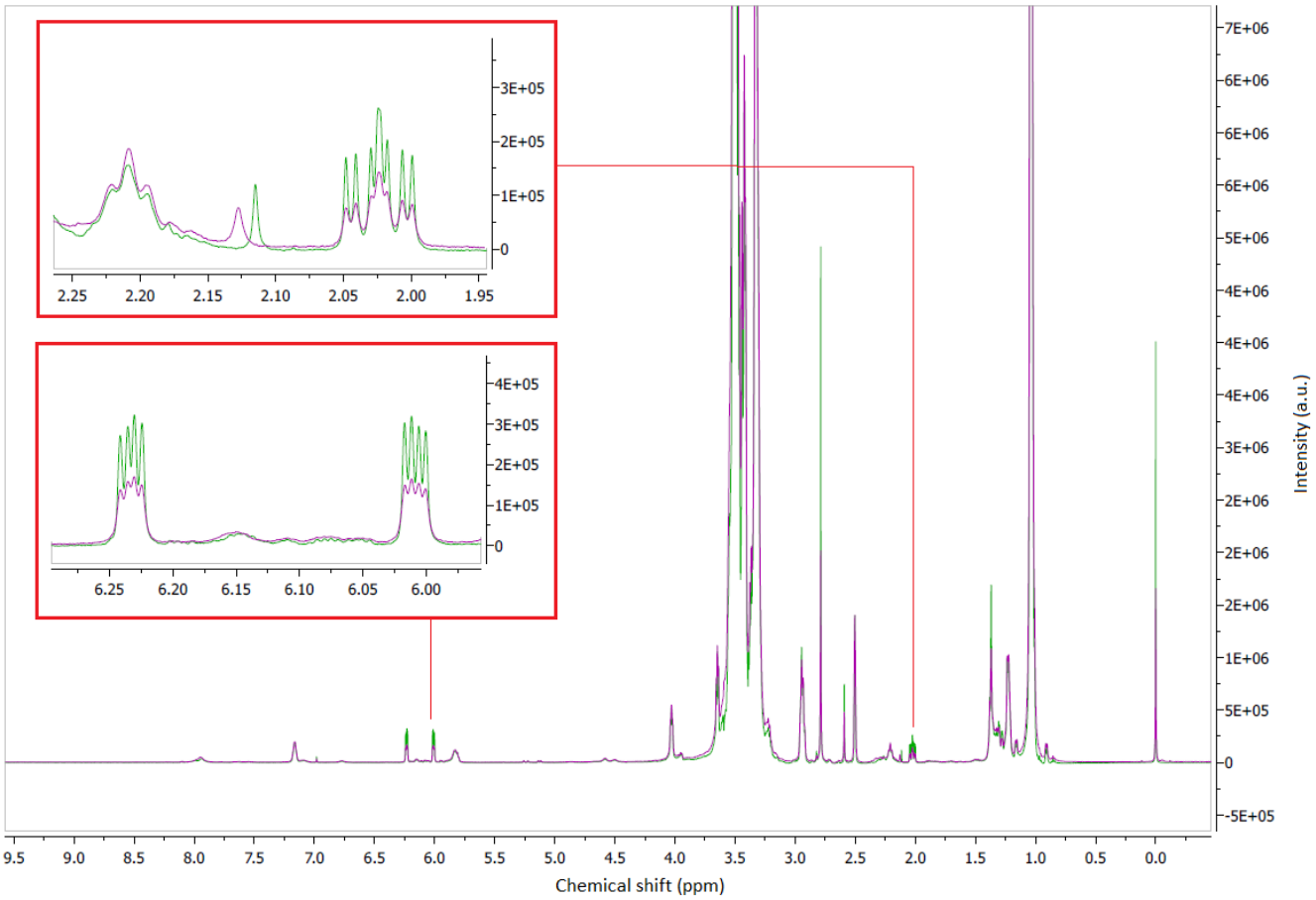

Figure 60 *^{1}H-NMR spectra of NB-DHP407/S-DHP407-system before (green) and after (pink) light exposure. The inserts highlight differences between the spectra.*

Figure 61 shows ^{13}C NMR spectra of NB-DHP407/S-SHP407-system before and after light exposure. Upon irradiation, the reduction of the bands at 132 and 138 ppm, ascribed to the resonance of norbornene double bonds, further confirmed the successful formation of the photo-induced cross-linked network and the presence of un-reacted functional groups in accordance with ^{1}H NMR results. Furthermore, ^{13}C NMR spectra of NB-DHP407/S-SHP407 systems showed another set of characteristic peaks at 170.3 and 170 ppm that could be ascribed to the carbonyl group involved in the amide bond between D-DHP407-NH and TGA preserving the free -SH moieties or converted in S-S bonds, respectively. Specifically, the reduction of the peak at 170.3 ppm, together with the reduction of the band at 6-6.2 ppm in the ^{1}H NMR spectrum, further proved the formation of covalent bonds between thiol and norbornene moieties. However, also a little amount of thiols still remained un-reacted. Furthermore, the invariance of the peak at 170 ppm suggested that no disulphide bonds were formed upon irradiation (in case of -S-S- bond formation this peak is expected to increase compared to the not-irradiated sample).

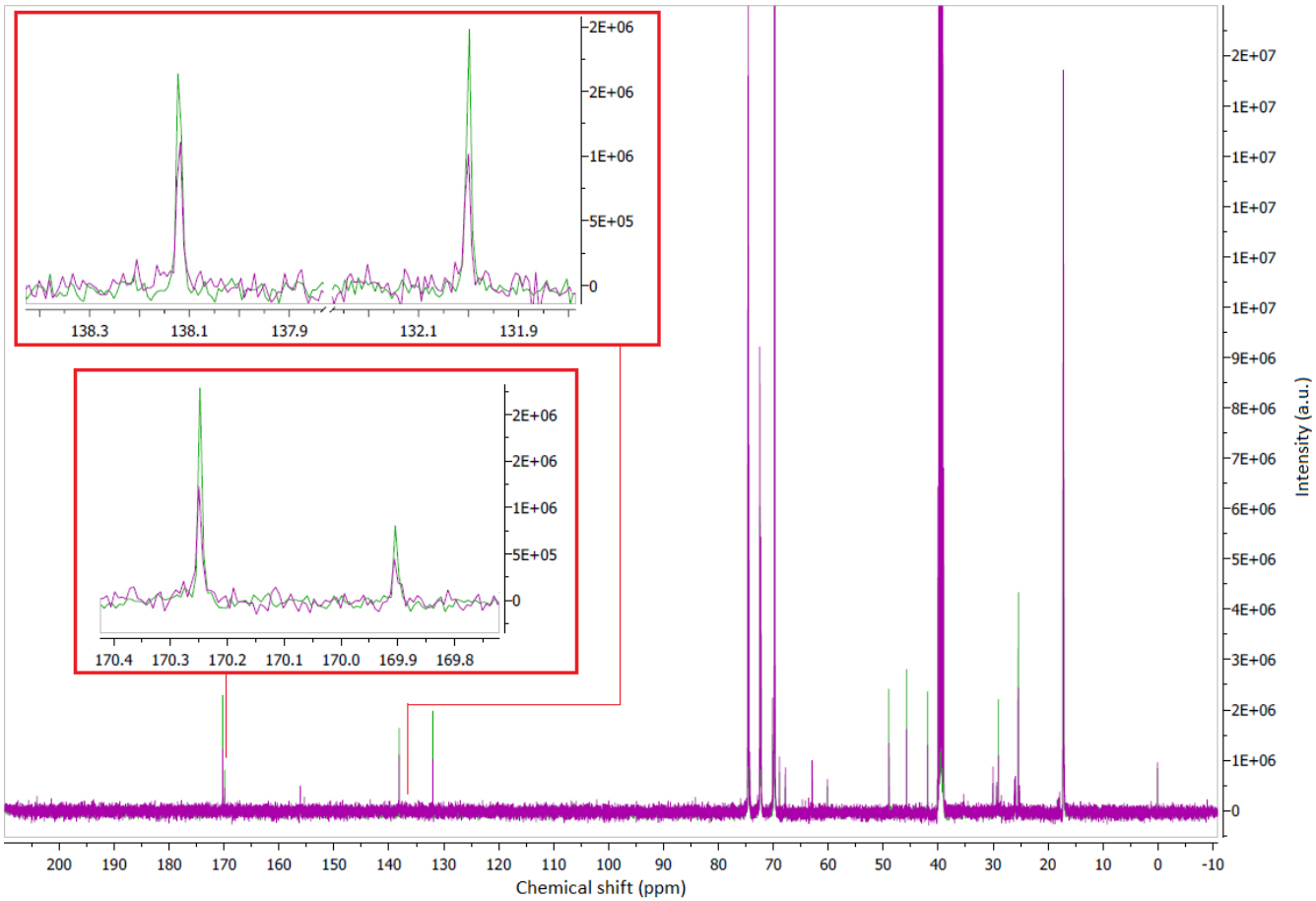

Figure 61 *^{13}C-NMR spectra of NB-DHP407/S-DHP407-system before (green) and after (pink) light exposure. The inserts highlight differences between the spectra*

Therefore, the presence of un-reacted thiols and double bonds opens the way to further improve the crosslinking efficiency by adjusting the irradiation parameters (e.g., irradiation time, light intensity).

4.2.4. Dynamic Light Scattering (DLS) analyses: measurement of the average micelle hydrodynamic diameter

The Dynamic Light Scattering (DLS) technique was used to investigate the influence of irradiation on the micelle hydrodynamic diameter of NB-DHP407/S-DHP407 samples. Specifically, samples were prepared as previously described and then diluted in physiological saline solution to reach a final 0.5% w/V concentration.

In **Table 2** (data obtained from size distribution profiles by intensity and volume are represented as mean ± standard deviation) it is possible to notice that upon irradiation, the mean hydrodynamic diameter of the micelles increased from 29.4±0.4 nm to 31±1.1 nm. This could be due to the thiol-

ene photo-crosslinking reaction occurring between the polymeric chains, which resulted in the formation of higher molecular weight polymeric chains that arranged in larger micelles. The same consideration can be obtained evaluating the mean hydrodynamic diameter obtained from size distribution profile by intensity.

Table 2 *Comparison between NB-DHP407/S-DHP407 sample hydrodynamic diameter at 37°C before and after light exposure*

	Diameter (nm) at 37°C INTENSITY	**Diameter (nm) at 37°C VOLUME**
NB-DHP407+S-DHP407 0.5% w/v_ pre-irradation	**46.3** ± 5.8	**29.4** ± 0.4
NB-DHP407+S-DHP407 0.5% w/v_post-irradiation	**47.8** ± 6.8	**31.10** ± 1.1

Figure 62 shows the size distribution profiles by intensity and by volume for NB-DHP407/S-DHP407 solutions at 0.5% w/v concentration before and after irradiation. After irradiation, the size distribution showed a slight shift towards higher hydrodynamic diameters that proved the formation of bigger structures, resulting from the crosslinking between the micelles through the thiol-ene photo-crosslinking.

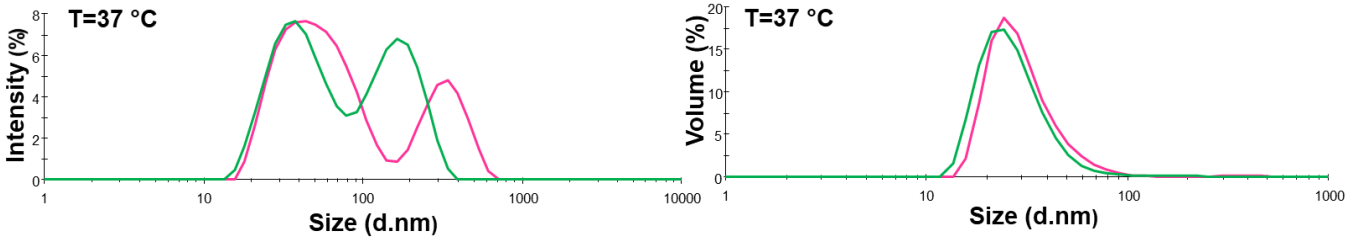

Figure 62 *DLS measurement results for a 0.5% w/v concentrated NB-DHP407/S-DHP407 solution before (green) and after (pink) light exposure.*

4.2. Rheological characterization

4.2.1 Frequency sweep tests

Frequency sweep tests were performed to study the kinetics of gel formation and development. To this aim, the storage (G') and the loss (G'') moduli were measured at three different temperatures (25 °C, 30 °C, 37 °C) as a function of applied angular frequency in the range 0.1-100 rad/s.

Furthermore, exploiting the possibility of the developed systems to return in a sol-state even after light exposure when temperature decreased under its critical gelation temperature, these tests were performed on photo-crosslinked hydrogels upon their gel-to-sol transition. Specifically, these tests aimed at:

1. Studying the efficiency of thiol-norbornene photo-crosslinking mechanism;
2. Investigating the role exerted by tyrosine as co-initiator;
3. Highlighting the differences, in terms of mechanical properties, between two different thiol-ene photo-crosslinked hydrogels (i.e., thiol-norbornene developed in this work and thiol-acrylate investigated in a previous work [86]).

Figure 63, 64 and **65** report the comparison between NB-DHP407/S-DHP407-based sol-gel systems at 18% w/V concentration added with photo-initiator EY (0.5mM) before and after light exposure.

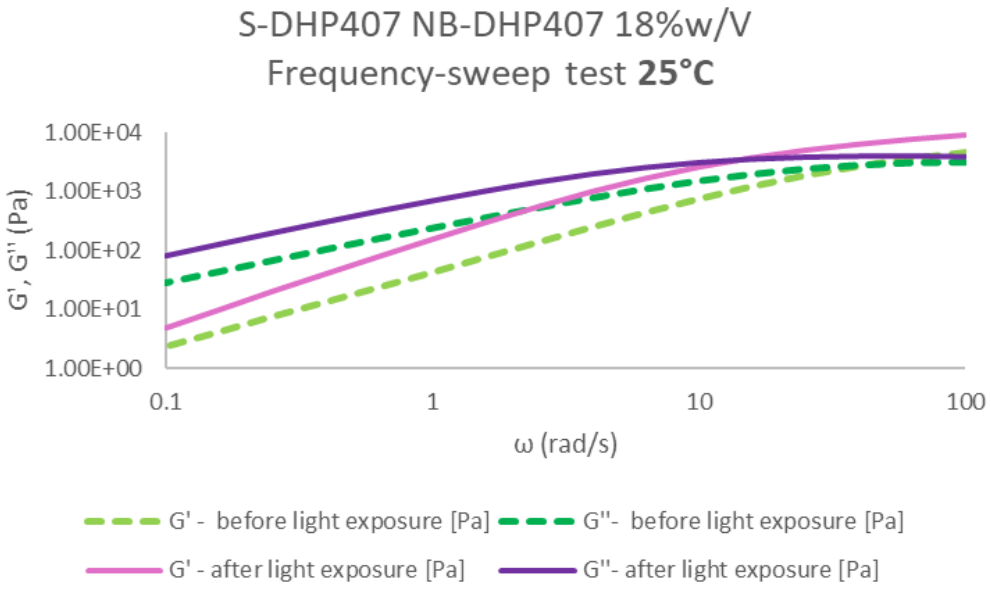

Figure 63 *Storage (G') and Loss (G'') moduli trend as a function of angular frequency for NB-DHP407/S-DHP407 sol-gel system at 18% w/v concentration at 25°C before (pink-purple) and after (green) light exposure.*

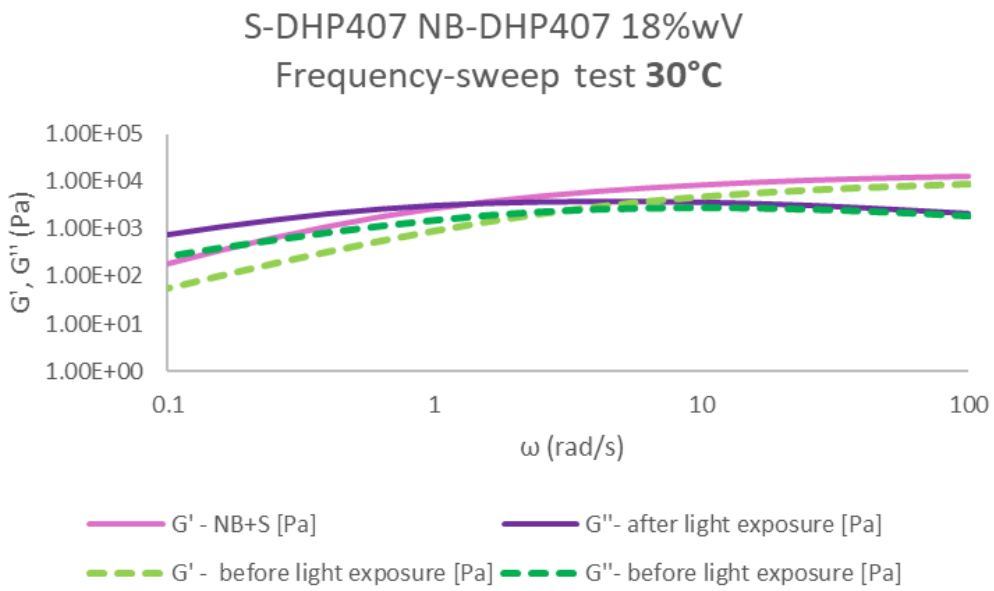

Figure 64 *Storage (G') and Loss (G'') moduli trend as a function of angular frequency for NB-DHP407/S-DHP407 sol-gel system at 18% w/v concentration at 30°C before (pink-purple) and after (green) light exposure.*

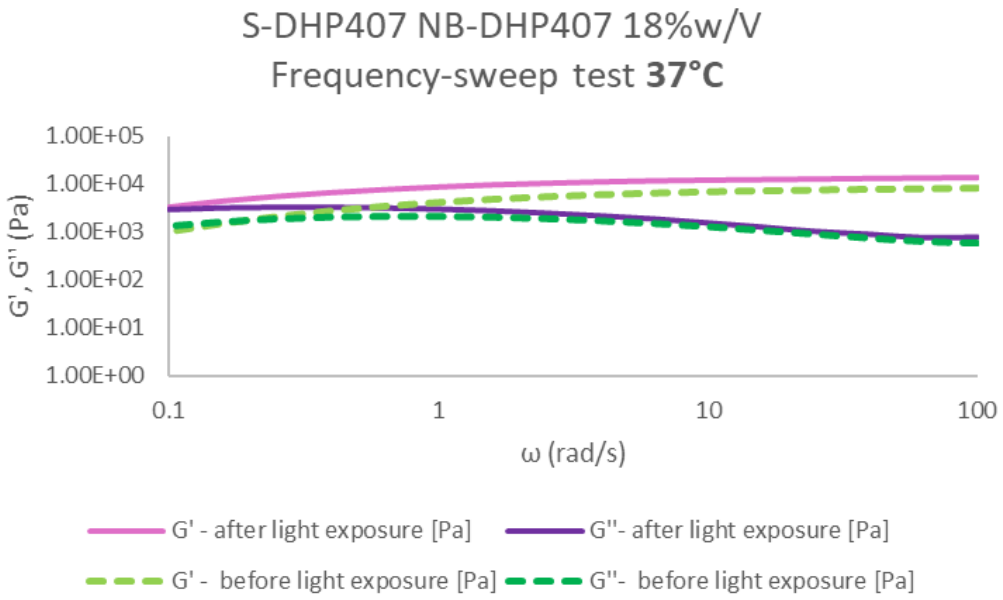

Figure 65 *Storage (G') and Loss (G'') moduli trend as a function of angular frequency for NB-DHP407/S-DHP407 sol-gel system at 18% w/v concentration at 37°C before (pink-purple) and after (green) light exposure.*

The crossover frequencies derived from the graphs for the two PEU-based hydrogels before and after light exposure (S-DHP407/NB-DHP407 pre-light and S-DHP407/NB-DHP407 light) are reported in **Table 3**.

Table 3 *Crossover frequencies for NB-DHP407/S-DHP407 photo-crosslinked hydrogel at 18% w/v concentration before (green) and after (pink) light irradiation in the presence of EY at 0.5 mM at three different temperatures (25°C, 30°C and 37 °C)*

	Crossover frequency (rad/s)		
	25 °C	30 °C	37 °C
S-DHP407/NB-DHP407 pre-light	41	3	0.18
S-DHP407/NB-DHP407 light	15	1.4	<0.1

These results can be used to investigate the hydrogel development upon light exposure. Comparing the cross-over frequencies between hydrogels before and after irradiation, lower crossover frequencies for S-DHP407/NB-DHP407-light were estimated. This result was indicative of more developed gels after light exposure, confirming successful photo-induced network formation.

Figure 66, 67 and **68** show the comparison between two photo-crosslinked hydrogels:

-NB-DHP407/S-DHP407-based sol-gel systems added with photo-initiator EY (0.5 mM) and co-initiator TYR (5 mM);

-NB-DHP407/S-DHP407-based sol-gel systems added with photo-initiator EY (0.5 mM)

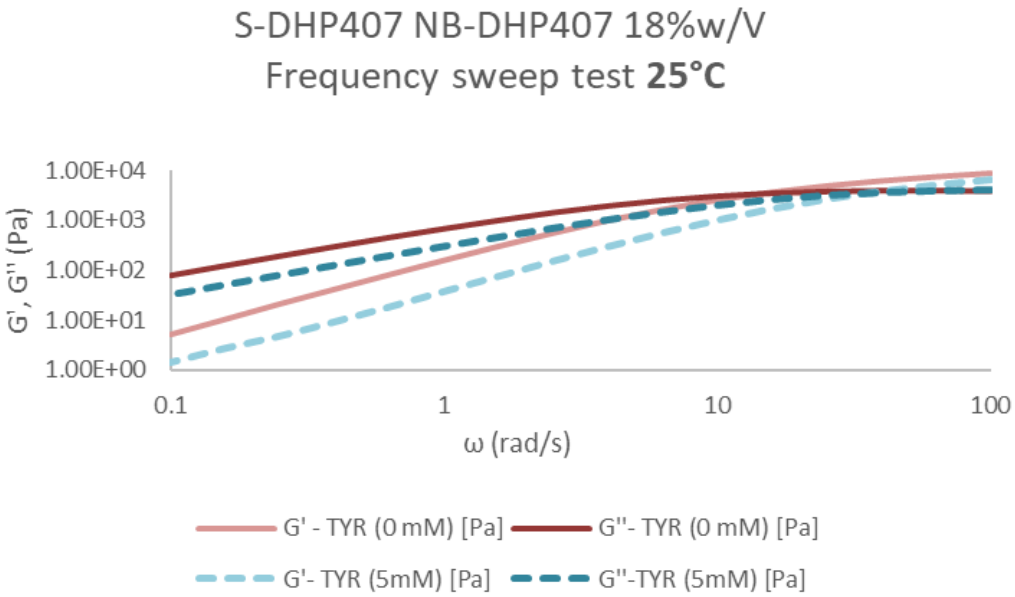

Figure 66 *Storage (G') and Loss (G'') moduli trend as a function of angular frequency for NB-DHP407/S-DHP407 sol-gel system at 18% w/v concentration at 25°C with (blue) and without (red) the addition of co-initiator TYR.*

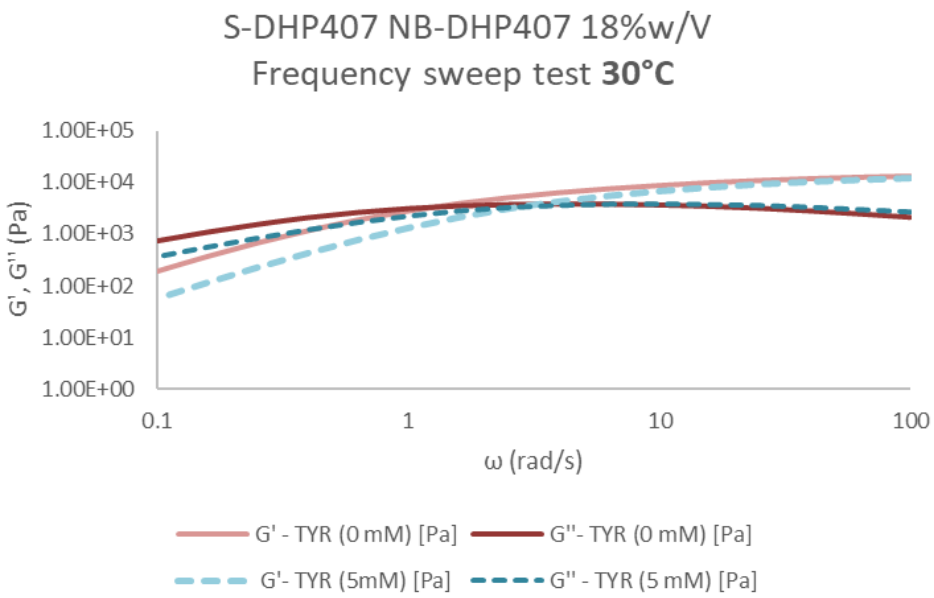

Figure 67 *Storage (G') and Loss (G'') moduli trend as a function of angular frequency for NB-DHP407/S-DHP407 sol-gel system at 18% w/v concentration at 30°C with (blue) and without (red) the addition of co-initiator TYR.*

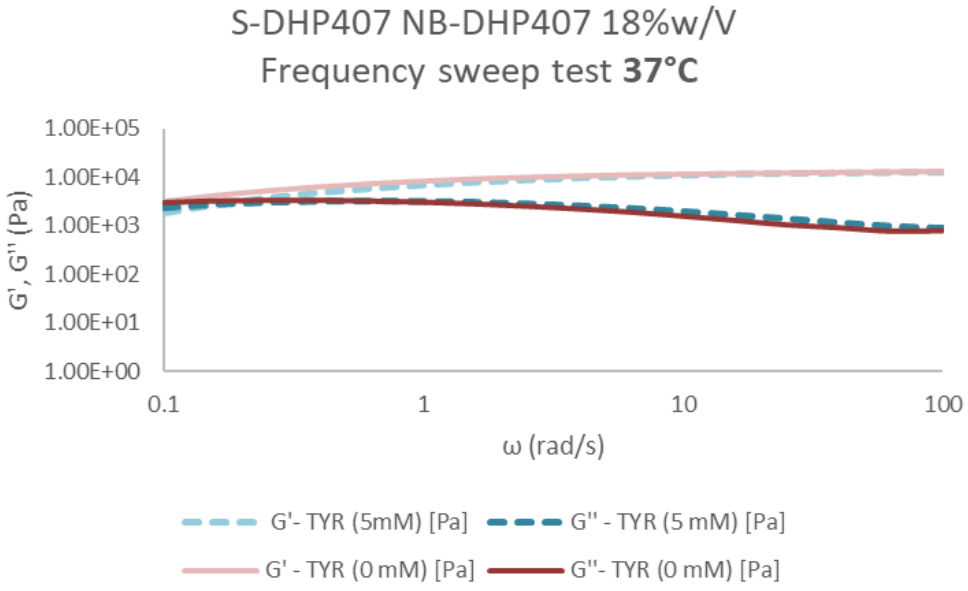

Figure 68 *Storage (G') and Loss (G'') moduli trend as a function of angular frequency for NB-DHP407/S-DHP407 sol-gel system at 18% w/v concentration at 37°C with (blue) and without (red) the addition of co-initiator TYR.*

In general, when the values of the storage modulus G' becomes higher than the loss modulus G'', the system state changes from sol to gel; the G'/G'' crossover frequency, which identifies the sol-to-gel transition, is expected to move towards lower frequencies as a consequence of temperature increase. The crossover values that can be derived from the graphs for the two PEU-based hydrogels are reported in **Table 4**.

Table 4 *Crossover frequencies of NB-DHP407/S-DHP407 photo-crosslinked hydrogels with 18% w/v concentration with (blue) or without (red) the addition of TYR as co-initiator at three different temperatures (25°C, 30°C and 37 °C)*

	Crossover frequency (rad/s)		
	25 °C	30 °C	37 °C
S-DHP407/NB-DHP407	15	1.4	<0.1
S-DHP407/NB-DHP407T-TYR 5mM	42	3.2	0.15

Comparing the cross-over frequencies between the two hydrogels with or without the addition of TYR (S-DHP407/NB-DHP407-TYR 5mM and S-DHP407/NB-DHP407, respectively) lower crossover frequencies were measured for S-DHP407/NB-DHP407 sample at each temperature. These evidences suggested the formation of more developed gels without the use of a co-initiator and thus, further confirmed the results obtained through UV-Vis spectroscopic analyses. However, both hydrogels at the selected concentrations were not fully developed gels at 37°C, since the difference between G' and G'' at 0.1 rad/s was less than an order of magnitude. For tissue engineering applications, it is generally required for the hydrogels to be fully developed at physiological temperature; however, in the perspective of using these materials as bioinks for RP techniques, this not fully gel state can be useful to provide a less stressful environment when cells are inserted in the solution and printed.

Finally, the rheological characterization was also exploited to compare two photo-crosslinked thiol-ene systems: thiol-norbornene (NB-DHP407/S-DHP407) and thiol-acrylate (A-DHP407/S-DHP407), respectively. Specifically, NB-DHP407/S-DHP407-based sol-gel systems containing 0.5mM EY was compared to A-DHP407/S-DHP407-based sol-gel system added with EY 1mM and triethanolamine (TEOA) 7.5mM as co-initiator (this second composition resulted from an optimization of the system carried out in a previous work [86]).

Figure 69, **70** and **71** show the results of frequency sweep test carried out on the two photo-crosslinked hydrogels at 18%w/V concentration at three different temperatures (25 °C, 30 °C and 37 °C).

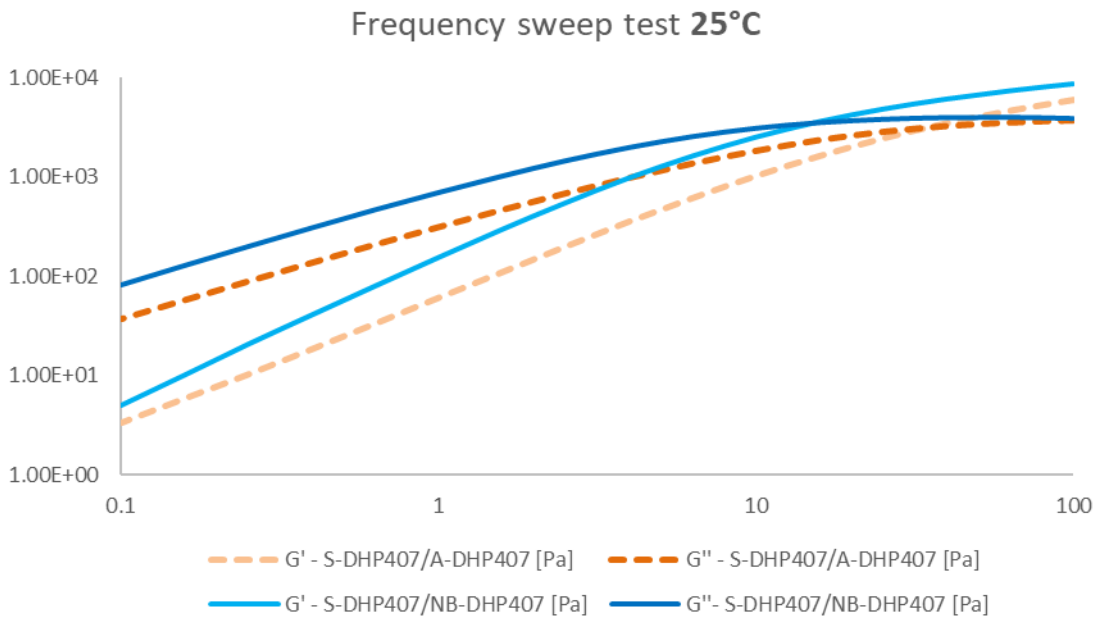

Figure 69 *Storage (G') and Loss (G'') moduli trend as a function of angular frequency for NB-DHP407/S-DHP407 (blue) and A-DHP407/S-DHP407 (orange) sol-gel system at 18% w/v concentration at 25°C.*

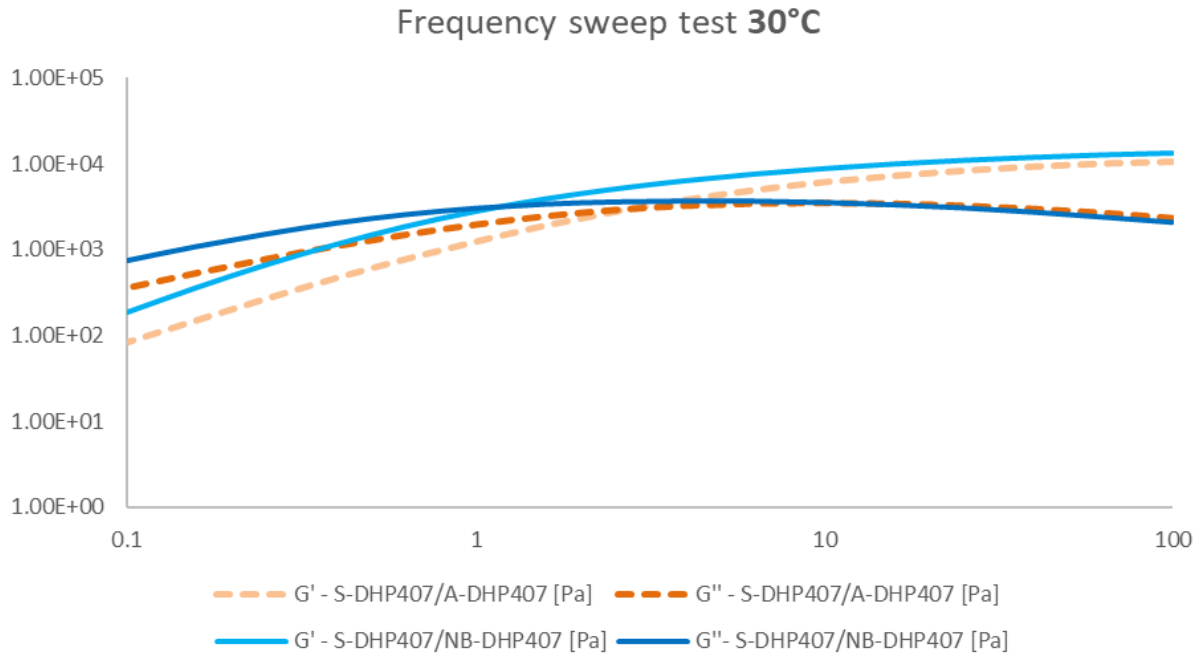

Figure 70 *Storage (G') and Loss (G'') moduli trend as a function of angular frequency for NB-DHP407/S-DHP407 (blue) and A-DHP407/S-DHP407 (orange) sol-gel system at 18% w/v concentration at 30°C.*

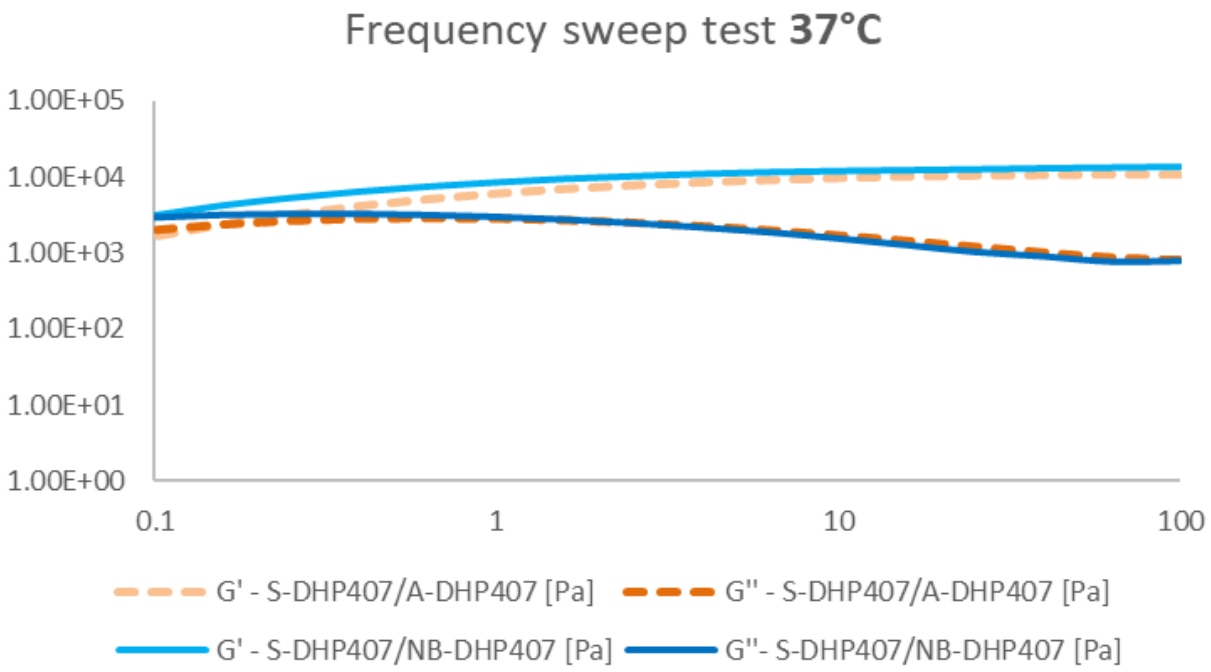

Figure 71 *Storage (G') and Loss (G'') moduli trend as a function of angular frequency for NB-DHP407/S-DHP407 (blue) and A-DHP407/S-DHP407 (orange) sol-gel system at 18% w/v concentration at 37°C.*

The crossover frequencies of these two thiol-ene systems (derived from the three previous graphs) are reported in **Table 5.**

Table 5 *Crossover frequencies of NB-DHP407/S-DHP407 (blue) and S-DHP407/A-DHP407 (orange) photo-crosslinked hydrogels at 18% w/v concentration added with the optimized concentration of initiator and/or co-initiator at three different temperatures (25, 30 and 37 °C)*

	Crossover frequency (rad/s)		
	25 °C	30 °C	37 °C
S-DHP407/NB-DHP407	15	1.4	<0.1
S-DHP407/A-DHP407	34	2.8	0.16

At each analysed temperature, the crossover frequency of S-DHP407/NB-DHP407 photo-crosslinked hydrogels turned out to be lower than that of S-DHP407/A-DHP407 gels, suggesting that thiol-norbornene photo-crosslinked hydrogels were more developed with respect to thiol-acrylate ones. The achievement of higher mechanical properties (loss and storage moduli) could be due to the photo-crosslinking mechanism itself, which is not affected by homo-polymerization and oxygen

inhibition [53]. Moreover, it was possible to assess that thiol-acrylate photo-crosslinking required a higher photo-initiator concentration (EY 1 mM) and the addition of a co-initiator (TEOA) with respect to thiol-norbornene system in which EY was present at 0.5 mM concentration and no co-initiator was required.

4.2.2 Strain sweep tests

In order to study hydrogel resistance to an applied deformation at 37 °C and constant frequency (10 Hz), strain sweep tests were performed on the previously analysed polyurethane-based systems.
All graphs (**Figure 72 - 74**) report the trend of storage (G') and loss (G'') moduli over strain within the range 0.1-500%. Initially, both moduli presented constant values; then, G' decreased and G'' increased after a critical value of deformation γ was reached before the breaking of the gel.
More in detail, **Figure 72** shows the comparison between NB-DHP407/S-DHP407-based sol-gel systems at 18% w/v concentration before and after irradiation, while **Figure 73** highlights the differences between NB-DHP407/S-DHP407-based sol-gel systems with or without the addition of tyrosine as co-initiator (5mM concentration) upon light exposure. **Figure 74**, instead, shows the comparison between thiol-norbornene and thiol-acrylate photo-crosslinked hydrogels. Each comparison did not show significant differences between the two gels in terms of resistance to applied strain. However, evaluating the differences between storage and loss moduli (ΔG =G'-G'') at 0.01% strain, listed for each system together with the graph, it was possible to have further information about gel development. Specifically, higher ΔG indicated more developed hydrogels at 37 °C. Results were in accordance with frequency sweep tests, further confirming previous analyses.

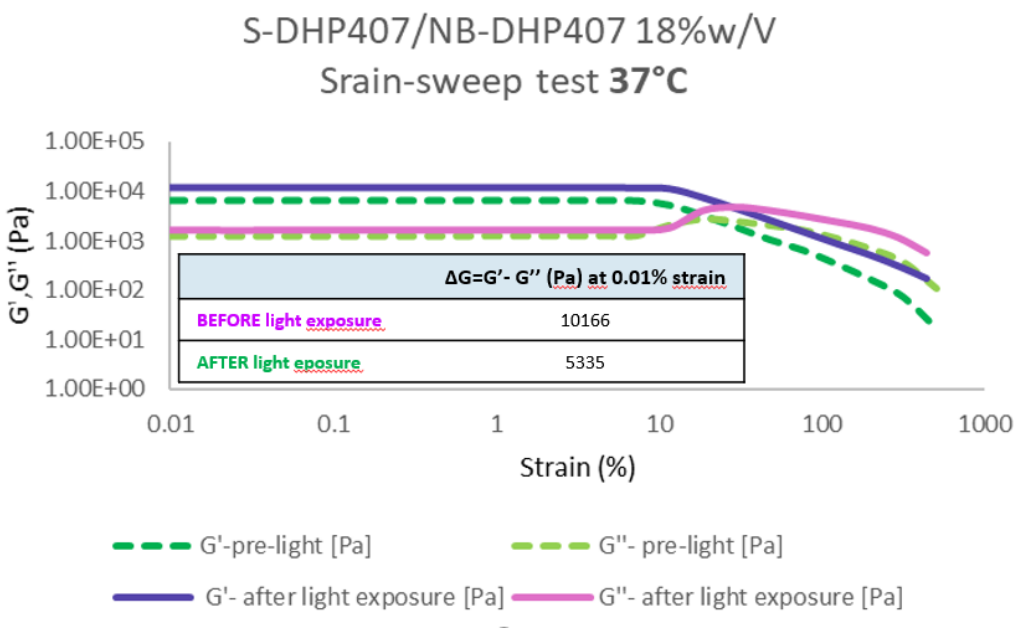

Figure 72 *Storage and Loss moduli trend as a function of applied strain for NB-DHP407/S-DHP407 sol-gel system at 18% w/v concentration at 37°C before (pink-purple) and after (green) light exposure.*

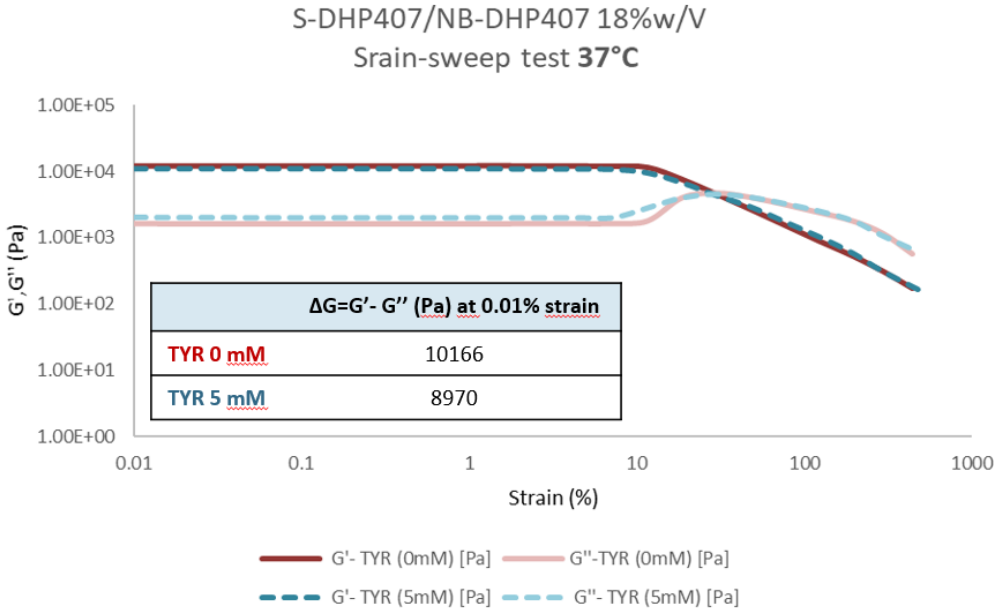

Figure 73 *Storage and Loss moduli trend as a function of applied strain for NB-DHP407/S-DHP407 sol-gel system at 18% w/v concentration at 37°C with (blue) or without (red) the addition of co-initiator TYR..*

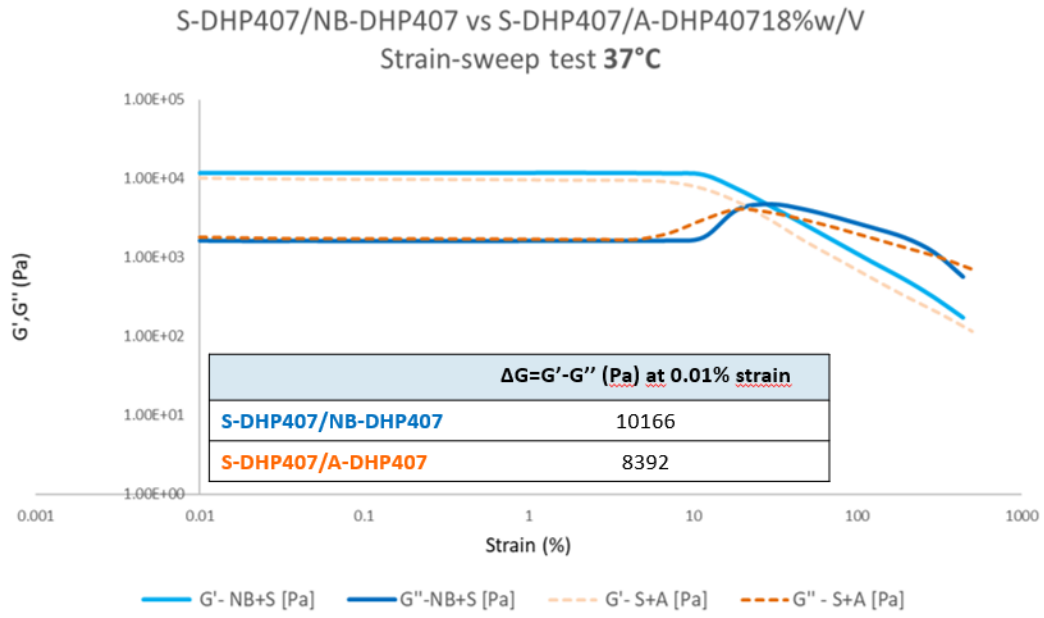

Figure 74 *Storage and Loss moduli trend as a function of applied strain for S-DHP40/NB-DHP407 (blue) and S-DHP407/A-DHP407(orange) sol-gel system at 18% w/v concentration at 37°C.*

The following tables summarize the resistance to deformation (i.e., strain at break γ) for thiol-ene based sol-gel systems at 18% w/v concentration in the previously analysed three different conditions:

- NB-DHP407/S-DHP407before and after light exposure (**Table 6**),
- NB-DHP407/S-DHP407 with or without the addition of TYR (5 mM concentration) upon light exposure (**Table 7**),
- Thiol-ene sol-gel systems, NB-DHP407/S-DHP407 and S-DHP407/A-DHP407, respectively, which undergo a different crosslinking reaction upon irradiation with visible light (**Table 8**).

Table 6 *Strain at break (γ) for NB-DHP407/S-DHP407 based sol-gel systems before and after light exposure*

	γ (%)
AFTER light exposure	11.6
BEFORE light exposure	7.3

Table 7 Strain at break (γ) for NB-DHP407/S-DHP407 based sol-gel systems with or without the addition of TYR upon light exposure

	γ (%)
TYR (0 mM)	11.6
TYR (5 mM)	7.3

Table 8 Strain at break (γ) for S-DHP407/NB-DHP407 and S-DHP407/A-DHP407based sol-gel systems after light exposure

	γ (%)
S-DHP407/NB-DHP407	11.6
S-DHP407/A-DHP407	6.2

Strain at break resulted to be higher for the systems which appeared to be more developed from the previous frequency sweep tests, confirming higher mechanical properties also in terms of hardening effect.

5. 3D bioprinting

Figure 75 shows the main steps of the 3D printing process. Specifically, the CAD 3D model of a square meshed grid (created using Solidworks as CAD softwareI), the sliced structure (obtained using Slice3r software) and the resulting G-code file (Repetier-Host software).

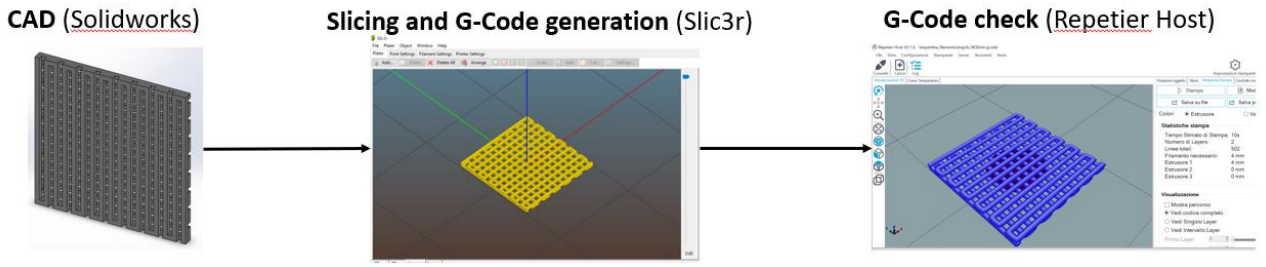

Figure 75 Schematic representation of the three main steps of 3D printing process: 3D modelling, slicing and G-code generation of a square meshed grid.

Among the tested parameters, those which turned out to give the *best square meshed grids* in term of shape fidelity and capability to obtain regular structures with a continuous filament turned out to be *G25 nozzle size, 100 kPa printer pressure and 30% feed-rate*.

Figure 76 shows a comparison between the printed grid before and after light exposure, obtained by exploiting first only hydrogel thermo-sensibility and then, also Vis light responsiveness. From this microscopic image is evident that the photo-crosslinking reaction is essential to obtain higher regular structures (e.g., the holes of the not-photo-crosslinked grid collapse rapidly after the printing process).

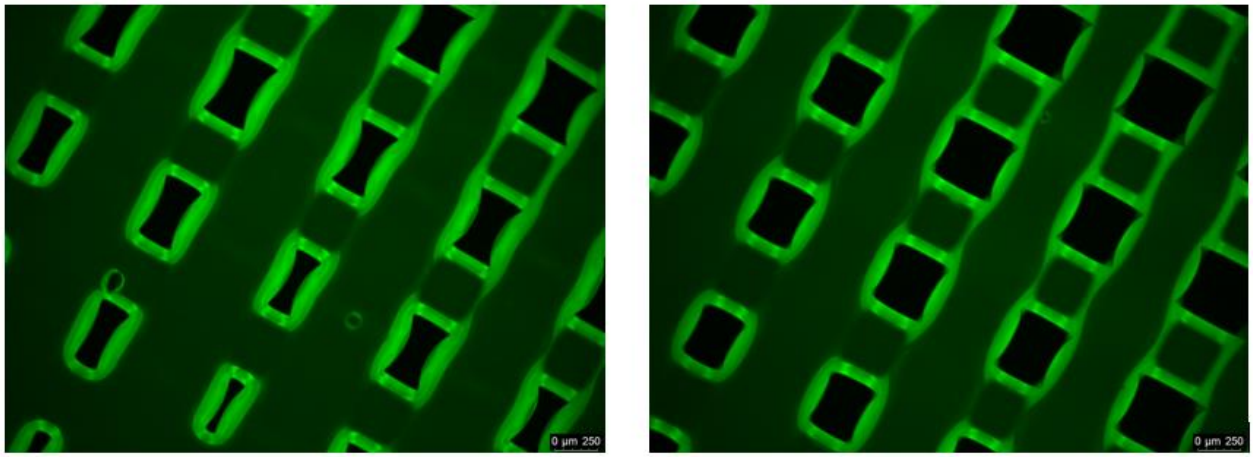

Figure 76 36 *Comparison between the printed grid before (left) and after (right) light exposure.*

However, from **Figure 77,** which shows the printing process of a two-layer square meshed grid, it is possible to confirm the printability of the bioink under the previously optimized conditions.

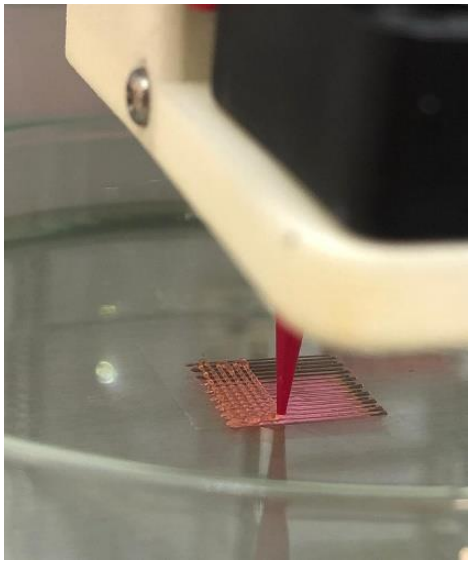

Figure 77 *Printing process of two-layer square meshed grid.*

Finally, in order to investigate more complex geometries able to better adapt to irregular tissue defects, the honeycomb-like structures of different sizes (hexagon dimension ranging from 2 to 5 mm) were printed and photo-crosslinked.

Figure 78 shows the main steps of the 3D printing process. Specifically, the CAD 3D model of a honeycomb-like structure (created using Solidworks as CAD softwareI), the sliced structure (obtained using Slice3r software) and the resulting G-code file (Repetier-Host software).

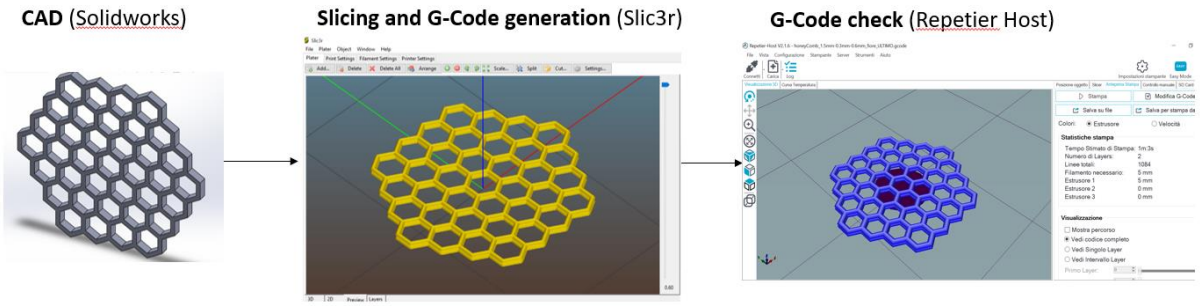

Figure 78 *Schematic representation of the three main steps of 3D printing process: 3D modelling, slicing and G-code generation of a honeycomb-like structure.*

For each honeycomb-like structure model the CAD 3D model, a photograph and a microscope image (representative of a mean structure dimension among the ten analysed) are reported. The comparison between the CAD-3D model and the printed filament dimension (obtained using microscope images) was used to evaluate the resulting printing resolution achieved for each construct-size. Indeed, the optimized printed parameters (nozzle size, printer pressure and feed-rate) are stated for each structure.

5 mm Honeycomb:

Figure 79 shows the 3D CAD model of the honeycomb-like structure, reporting the dimensions in millimetres (hexagon hole dimension: 5 mm, filament dimension: 0.7mm), modelled using Solidworks as CAD software. Therefore, the nozzle diameter used to print this structure was a G22 nozzle.

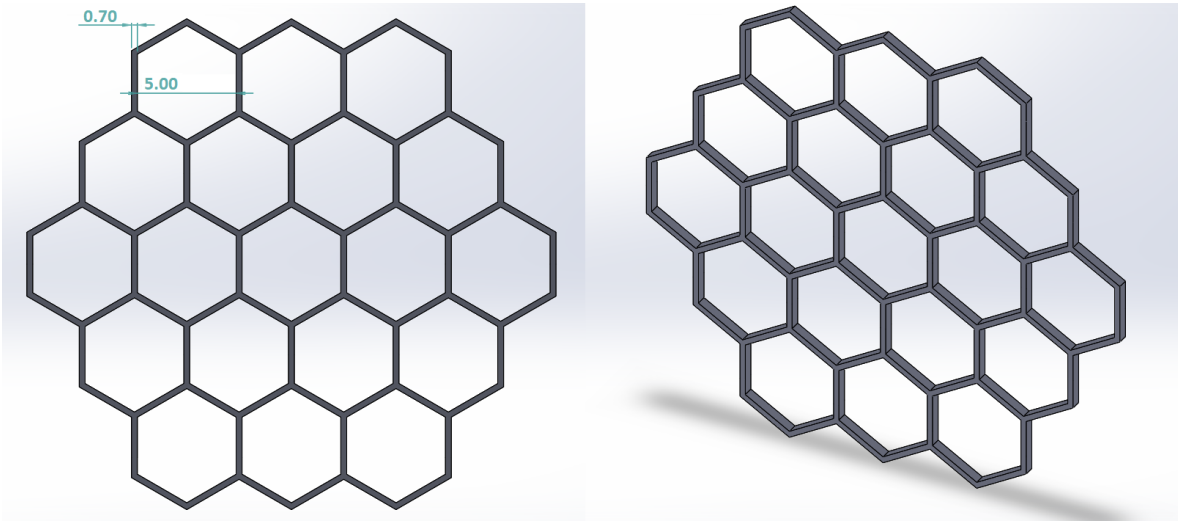

Figure 79 *CAD model: 2D- view (left) and 3D-view (right)*

Figure 80 shows a photograph of the printed and photo-crosslinked honeycomb-like structure. The optimized printing conditions able to give a good resolution, turned out to be a printer pressure and a feed rate of 100 kPa and 40%, respectively.

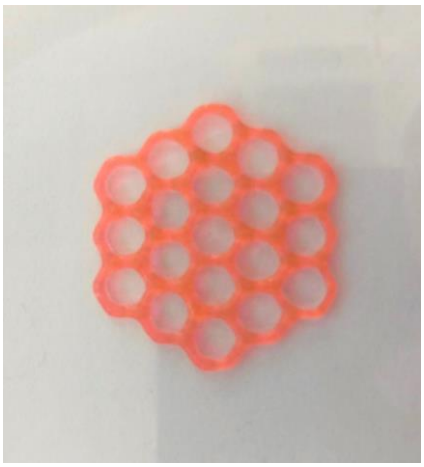

Figure 80 *Photograph of the 5mm dimension honeycomb-like structure.*

Figure 81 shows the microscope image of the honeycomb-like structure representative of a mean filament dimension. The mean printed filament diameter was 1.42 mm, confirming the high printing resolution achieved with the printing process.

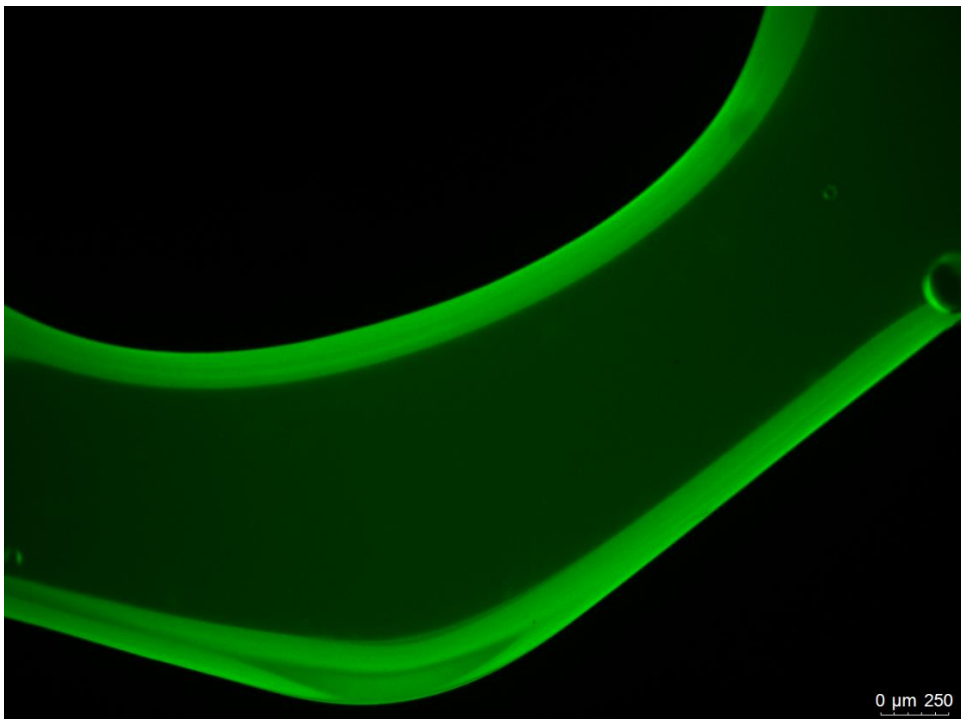

Figure 81 *Microscope image representative of a mean printed filament dimension*

4 mm Honeycomb:

Figure 82 shows the 3D CAD model of the honeycomb-like structure, reporting the dimensions in millimetres (hexagon hole dimension: 4 mm, filament dimension: 0.5 mm), modelled using Solidworks as CAD software. Therefore, the nozzle diameter used to print this structure was a G25 nozzle.

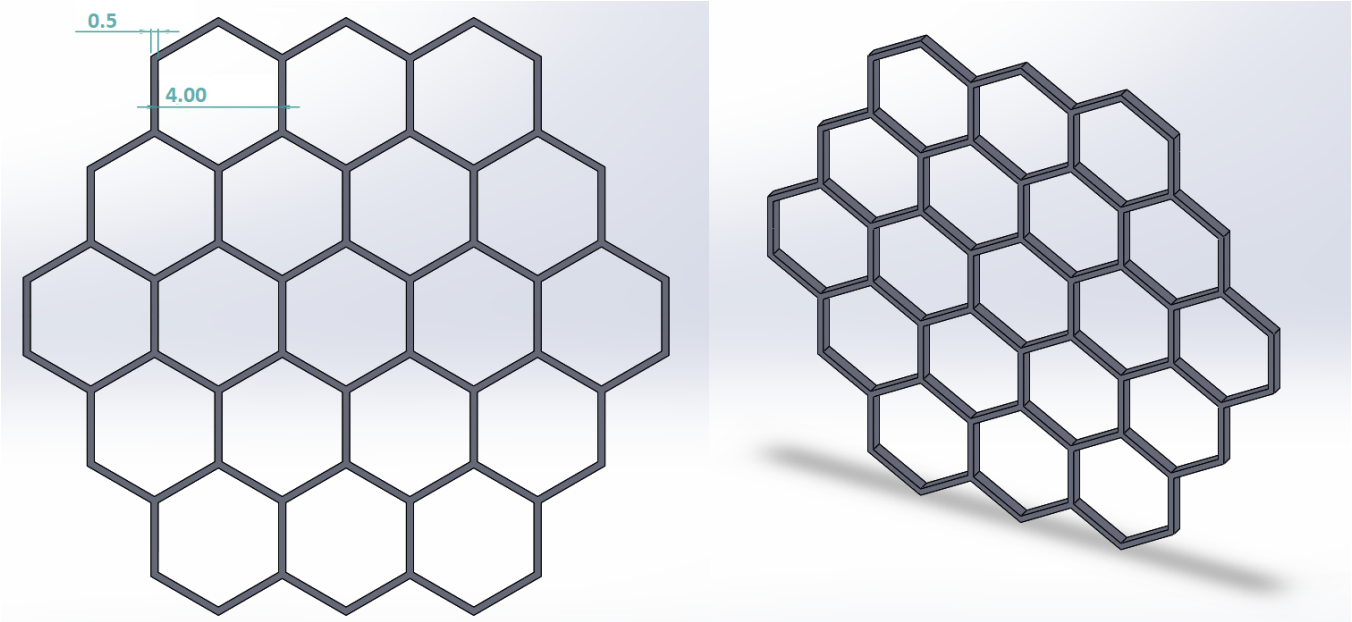

Figure 82 *CAD model: 2D- view (left) and 3D-view (right)*

Figure 83 shows a photograph of the printed and photo-crosslinked honeycomb-like structure. The optimized printing conditions able to give a good resolution, turned out to be a printer pressure and a feed rate of 100 kPa and 20%, respectively.

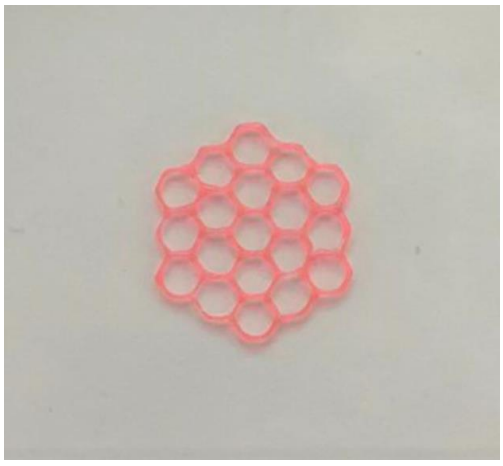

Figure 83 *Photograph of the 4mm dimension honeycomb-like structure*

Figure 84 shows the microscope image of the honeycomb-like structure representative of a mean filament dimension. The mean printed filament diameter was 1.12 mm, confirming the high printing resolution achieved with the printing process.

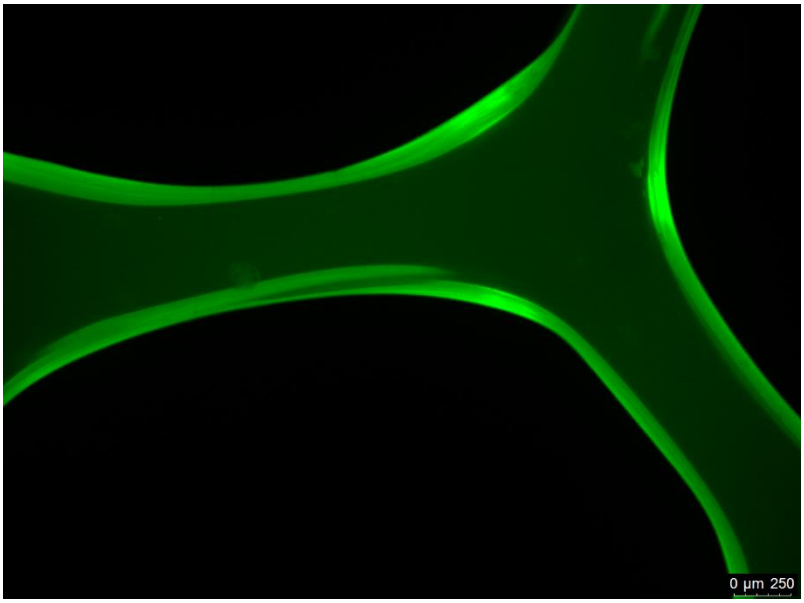

Figure 84 *Microscope image representative of a mean printed filament dimension*

3 mm Honeycomb:

Figure 85 shows the 3D CAD model of the honeycomb-like structure, reporting the dimensions in millimetres (hexagon hole dimension: 3 mm, filament dimension: 0.4 mm), modelled using Solidworks as CAD software. Therefore, the nozzle diameter used to print this structure was a G27 nozzle.

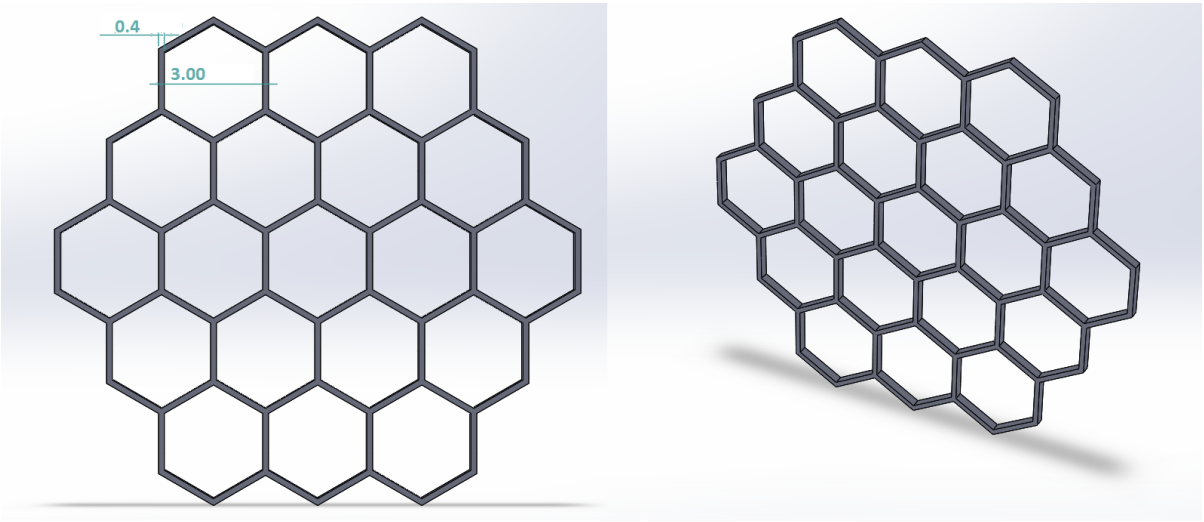

Figure 85 *CAD model: 2D- view (left) and 3D-view (right)*

Figure 86 shows a photograph of the printed and photo-crosslinked honeycomb-like structure. The optimized printing conditions able to give a good resolution, turned out to be a printer pressure and a feed rate of 125 kPa and 20%, respectively.

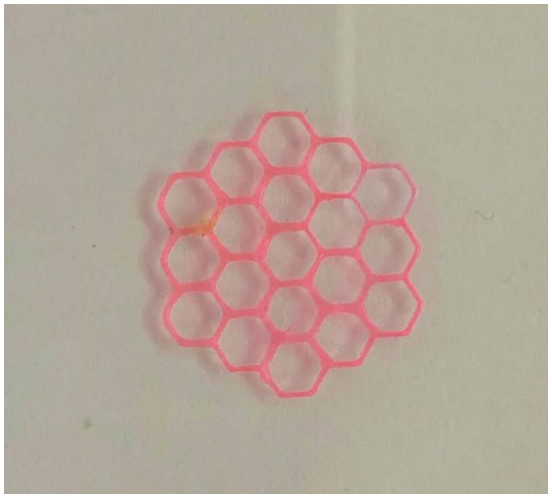

Figure 86 *Photograph of the 3mm dimension honeycomb-like structure.*

Figure 87 shows the microscope image of the honeycomb-like structure representative of a mean filament dimension. The mean printed filament diameter was 0.83 mm, confirming the high printing resolution achieved with the printing process.

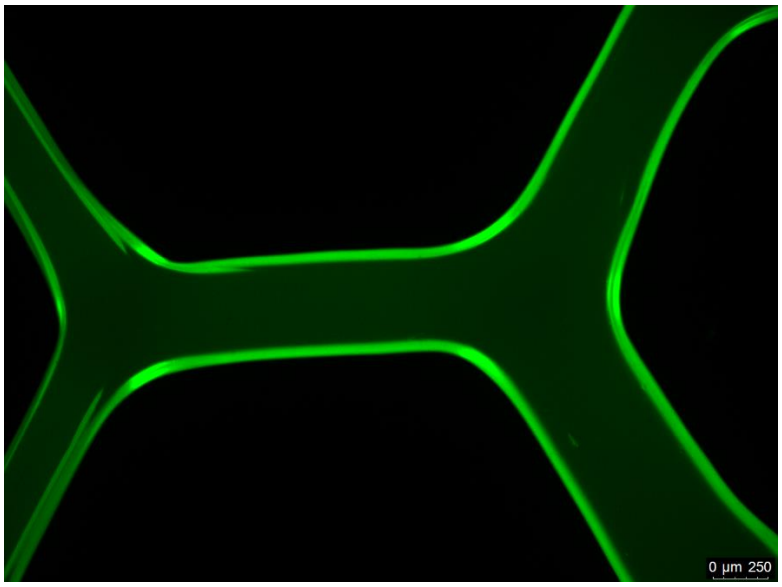

Figure 87 *Microscope image representative of a mean printed filament dimension*

2 mm Honeycomb:

Figure 88 shows the 3D CAD model of the honeycomb-like structure, reporting the dimensions in millimetres (hexagon hole dimension: 2 mm, filament dimension: 0.4 mm), modelled using Solidworks as CAD software. Therefore, the nozzle diameter used to print this structure was a G27 nozzle.

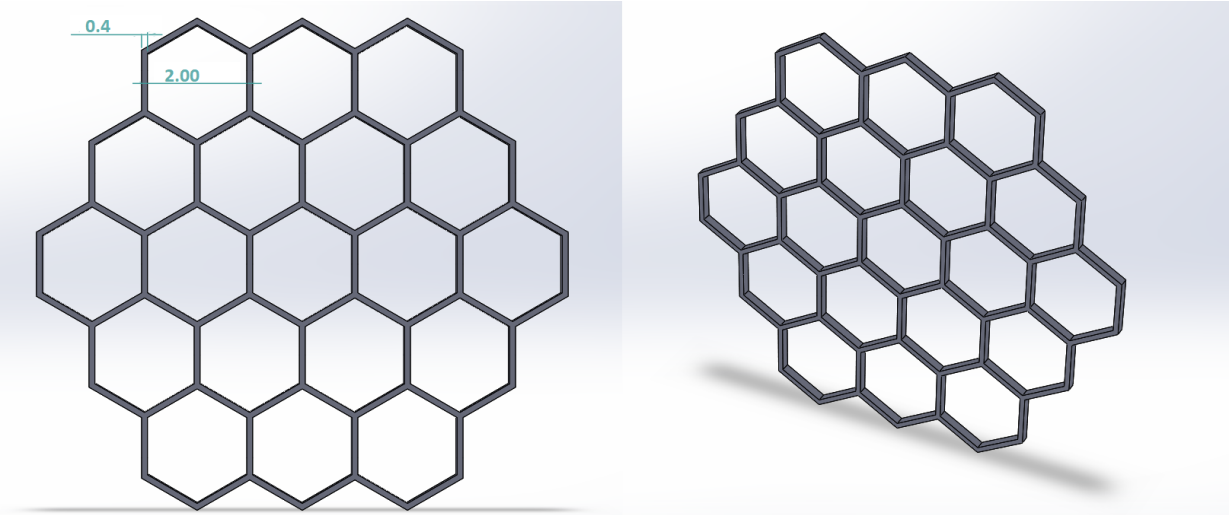

Figure 88 *CAD model: 2D- view (left) and 3D-view (right)*

Figure 89 shows a photograph of the printed and photo-crosslinked honeycomb-like structure. The optimized printing conditions able to give a good resolution, turned out to be a printer pressure and a feed rate of 125 kPa and 20%, respectively.

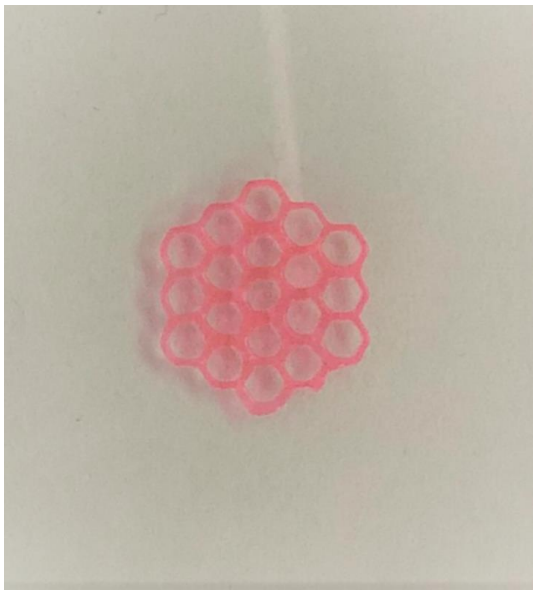

Figure 89 *Photograph of the 2mm dimension honeycomb-like structure.*

Figure 90 shows the microscope image of the honeycomb-like structure representative of a mean filament dimension. The mean printed filament diameter was 1.2 mm, so it resulted to be higher than the CAD model, suggesting the necessity of further optimization of the adopted printing parameters.

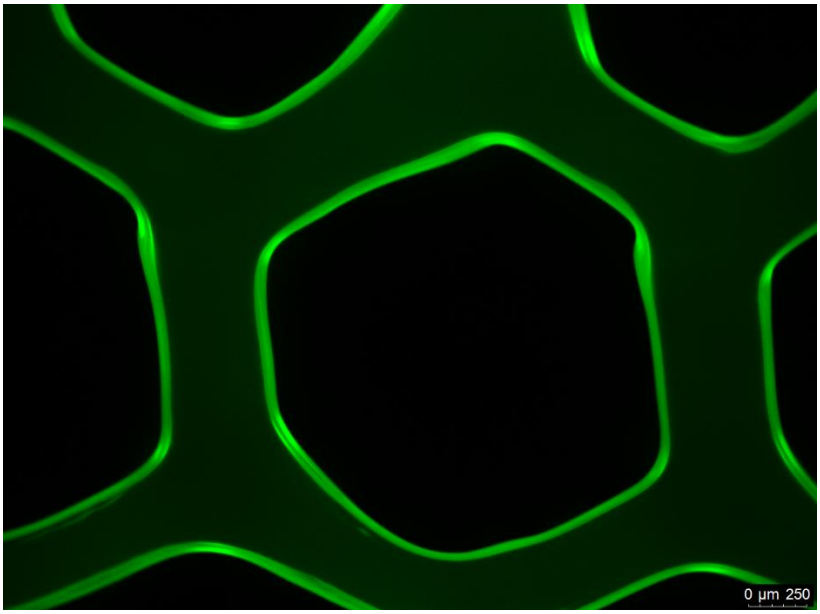

Figure 90 *Microscope image representative of a mean printed filament dimension*

Conclusion and Future Developments

The use of 3D-bioprinting in tissue engineering is gaining increasing importance since it permits to design bioengineered constructs (possibly loaded with cells or biomolecules) with custom-designed geometries suitable for replacing diseased tissues or even whole organs. In this process, the bioink plays a fundamental role and must comply with different strict requirements: (i) easy printability at low pressure to avoid cell damage; (ii) capability to maintain its printed shape; (iii) good cytocompatibility, and (iv) high stability in a watery environment. In this context, the high chemical versatility of polyurethanes, which allows the synthesis of polymers with tuneable properties by simply changing their building blocks (macrodiol, diisocyanate and chain extender), could be exploited to develop smart bioinks.

In this work new thermo- and photo-sensitive polyurethane-based hydrogels were designed and characterized in order to obtain suitable bioinks to create 3D-constructs able to fill tissue defects with complex geometry.

Specifically, an amphiphilic polyurethane (DHP407, M_n 20000 Da), based on Poloxamer® 407 as macrodiol, 1,6 hexamethylene diisocyanate and a chain extender containing Boc-protected amino groups, was successfully synthesised to design thermosensitive hydrogels able to undergo sol-to-gel transition upon temperature increase within the physiological range (30-37°C). Subsequently, secondary amino groups present along DHP407 backbone were Boc-deprotected (D-DHP407) through an acidic treatment to expose secondary amines (10^{19} units/$g_{D\text{-}DHP407}$ as calculated through Orange II Sodium salt assay). Then, the exposed functional groups were exploited to graft photosensitive moieties (i.e., 5-Norbornene 2-Carboxylic acid (NBE) and Thioglycolic acid (TGA) giving NB-DHP407 and S-DHP407, respectively) through carbodiimide chemistry, thus providing the resulting polymer with responsiveness to UV/Vis light irradiation. The successful functionalization procedure was first confirmed by chemical characterization through ATR-FTIR spectroscopy and then, the number of grafted thiol and norbornene groups was quantified through the colorimetric Ellman's method (10^{19} groups/$g_{S\text{-}DHP407}$) and ^{1}H-NMR spectroscopy (10^{17} groups/$g_{NB\text{-}DHP407}$), respectively. Then, the thermo-responsiveness of the newly designed polymers was proved through Dynamic Light Scattering (DLS) analyses by evaluating the changes in micelle hydrodynamic diameters upon heating S-DHP407 and NB-DHP407 aqueous solutions up to 45 °C. Furthermore, the photo-click reaction mechanism occurring between NB-DHP407 and S-DHP407 upon visible light irradiation at 80000 Lux for 10 minutes was first studied through UV-Vis spectroscopy on solutions

containing the virgin molecules (TGA and NBE) to identify the optimal photo-crosslinking parameters (i.e., photoinitiator Eosin Y and co-initiator tyrosine concentration). Among the tested conditions, the use of Eosin Y (EY) 0.5 mM as the only photo-initiator (i.e., without the need of a co-initiator) turned out to be the most promising condition to enhance the formation of covalent bonds between thiol and norbornene groups upon irradiation. The optimized concentration of EY was then used to prepare hydrogels through thiol-ene photo-click chemistry. ^{1}H NMR and ^{13}C NMR analyses were then exploited to confirm the success of visible light-initiated photo-crosslinking and thus the formation of new bonds among polymeric chains, through the decreasing intensity of the bands ascribed to norbornene and thiol groups. Moreover, DLS analyses performed on photo-crosslinked hydrogels further proved the success of the thiol-ene photo-crosslinking occurred between the polymeric chains, through the measurement of an increased micelle hydrodynamic diameter after light exposure with respect to the control (not-irradiated gels). Subsequently, photo-crosslinked hydrogels were rheologically characterized by exploiting their retained thermo-reversibility upon exposure to green light. The formation of significantly more developed gels with respect to the control (not photo-crosslinked hydrogels) at each analysed temperature was a further confirmation of the occurred thiol-ene photo-click reaction.

Finally, the optimized bioink formulation was successfully 3D-printed according to two different CAD models, i.e. square grid and honeycomb structure, by properly adjusting the working pressure, temperature and feed-rate.

To conclude, this novel smart bioink represents a promising platform to be used in the design of cellularized constructs due to their easy printability at low pressure and the possibility to further stabilize the 3D-printed structures via a rapid and cell-friendly photo-crosslinking mechanism (i.e., visible light irradiation, use of a cell-friendly photoinitiator). Moreover, hydrogel capability to undergo gel-to-sol transition upon irradiation paves the way to the design of a very versatile system as it could be also exploited as an injectable drug delivery system with improved mechanical properties with respect to the not photo-crosslinked hydrogels. However, further improvements in terms of hydrogel mechanical properties could be potentially achieved by working on the photo-crosslinking parameters (e.g., irradiation time, light intensity) as un-reacted thiol and norbornene groups were still present in the photo-crosslinked gels.

BIBLIOGRAPHY

[1] S. Van Vlierberghe, P. Dubruel, and E. Schacht, “Biopolymer-based hydrogels as scaffolds for tissue engineering applications: A review,” *Biomacromolecules*, vol. 12, no. 5, pp. 1387–1408, 2011.

[2] L. R. Feksa, E. A. Troian, C. D. Muller, F. Viegas, A. B. Machado, and V. C. Rech, “Hydrogels for biomedical applications,” *Nanostructures Eng. Cells, Tissues Organs From Des. to Appl.*, vol. 64, pp. 403–438, 2018.

[3] Y. Sekine, H. Takagi, S. Sudo, Y. Kajiwara, H. Fukazawa, and T. Ikeda-Fukazawa, “Dependence of structure of polymer side chain on water structure in hydrogels,” *Polymer (Guildf).*, vol. 55, no. 24, pp. 6320–6324, 2014.

[4] W. E. Hennink and C. F. van Nostrum, “Novel crosslinking methods to design hydrogels,” *Adv. Drug Deliv. Rev.*, vol. 64, no. SUPPL., pp. 223–236, 2012.

[5] X. Zhao, N. Huebsch, D. J. Mooney, and Z. Suo, “Stress-relaxation behavior in gels with ionic and covalent crosslinks,” *J. Appl. Phys.*, vol. 107, no. 6, 2010.

[6] H. Geckil, X. Zhang, S. Moon, and U. Demirci, “Engineering hydrogels as extracellular matrix mimics R eview,” *Lab Chip*, vol. 11, no. 5, pp. 469–484, 2013.

[7] C. B. Hutson *et al.*, “Synthesis and characterization of tunable poly(ethylene glycol): Gelatin methacrylate composite hydrogels,” *Tissue Eng. - Part A*, vol. 17, no. 13–14, pp. 1713–1723, 2011.

[8] J. L. Ifkovits and J. A. Burdick, “Review: Photopolymerizable and degradable biomaterials for tissue engineering applications,” *Tissue Eng.*, vol. 13, no. 10, pp. 2369–2385, 2007.

[9] F. Ullah, M. B. H. Othman, F. Javed, Z. Ahmad, and H. M. Akil, “Classification, processing and application of hydrogels: A review,” *Mater. Sci. Eng. C*, vol. 57, pp. 414–433, 2015.

[10] J. Zhu, “Stress Risk Assessment Form,” vol. 8, no. 5, pp. 1–8, 2011.

[11] M. W. Tibbitt and K. S. Anseth, “Hydrogels as extracellular matrix mimics for 3D cell culture,” *Biotechnol. Bioeng.*, vol. 103, no. 4, pp. 655–663, 2009.

[12] C. A. Durst, M. P. Cuchiara, E. G. Mansfield, J. L. West, and K. J. Grande-Allen, “Flexural

characterization of cell encapsulated PEGDA hydrogels with applications for tissue engineered heart valves," *Acta Biomater.*, vol. 7, no. 6, pp. 2467–2476, 2011.

[13] J. Yeh *et al.*, "Micromolding of shape-controlled, harvestable cell-laden hydrogels," *Biomaterials*, vol. 27, no. 31, pp. 5391–5398, 2006.

[14] G. Sun, Y. I. Shen, S. Kusuma, K. Fox-Talbot, C. J. Steenbergen, and S. Gerecht, "Functional neovascularization of biodegradable dextran hydrogels with multiple angiogenic growth factors," *Biomaterials*, vol. 32, no. 1, pp. 95–106, 2011.

[15] K. H. Park, K. Na, and H. M. Chung, "Enhancement of the adhesion of fibroblasts by peptide containing an Arg-Gly-Asp sequence with poly(ethylene glycol) into a thermo-reversible hydrogel as a synthetic extracellular matrix," *Biotechnol. Lett.*, vol. 27, no. 4, pp. 227–231, 2005.

[16] J. J. Moon *et al.*, "Biomimetic hydrogels with pro-angiogenic properties," *Biomaterials*, vol. 31, no. 14, pp. 3840–3847, 2010.

[17] J. E. Leslie-Barbick, J. E. Saik, D. J. Gould, M. E. Dickinson, and J. L. West, "The promotion of microvasculature formation in poly(ethylene glycol) diacrylate hydrogels by an immobilized VEGF-mimetic peptide," *Biomaterials*, vol. 32, no. 25, pp. 5782–5789, 2011.

[18] J. Teßmar, F. Brandl, and A. Göpferich, "Hydrogels for tissue engineering," *Fundam. Tissue Eng. Regen. Med.*, vol. 101, no. 7, pp. 495–517, 2009.

[19] T. R. Hoare and D. S. Kohane, "Hydrogels in drug delivery: Progress and challenges," *Polymer (Guildf).*, vol. 49, no. 8, pp. 1993–2007, 2008.

[20] K. Deligkaris, T. S. Tadele, W. Olthuis, and A. van den Berg, "Hydrogel-based devices for biomedical applications," *Sensors Actuators, B Chem.*, vol. 147, no. 2, pp. 765–774, 2010.

[21] P. Eiselt, K. Y. Lee, and D. J. Mooney, "Rigidity of two-component hydrogels prepared from alginate and poly(ethylene glycol)-diamines," *Macromolecules*, vol. 32, no. 17, pp. 5561–5566, 1999.

[22] J. J. Sperinde and L. G. Griffith, "Control and prediction of gelation kinetics in enzymatically cross-linked poly(ethylene glycol) hydrogels," *Macromolecules*, vol. 33, no. 15, pp. 5476–5480, 2000.

[23] A. K. Bajpai, J. Bajpai, R. Saini, and R. Gupta, “Responsive polymers in biology and technology,” *Polym. Rev.*, vol. 51, no. 1, pp. 53–97, 2011.

[24] K. S. Soppimath, T. M. Aminabhavi, A. M. Dave, S. G. Kumbar, and W. E. Rudzinski, “Stimulus-responsive ‘smart’ hydrogels as novel drug delivery systems,” *Drug Dev. Ind. Pharm.*, vol. 28, no. 8, pp. 957–974, 2002.

[25] J. F. Mano, “Stimuli-responsive polymeric systems for biomedical applications,” *Adv. Eng. Mater.*, vol. 10, no. 6, pp. 515–527, 2008.

[26] D. J. Beebe *et al.*, “Functional hydrogel structures for autonomous flow control inside microfluidic channels,” *Nature*, vol. 404, no. 6778, pp. 588–590, 2000.

[27] H. Ghandehari, P. Kopečkové, and J. Kopeček, “In vitro degradation of pH-sensitive hydrogels containing aromatic azo bonds,” *Biomaterials*, vol. 18, no. 12, pp. 861–872, 1997.

[28] R. A. Siegel, M. Falamarzian, B. A. Firestone, and B. C. Moxley, “pH-Controlled release from hydrophobic/polyelectrolyte copolymer hydrogels,” *J. Control. Release*, vol. 8, no. 2, pp. 179–182, 1988.

[29] D. Schmaljohann, “Thermo- and pH-responsive polymers in drug delivery,” *Adv. Drug Deliv. Rev.*, vol. 58, no. 15, pp. 1655–1670, 2006.

[30] Q. H. B. T. Films and L. D. M. L. Scattering, “<Nature (399, 1999, 766).pdf>,” vol. 399, no. June, 1999.

[31] L. Serra, J. Doménech, and N. A. Peppas, “Drug transport mechanisms and release kinetics from molecularly designed poly(acrylic acid-g-ethylene glycol) hydrogels,” *Biomaterials*, vol. 27, no. 31, pp. 5440–5451, 2006.

[32] L. Altomare *et al.*, “Biopolymer-based strategies in the design of smart medical devices and artificial organs,” *Int. J. Artif. Organs*, 2018.

[33] L. Klouda and A. G. Mikos, “Thermoresponsive hydrogels in biomedical applications,” *Eur. J. Pharm. Biopharm.*, vol. 68, no. 1, pp. 34–45, 2008.

[34] M. Boffito, P. Sirianni, A. M. Di Rienzo, and V. Chiono, “Thermosensitive block copolymer hydrogels based on poly(E-caprolactone) and polyethylene glycol for biomedical applications: State of the art and future perspectives,” *J. Biomed. Mater. Res. - Part A*, vol.

103, no. 3, pp. 1276–1290, 2015.

[35] S. Fujishige, K. Kubota, and I. Ando, “Phase transition of aqueous solutions of poly(N-isopropylacrylamide) and poly(N-isopropylmethacrylamide),” *J. Phys. Chem.*, vol. 93, no. 8, pp. 3311–3313, 1989.

[36] M. Nakayama, T. Okano, T. Miyazaki, F. Kohori, K. Sakai, and M. Yokoyama, “Molecular design of biodegradable polymeric micelles for temperature-responsive drug release,” *J. Control. Release*, vol. 115, no. 1, pp. 46–56, 2006.

[37] X. Z. Zhang, Y. Y. Yang, T. S. Chung, and K. X. Ma, “Preparation and characterization of fast response macroporous poly(N-isopropylacrylamide) hydrogels,” *Langmuir*, vol. 17, no. 20, pp. 6094–6099, 2001.

[38] A. Organs, “Environment responsive gelling copolymer,” vol. 2, no. 12, 2001.

[39] B. Jeong, S. W. Kim, and Y. H. Bae, “Thermosensitive sol-gel reversible hydrogels,” *Adv. Drug Deliv. Rev.*, vol. 64, no. SUPPL., pp. 154–162, 2012.

[40] Ron and Bromberg, “Temperature-responsive gels and thermogelling polymer matrices for protein and peptide delivery.,” *Adv. Drug Deliv. Rev.*, vol. 31, no. 3, pp. 197–221, 1998.

[41] V. Lenaerts, C. Triqueneaux, M. Quartern, F. Rieg-Falson, and P. Couvreur, “Temperature-dependent rheological behavior of Pluronic F-127 aqueous solutions,” *Int. J. Pharm.*, vol. 39, no. 1–2, pp. 121–127, 1987.

[42] Y. Yang, J. C. Wang, X. Zhang, W. L. Lu, and Q. Zhang, “A novel mixed micelle gel with thermo-sensitive property for the local delivery of docetaxel,” *J. Control. Release*, vol. 135, no. 2, pp. 175–182, 2009.

[43] J. M. Brunet-Maheu Jean-Marc, J. C. Fernandes, C. A. V. de Lacerda, Q. Shi, M. Benderdour, and P. Lavigne, “Pluronic F-127 as a cell carrier for bone tissue engineering,” *J. Biomater. Appl.*, vol. 24, no. 3, pp. 275–287, 2009.

[44] D. Cohn, A. Sosnik, and A. Levy, “Improved reverse thermo-responsive polymeric systems,” *Biomaterials*, vol. 24, no. 21, pp. 3707–3714, 2003.

[45] M. Boffito *et al.*, “Novel polyurethane-based thermosensitive hydrogels as drug release and tissue engineering platforms: Design and in vitro characterization,” *Polym. Int.*, vol. 65, no.

7, pp. 756–769, 2016.

[46] M. R. Matanović, J. Kristl, and P. A. Grabnar, “Thermoresponsive polymers: Insights into decisive hydrogel characteristics, mechanisms of gelation, and promising biomedical applications,” *Int. J. Pharm.*, vol. 472, no. 1–2, pp. 262–275, 2014.

[47] B. Jeong, Y. H. Bae, and S. W. Kim, “Thermoreversible gelation of PEG-PLGA-PEG triblock copolymer aqueous solutions,” *Macromolecules*, vol. 32, no. 21, pp. 7064–7069, 1999.

[48] C. C. Lin, C. S. Ki, and H. Shih, “Thiol-norbornene photoclick hydrogels for tissue engineering applications,” *J. Appl. Polym. Sci.*, vol. 132, no. 8, pp. 1–11, 2015.

[49] “Polyurethane-based thiomers : a new multifunctional copolymer platform for biomedical applications,” pp. 1–35.

[50] T. Greene, T. Y. Lin, O. M. Andrisani, and C. C. Lin, “Comparative study of visible light polymerized gelatin hydrogels for 3D culture of hepatic progenitor cells,” *J. Appl. Polym. Sci.*, vol. 134, no. 11, pp. 1–10, 2017.

[51] D. Zhou and Y. Ito, “Visible light-curable polymers for biomedical applications,” *Sci. China Chem.*, vol. 57, no. 4, pp. 510–521, 2014.

[52] J. L. West and K. T. Nguyen, “Photopolymerizable hydrogels for tissue engineering applications,” *Biomaterials*, vol. 23, no. 22, pp. 4307–4314, 2002.

[53] A. E. Rydholm, C. N. Bowman, and K. S. Anseth, “Degradable thiol-acrylate photopolymers: Polymerization and degradation behavior of an in situ forming biomaterial,” *Biomaterials*, vol. 26, no. 22, pp. 4495–4506, 2005.

[54] S. Han and L. Chien-Chi, “Visible-Light-Mediated Thiol-Ene Hydrogelation Using Eosin-Y as the Only Photoinitiator,” *Macromol. Rapid Commun.*, vol. 34, no. 3, pp. 269–273, 2013.

[55] M. A. Shaker and H. M. Younes, “Photo-irradiation paradigm: Mapping a remarkable facile technique used for advanced drug, gene and cell delivery,” *J. Control. Release*, vol. 217, pp. 10–26, 2015.

[56] A. S. Sawhney, C. P. Pathak, and J. A. Hubbell, “Bioerodible Hydrogels Based on Photopolymerized Poly(ethylene glycol)-co-poly (α-hydroxy acid) Diacrylate Macromers,” *Macromolecules*, vol. 26, no. 4, pp. 581–587, 1993.

[57] I. S. Kim, Y. Il Jeong, and S. H. Kim, “Self-assembled hydrogel nanoparticles composed of dextran and poly(ethylene glycol) macromer,” *Int. J. Pharm.*, vol. 205, no. 1–2, pp. 109–116, 2000.

[58] P. Martens and K. S. Anseth, “Characterization of hydrogels formed from acrylate modified poly(vinyl alcohol) macromers,” *Polymer (Guildf).*, vol. 41, no. 21, pp. 7715–7722, 2000.

[59] L. I. N. Lin, Y. Morisaki, and Y. Chujo, “Synthesis of Through-Space Conjugated Polymers in the Main Chain,” pp. 7003–7011, 2009.

[60] S. C. Ligon-Auer, M. Schwentenwein, C. Gorsche, J. Stampfl, and R. Liska, “Toughening of photo-curable polymer networks: A review,” *Polym. Chem.*, vol. 7, no. 2, pp. 257–286, 2016.

[61] E. M. Saffer, M. A. Lackey, D. M. Griffin, S. Kishore, G. N. Tew, and S. R. Bhatia, “SANS study of highly resilient poly(ethylene glycol) hydrogels,” *Soft Matter*, vol. 10, no. 12, pp. 1905–1916, 2014.

[62] J. Cui, M. A. Lackey, G. N. Tew, and A. J. Crosby, “Mechanical Properties of End-Linked PEG/PDMS Hydrogels,” 2012.

[63] H. Shih, H. Y. Liu, and C. C. Lin, “Improving gelation efficiency and cytocompatibility of visible light polymerized thiol-norbornene hydrogels via addition of soluble tyrosine,” *Biomater. Sci.*, vol. 5, no. 3, pp. 589–599, 2017.

[64] J. O. Akindoyo, M. D. H. Beg, S. Ghazali, M. R. Islam, N. Jeyaratnam, and A. R. Yuvaraj, “Polyurethane types, synthesis and applications-a review,” *RSC Adv.*, vol. 6, no. 115, pp. 114453–114482, 2016.

[65] S. A. Guelcher, “Biodegradable polyurethanes: Synthesis and applications in regenerative medicine,” *Tissue Eng. - Part B Rev.*, vol. 14, no. 1, pp. 3–17, 2008.

[66] P. A. Gunatillake, R. Adhikari, and N. Gadegaard, “Biodegradable synthetic polymers for tissue engineering,” *Eur. Cells Mater.*, vol. 5, pp. 1–16, 2003.

[67] H. B. L. and J. D. A. JIN HO LEE, “14-Prog. Polym. Sci., 1995, 20, 1043.pdf,” vol. 20, no. 95, pp. 1043–1079, 1995.

[68] J. Joseph, R. M. Patel, A. Wenham, and J. R. Smith, “Biomedical applications of polyurethane materials and coatings,” *Trans. Inst. Met. Finish.*, vol. 96, no. 3, pp. 121–129, 2018.

[69] J. H. Silver, C. W. Myers, F. Lim, and S. L. Cooper, “Effect of polyol molecular weight on the physical properties and haemocompatibility of polyurethanes containing polyethylene oxide macroglycols,” *Biomaterials*, vol. 15, no. 9, pp. 695–704, 1994.

[70] H. J. Yoo and H. Do Kim, “Synthesis and properties of waterborne polyurethane hydrogels for wound healing dressings,” *J. Biomed. Mater. Res. - Part B Appl. Biomater.*, vol. 85, no. 2, pp. 326–333, 2008.

[71] L. Zhou *et al.*, “Synthesis and characterization of pH-sensitive biodegradable polyurethane for potential drug delivery applications,” *Macromolecules*, vol. 44, no. 4, pp. 857–864, 2011.

[72] L. Zhou *et al.*, “The degradation and biocompatibility of pH-sensitive biodegradable polyurethanes for intracellular multifunctional antitumor drug delivery,” *Biomaterials*, vol. 33, no. 9, pp. 2734–2745, 2012.

[73] B. Liu, J. Hu, and Q. Meng, “Nonwoven supported temperature-sensitive poly(N-isopropylacrylamide)/ polyurethane copolymer hydrogel with antibacterial aetivity,” *J. Biomed. Mater. Res. - Part B Appl. Biomater.*, vol. 89, no. 1, pp. 1–8, 2009.

[74] T. Billiet, M. Vandenhaute, J. Schelfhout, S. Van Vlierberghe, and P. Dubruel, “A review of trends and limitations in hydrogel-rapid prototyping for tissue engineering,” *Biomaterials*, vol. 33, no. 26, pp. 6020–6041, 2012.

[75] R. Suntornnond, J. An, and C. K. Chua, “Bioprinting of Thermoresponsive Hydrogels for Next Generation Tissue Engineering: A Review,” *Macromol. Mater. Eng.*, vol. 302, no. 1, pp. 1–15, 2017.

[76] E. Sachs, M. Cima, P. Williams, D. Brancazio, and J. Cornie, “Three dimensional printing: Rapid tooling and prototypes directly from a CAD model,” *J. Manuf. Sci. Eng. Trans. ASME*, vol. 114, no. 4, pp. 481–488, 1992.

[77] F. Gao, C. Ruan, and W. Liu, “High-strength hydrogel-based bioinks,” *Mater. Chem. Front.*, 2019.

[78] I. Mironi-Harpaz, D. Y. Wang, S. Venkatraman, and D. Seliktar, “Photopolymerization of cell-encapsulating hydrogels: Crosslinking efficiency versus cytotoxicity,” *Acta Biomater.*, vol. 8, no. 5, pp. 1838–1848, 2012.

[79] Y. He, F. Yang, H. Zhao, Q. Gao, B. Xia, and J. Fu, “Research on the printability of hydrogels in 3D bioprinting,” *Sci. Rep.*, vol. 6, pp. 1–13, 2016.

[80] S. Bandyopadhyay and J. J. Hablitz, “A Review of 3D Printing in Tissue Engineering,” *J. Neurophysiol.*, vol. 97, no. 6, pp. 4120–4128, 2007.

[81] F. P. W. Melchels, M. A. N. Domingos, T. J. Klein, J. Malda, P. J. Bartolo, and D. W. Hutmacher, “Additive manufacturing of tissues and organs,” *Prog. Polym. Sci.*, vol. 37, no. 8, pp. 1079–1104, 2012.

[82] A. Skardal, J. Zhang, L. McCoard, X. Xu, S. Oottamasathien, and G. D. Prestwich, “Photocrosslinkable hyaluronan-gelatin hydrogels for two-step bioprinting,” *Tissue Eng. - Part A*, vol. 16, no. 8, pp. 2675–2685, 2010.

[83] L. A. Hockaday *et al.*, “Rapid 3D printing of anatomically accurate and mechanically heterogeneous aortic valve hydrogel scaffolds,” *Biofabrication*, vol. 4, no. 3, 2012.

[84] M. Müller, J. Becher, M. Schnabelrauch, and M. Zenobi-Wong, “Nanostructured Pluronic hydrogels as bioinks for 3D bioprinting,” *Biofabrication*, vol. 7, no. 3, p. 35006, 2015.

[85] R. Laurano, C. Cassino, G. Ciardelli, V. Chiono, and M. Boffito, “Polyurethane-based thiomers: A new multifunctional copolymer platform for biomedical applications,” *React. Funct. Polym.*, vol. 146, no. August 2019, p. 104413, 2020.

[86] R. Pappalardo, “Design of stimuli responsive polyurethane-based hydrogels for 3D printing applications,” 2019.

[87] C. E. Schanté, G. Zuber, C. Herlin, and T. F. Vandamme, “Chemical modifications of hyaluronic acid for the synthesis of derivatives for a broad range of biomedical applications,” *Carbohydr. Polym.*, vol. 85, no. 3, pp. 469–489, 2011.

[88] M. D’Este, D. Eglin, and M. Alini, “A systematic analysis of DMTMM vs EDC/NHS for ligation of amines to Hyaluronan in water,” *Carbohydr. Polym.*, vol. 108, no. 1, pp. 239–246, 2014.

[89] H. Shih, A. K. Fraser, and C. C. Lin, “Interfacial thiol-ene photoclick reactions for forming multilayer hydrogels,” *ACS Appl. Mater. Interfaces*, vol. 5, no. 5, pp. 1673–1680, 2013.